THEORETICAL STUDIES OF THE NONLINEAR INFRARED PROPERTIES OF p-TYPE SEMICONDUCTORS

Thesis by

Ralph B. James

In Partial Fulfillment of the Requirements

for the Degree

of

Doctor of Philosophy

California Institute of Technology

Pasadena, California

1981

(Submitted October 30, 1980)

Dedicated to my wife

Patricia

and to my parents

John and Gladys James

ACKNOWLEDGEMENTS

I would like to express my appreciation and thanks to Dr. Darryl L. Smith and Dr. Thomas C. McGill for their valuable guidance and advice with this work.

I have also profited much from useful discussions with Murray Daw, Dr. Gordon Osbourn, and Edgard Schweig. I would also like to thank Andy Hunter, Dr. Ken Elliott, Dr. Joel Schulman, Dr. Y. C. Chang, Gordon Mitchard, Randy Feenstra, Mike Weimer, Anne Hofmeister, Arati Prabhakar, Barton Zwiebach, Tom Koch, Mark Boslough, and Andy Gabriel for providing a stimulating research environment. I am indebted to Dr. Darryl Smith, Dr. Thomas McGill, Dr. Amnon Yariv, Dr. Noel Corngold, and Dr. James McCaldin for their suggestions with regard to my graduate work and for their assistance with my job placement following the completion of my graduate program. I also very much appreciate Vere Snell for her friendly assistance and for typing this thesis.

I am thankful for financial support received from the California Institute of Technology, the ARCS Foundation, and the Department of the Air Force.

Finally, I would like to express my deepest appreciation to my wife, Patricia, for her constant support and encouragement while I completed the work in this thesis.

ABSTRACT

This thesis presents theoretical studies of the nonlinear optical properties of p-type semiconductors. Chapter 2 is concerned with the intensity dependence of the complex dielectric constant of p-type germanium for light with a wavelength in the 9-11 μm region. The nonlinear absorption is described by the imaginary part of the complex dielectric constant, and the nonlinear dispersive properties are described by the intensity dependence of the real part of the dielectric constant. Chapter 3 deals with the saturation characteristics of practically all Groups IV and III-V p-type semiconductors and includes a discussion of the systematic dependence of the saturation intensity on the material parameters. Chapters 4 and 5 are concerned with several "pump-and-probe" experiments. Here, the transmission of a low-intensity light beam (probe) can be altered by the presence of a high-intensity laser (pump). In these chapters the modulation of the probe transmission is analyzed as a function of the intensity of the pump laser. Chapter 6 treats the intensity dependence of the conductivity of p-Ge for light with a wavelength of 10.6 μm.

In Chapter 2, we present a theory of the saturation of heavy- to light-hole band transitions in p-type germanium by high-intensity light with a wavelength near 10 μm. The free-hole distribution function is modified by the high-intensity light, which leads to an intensity dependence in the absorption coefficient and the index of refraction.

The absorption coefficient is found to decrease with intensity in a manner closely approximated by an inhomogeneously broadened two-level model. For temperatures and hole concentrations where hole-phonon dominates hole-impurity and hole-hole scattering, the saturation intensity is independent of the hole concentration. For larger hole densities, the saturation intensity is found to increase monotonically with increasing hole concentration. We calculate the saturation intensity as a function of excitation wavelength and temperature for p-Ge. The saturation intensity is found to increase with increasing photon energy and temperature. The calculated results for the absorption saturation are compared with the available experimental data and good agreement is found. In addition to the nonlinear absorption, there exist laser-induced changes in the index of refraction resulting from the saturation of the intervalence-band transitions. Calculations of the intensity dependence of the real part of the dielectric constant are performed for room temperature and for light with a wavelength of 10.6 μm. The index of refraction is found to increase monotonically with increasing intensity.

In Chapter 3, we present the results of the theory describing the saturation behavior of most p-type semiconductors with the diamond or zincblende crystal structure by high-intensity CO_2 light. For materials with large spin-orbit splittings as compared to the excitation wavelength (as for Ge), the dominant absorption mechanism is direct intervalence-band transitions where a free hole in the heavy-hole band absorbs a photon and makes a transition to the light-hole

band. For materials with small spin-orbit splittings as compared to the excitation wavelength (as for Si), direct intervalence-band transitions are allowed between the heavy-hole and light-hole, heavy-hole and split-off, and light-hole and split-off hole bands. In each material, values of the saturation intensity are reported as a function of the photon energy and temperature.

In Chapter 4, we present a theory to describe the enhanced transmission of a weak tunable probe laser with a wavelength near 3 μm in the presence of a high-intensity saturating beam with a wavelength near 10 μm in p-Ge. The mechanism responsible for the increasing transmission of the probe laser is the depletion of holes in the heavy-hole band by the saturating beam. Room temperature values of the absorption coefficient of the probe are predicted as a function of the intensity of the pump beam.

In Chapter 5, we present a theory of the absorption lineshape of a low-intensity probe laser which is tuned in the vicinity of a high-intensity pump laser with a wavelength of 10.6 μm. Values for the absorption coefficient of the probe are calculated at room temperature as a function of the intensity of the pump laser. We find the probe absorption can be divided into two contributions: one being due to the depletion of holes in the resonant region of the heavy-hole band by the saturable pump, and the other being due to a coupling of the pump and probe beams which allow the pump photons to be scattered into the probe and vice versa. The calculated results for the composite line-

shape of the probe are compared with the experimental data and good agreement is found.

In Chapter 6, we show how the modification of the free-hole distribution function by the saturating beam leads to a change in the conductivity of p-Ge. The photoconductive response is calculated as a function of the doping level, temperature and light intensity.

Parts of this thesis have been or will be published under the following titles:

Chapter 2:

Theory of Nonlinear Infrared Absorption in p-type Germanium, R. B. James and D. L. Smith, Phys. Rev. Lett. 42, 1495 (1979).

Saturation of Intervalence-Band Transitions in p-type Semiconductors, R. B. James and D. L. Smith, Phys. Rev. B21, 3502 (1980).

Dependence of the Saturation Intensity of p-type Germanium on Impurity Concentration and Residual Absorption at 10.59 μm, R. B. James and D. L. Smith, Solid State Commun. 33, 395 (1980).

Laser-Induced Changes in the Dispersive Properties of p-Ge Due to Intervalence-Band Transitions, R. B. James and D. L. Smith (submitted to Physical Review).

Chapter 3:

Saturation Characteristics of p-type Semiconductors over the CO_2 Laser-Spectrum, R. B. James and D. L. Smith, J. of Appl. Phys. 51, 2836 (1980).

Absorption of High-Intensity CO_2 Laser Light in p-type Semiconductors with Small Spin-Orbit Splittings, R. B. James and D. L. Smith, (submitted to J. of Appl. Phys.).

Chapter 4:

Calculation of 3 μm Probe Transmission in p-Ge Excited by a CO_2 Laser, R. B. James and D. L. Smith, (accepted for publication in Solid State Commun.)

Chapter 5:

Nonlinear Absorption of a Weak Tunable CO_2 Laser in p-Ge in the Presence of a High-Intensity Laser at 10.6 μm, R. B. James and D. L. Smith, (to be submitted to Physical Review).

Chapter 6:

Theoretical Description of the Intervalence-Band Photoconductivity of p-Ge at 10.6 μm, R. B. James and D. L. Smith, (submitted to Physical Review).

TABLE OF CONTENTS

CHAPTER 1

I. BACKGROUND

The study of nonlinear optics deals with phenomena that occur at high light intensities obtainable by laser beams. It represents one of the most interesting fields of research made possible by the development of powerful lasers. There is great current experimental and theoretical interest in the nonlinear dielectric properties of semiconductors in which, in addition to the linear response, polarization of the medium is produced which is not directly proportional to the electric field that induces it [1]. These nonlinear phenomena have many important applications as frequency conversion devices, three of the most important applications being: (1) parametric oscillation in which a high-power pump wave at frequency ω causes the simultaneous generation of radiation at ω_1 and ω_2, where $\omega = \omega_1 + \omega_2$; (2) frequency-up conversion in which a weak signal at ω_1 is converted to a signal at a higher frequency ω_3 by mixing with a strong pump laser at ω_2, where $\omega_2 = \omega_3 - \omega_1$; (3) and second-harmonic generation in which part of the energy of a laser beam at frequency ω is converted to that of a wave with frequency at 2ω.

Some other nonlinear properties in semiconductors which are of active interest in the control of laser beams include the electro-optic effect, photoelastic effect, Raman scattering, self-focusing actions, and saturable absorption. In this thesis I present a theory of the absorption saturation of several p-type semiconductors by high-intensity light with a wavelength near 10 μm. The results of the theory

can also be used to analyze the importance of self-focusing actions in p-type semiconductors for given experimental conditions. These self-focusing actions are due to an intensity dependence in the index of refraction of the material and are of great concern to experimentalists working with high power laser pulses since the spatial and temporal behavior of the laser pulse is modified as the pulse propagates through the medium.

When radiation at a given frequency interacts with a material with a transition near the frequency, a resonant interaction occurs, and several nonlinear phenomena associated with the resonance may also occur. For materials in thermal equilibrium, the radiation is absorbed as it propagates through the material, resulting in the attenuation of the wave, where the decay of a wave propagating in the z-direction is given by

$$\frac{dI}{dz} = -\alpha I \quad . \tag{1}$$

Here, I is the light intensity and α is the absorption coefficient. The absorption of light by several p-type semiconductors becomes a nonlinear function at high light intensities. At low light intensities (linear regime), the absorption coefficient of the medium is independent of the intensity; however, at sufficiently high intensities, the absorption coefficient is significantly reduced, and the radiation

passes through the material relatively unattenuated. This effect is often termed saturation of the resonant transition and has many important applications in the design of laser systems. Most of the experimental information on the saturable absorption of p-type semiconductors exists for germanium for wavelengths in the 9-11 μm region, which corresponds to the CO_2 laser spectrum [2-5]. The measurements indicate that the reduction in the absorption coefficient with increasing intensity is approximately given by

$$\alpha(I) = \frac{\alpha_o(\omega)}{\sqrt{1 + I/I_s}} \quad , \tag{2}$$

where $\alpha_o(\omega)$ is the absorption coefficient at low intensity, and I_s is the saturation intensity [3-5]. This functional form for the intensity dependence of $\alpha(I)$ is predicted for an inhomogeneously broadened two-level system in which the medium can be characterized by a smooth distribution of resonant frequencies, as is the case for low-pressure gases due to the Doppler effect.

This nonlinear infrared absorption has several applications in the control of lasers to obtain large peak output powers. For example, the saturation property allows a means of passively mode locking a CO_2 laser by simply inserting a slice of a suitable p-type semiconductor into the optical path of the cavity. The saturable absorber causes the laser to oscillate in a pulsed fashion since this mode of oscillation undergoes less loss than one in which the energy is spread more

uniformly [6-8]. Once the pumping begins, the largest of the intensity fluctuations in the optical resonator grows at a larger rate than smaller intensity peaks, since the smaller intensities see greater loss. That is, the loss is a minimum when the phases of the oscillating modes are locked and the energy distribution inside the resonator corresponds to a narrow traveling pulse with a period equal to the round trip transit time of the resonator. Experiments have demonstrated that a CO_2 laser with p-Ge as a saturable absorber can be used to generate passively mode-locked pulses of subnanosecond duration [9-11], where the pulse duration is limited by the gain linewidth of the laser. Considerably shorter pulses on the order of a few picoseconds should be possible by operating the laser at higher pressures [11]. At sufficiently high gas pressure where the gain linewidth is much greater than the rate of the recovery of the saturable absorber, the mode-locked pulses have a duration approximately equal to the recovery time of the saturable absorber (about 1 psec in p-germanium).

The saturable absorption characteristics of p-type semiconductors have also been used to achieve isolation of high power CO_2 oscillator-amplifier systems [4-5]. One of the most important problems facing the design of fusion-oriented CO_2 lasers is the provision for adequate interstage isolation. The isolation devices must prevent spontaneous lasing in the high gain amplifiers and suppress retrodirected signals which can arise from windows and targets as well as other laser systems in a multiple beam irradiation experiment. By inserting a slice of p-

germanium as an isolation device, low-level oscillations as well as reflections would be attenuated, while the material would be transparent to the high intensity pulses which are to be amplified. In addition, p-type semiconductors have some distinct advantages over gaseous saturable absorbers, such as a high damage threshold, integrability into a beam transport system, picosecond recovery time and a broadband performance under saturation conditions.

The nonlinear absorption has also been used to temporally compress laser pulses [6,12]. That is, for a pulse of Gaussian lineshape, the tails of the pulse see a high absorption coefficient while the peak of the pulse propagates relatively unattenuated, which leads to a pulse shortening effect. For many applications, particularly in inertial fusion experiments, a pulse width of specified duration is strongly desired and pulse compression is required to achieve these durations.

In order to analyze the saturation properties of p-type semiconductors, one must first understand the nature of the absorption process. The dominant absorption mechanism in p-Ge at room temperature has been shown to be direct intervalence-band transitions for light in the 2-25 μm region and hole concentrations greater than about 10^{14} cm^{-3} [13-15]. The observed character of the absorption spectrum in the 9-11 μm region is primarily determined by two factors: the shape of the valence band structure and the steady-state distribution of free holes.

The valence band structure for small k is determined by degenerate

$\underset{\sim}{k}\cdot\underset{\sim}{p}$ perturbation theory by a method developed by Kane [16] based on measured values of the cyclotron resonance parameters. In Figure 1, the valence band structure of germanium is shown for $\underset{\sim}{k}$ in the [100] direction. There exist three bands each of which are two-fold degenerate. The six bands correspond to states constructed from the atomic p functions of the individual atoms times the two spin functions, spin up and spin down. The heavy-(h) and light-(ℓ) hole bands are degenerate at k=0, and the split-off hole band (s) is separated at k=0 from the heavy- and light-hole bands by the spin-orbit interaction. Here, the spin-orbit interaction lowers the two $j = 1/2$ bands with respect to the four $j = 3/2$ bands. Figure 2 illustrates the nonparabolic and anisotropic nature of the bands for k in the [100], [111], [110] and [γ] direction. The [γ] direction is defined to be the direction in $\underset{\sim}{k}$-space which makes equal angles with the [100], [111] and [110] directions [16]. According to the band structure calculations given by Kane, for a given direction in $\underset{\sim}{k}$-space the heavy-hole band may be taken as parabolic, the light-hole band effective mass increases with energy, and the split-off hole band effective mass decreases with energy. These qualitative features also hold for the valence band structures of other semiconductors with the diamond or zincblende structure; however, the effective masses and spin-orbit splittings are different for the different materials. We now consider the absorption spectrum of p-Ge at room temperature conditions. For light with wavelength between about 5 and 25 μm, the dominant transi-

Figure 1. Valence band structure of germanium for small k in the [100] direction. Here, an increase in hole energy corresponds to going vertically downward.

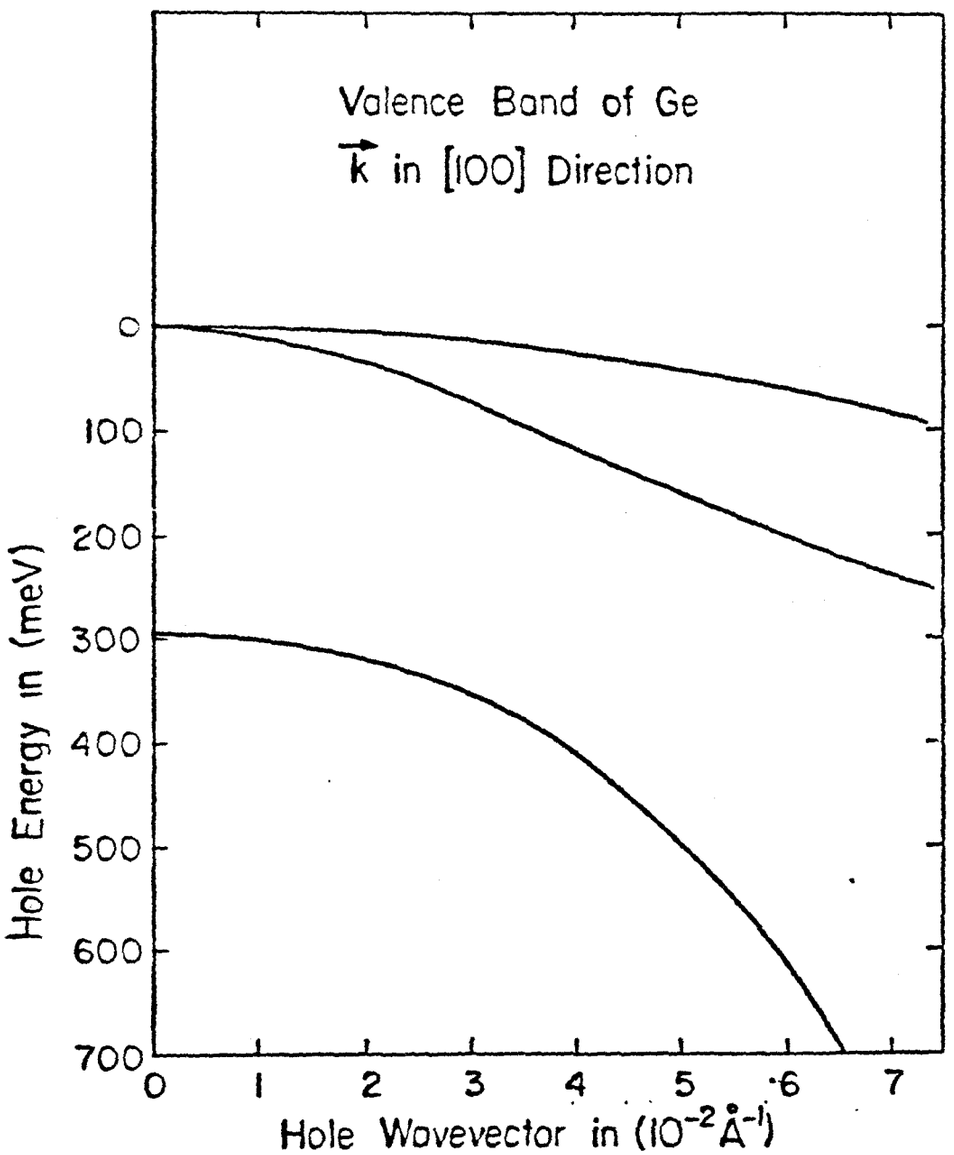
Valence Band of Ge
$\vec{k}$ in [100] Direction
Hole Energy in (meV)
0
100
200
300
400
500
600
700
0
1
2
3
4
5
6
7
Hole Wovevector in (10^{-2} Å^{-1})

Figure 2. Hole energy vs k^2 in germanium for k in the [100], [110], [111] and [γ] directions. The figure shows the anisotropy of the heavy- and light-hole bands. The [γ] direction is a direction which makes equal angles with the [100], [110] and [111] directions. Here the band structure graphs are inverted so that increasing hole energy corresponds to going vertically upward. The arrows indicate intervalence-band resonances for light with a wavelength of 10.6 μm. In these resonant processes, a hole in the heavy-hole band absorbs a photon and is excited to the light-hole band.

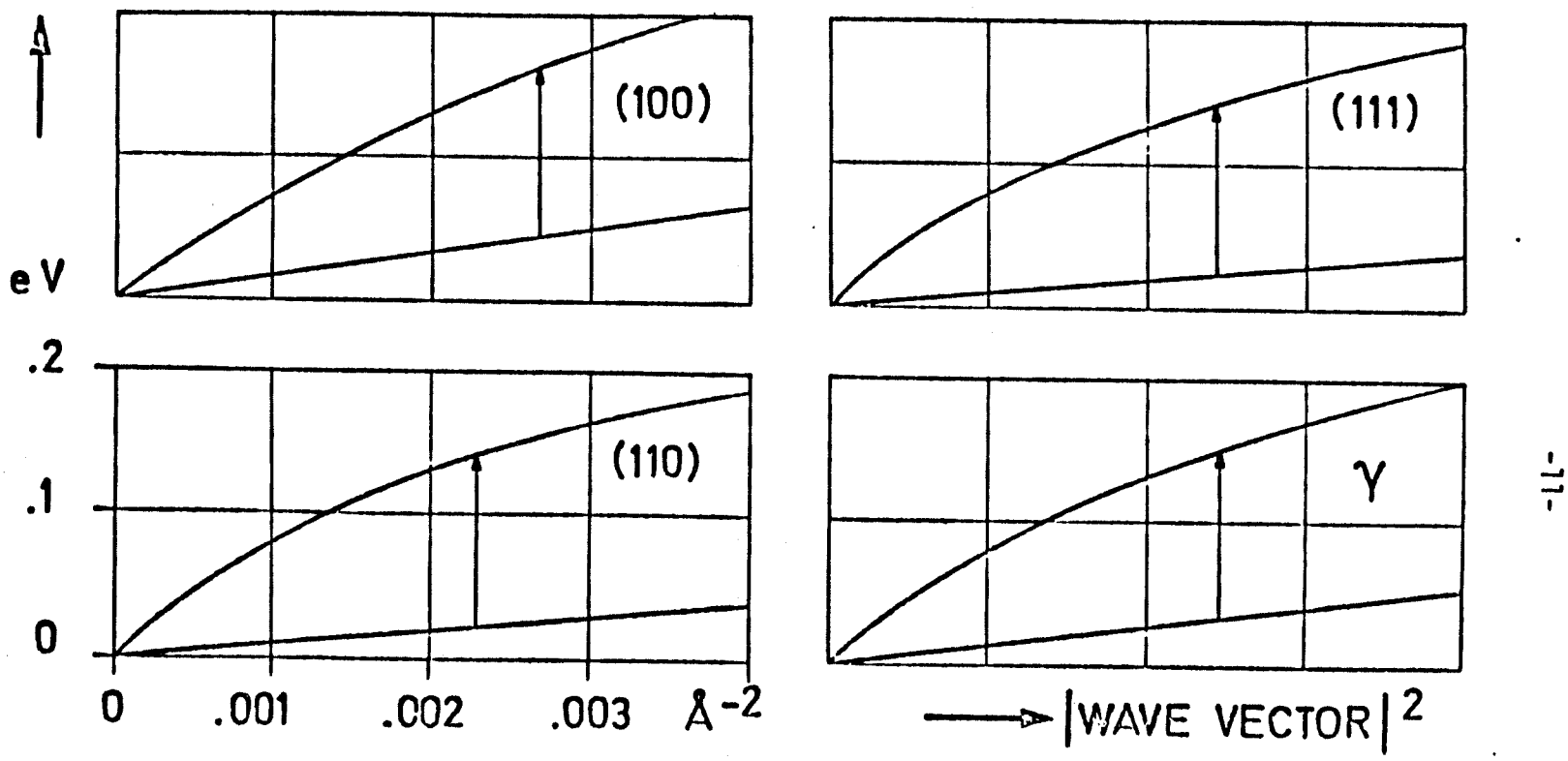
HOLE ENERGY
eV
.2
.1
0
(100)
(111)
(110)
γ
0
.001
.002
.003
Å-2
|WAVE VECTOR|2

tion occurs between the heavy- and light-hole bands; for wavelengths between about 4 and 5 μm, the dominant transition occurs between the light- and split-off hole bands; and for wavelengths about 2 and 4 μm, the dominant transition occurs between the heavy- and split-off hole bands. These three regions of absorption due to the three sets of valence bands are shown in Figure 3. For the 9-11 μm region, which corresponds to the CO_2 laser spectrum, the absorption cross section is about 6.0×10^{-16} cm^2, as explicitly shown in Figure 3. Similar intervalence-band absorption has been observed in several other p-type semiconductors as well [13-22]; however, the range of wavelengths which correspond to the three sets of intervalence-band transitions vary for the different materials.

Both energy and wavevector are conserved in the intervalence-band optical transition. Thus only holes in a narrow region of the heavy-hole band can directly participate in the absorption. For light with a wavelength of 10.6 μm, the resonant regions are shown by the arrows in Fig. (2) for $\underset{\sim}{k}$ in the [100] , [111] , [110] and [γ] directions. The variation in the magnitude of k^2 for which the resonance occurs is a consequence of the anisotropic nature of the band structure. Since the absorption coefficient is governed by the population of the pertinent initial hole states, the absorption becomes a nonlinear function for intensities sufficiently high that the distribution of hole states cannot maintain its equilibrium value. The absorption in the 9-11 μm region has been shown to saturate in p-Ge [2-5] and p-GaAs [2] due to this depletion of the initial hole states.

Figure 3. Absorption cross section of p-type germanium at room temperature. The lattice absorption independent of carrier concentration has been subtracted. The shaded region shows the 9-11 μm region. Experimental data were taken from Ref. (15).

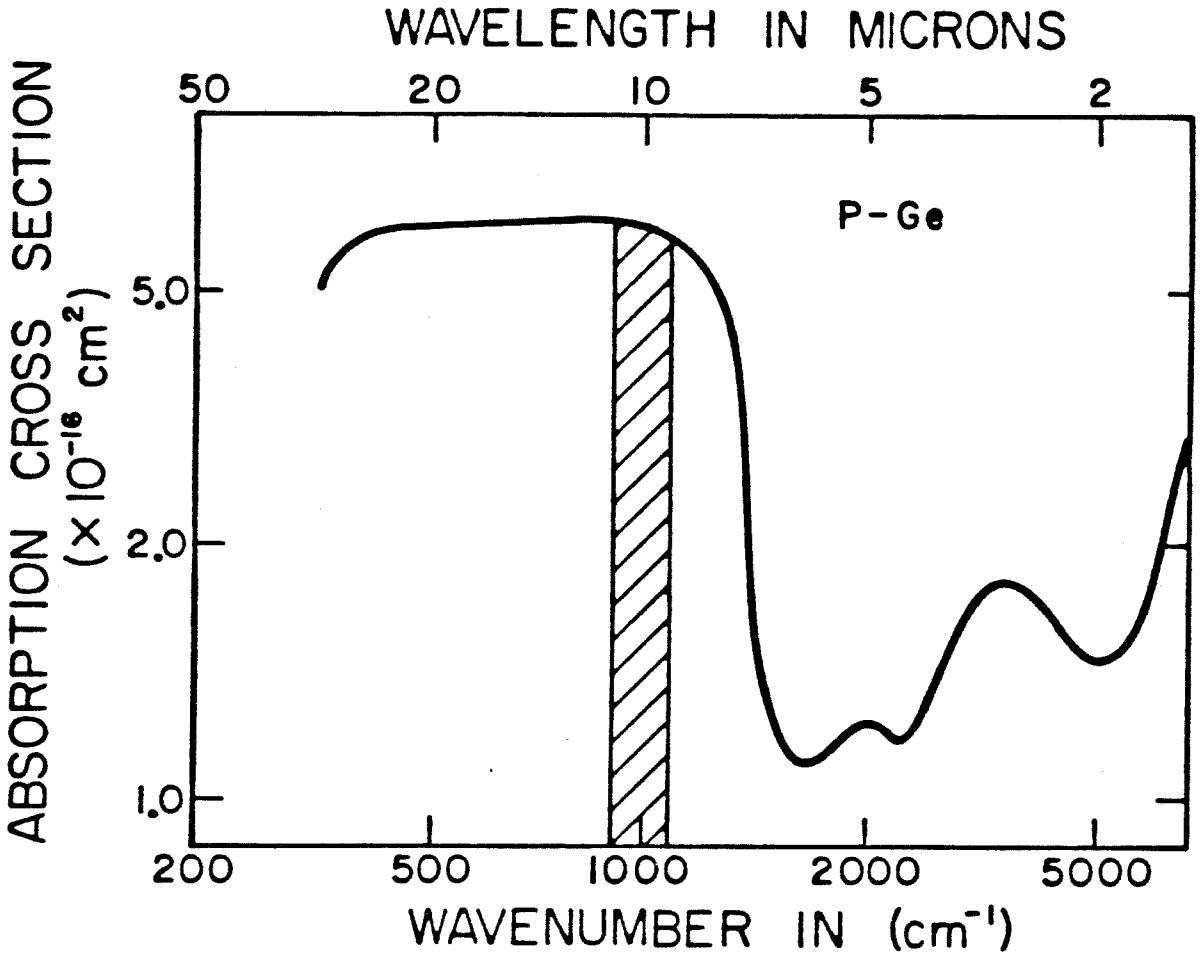
WAVELENGTH IN MICRONS
50
20
10
5
2
P-Ge
ABSORPTION CROSS SECTION
(X 10⁻¹⁶ cm²)
5.0
2.0
1.0
200
500
1000
2000
5000
WAVENUMBER IN (cm⁻¹)

Thus in order to calculate the intensity dependence of the absorption coefficient, we must first calculate the hole distribution in the heavy- and light-hole bands as a function of the light intensity. Here, we must include the interaction of the free-holes with the optical excitation and the dominant relaxation mechanisms. For hole concentrations and temperatures at which most saturable absorption measurements have been performed (room temperature, $N_h \lesssim 4 \times 10^{15} cm^{-3}$), phonon scattering is the dominant relaxation mechanism. Here, the scattering time due to lattice scattering is on a subpicosecond time scale for the hole states of interest. Phonon scattering was calculated on the basis of the deformable potential model, where the deformation parameters were taken to fit the temperature dependence of the measured mobility [23]. For more heavily doped material, the scattering of holes with ionized impurities and other free holes is included in the calculation.

Having calculated the distribution of hole states as a function of intensity, we relate the distribution to the absorption coefficient to determine the functional form for the reduction in the absorption coefficient with increasing intensity. The calculated intensity dependence of $\alpha(I)$ of p-Ge can be fit to high accuracy to the functional form of Eq. (2), and values of the saturation intensity are determined as a function of the photon energy and temperature. In Chapter 3, we examine the systematic dependences of the saturation characteristics for the various p-type semiconductors and find the

most important material parameters to be the average effective masses of the valence bands and the hole mobility.

Using this theory, we have determined the hole distribution as a function of the light intensity and frequency. This information allows an interpretation of several "pump-and-probe" experiments. The "pump-and-probe" approach is often used to measure the distribution function of optically pumped semiconductors. Here, one measures the transmission of a low-intensity light beam (probe) as a function of frequency in the presence of a high-intensity laser (pump) of fixed frequency. The probe pulse can be distinguished by using a different wavelength, direction, or polarization from the pump.

With a high intensity pump laser saturating the heavy- to light-hole band transition, the transmission of a low intensity probe resonant between the heavy- and split-off hole bands is altered. If the wavelength of the pump laser is fixed and the wavelength of the probe is tuned, there is a spectral region for the probe in which the two optical transitions are coupled due to their sharing of common initial states in the heavy-hole band. Thus the absorption coefficient of the probe depends on the intensity of the pump laser through the distribution function in the heavy-hole band. As the pump laser depletes the distribution in the resonant region of the heavy-hole band, we expect an enhancement in the transmission of the probe due to their sharing of common initial hole states. In Chapter

4, we examine the response of a probe resonant between the heavy- and split-off hole bands in p-Ge in the presence of a high-intensity pump at 10.6 μm resonant between the heavy- and light-hole bands. These features have been experimentally observed in p-Ge by Keilmann and Kuhl [24].

We also consider the case of a high intensity pump saturating the heavy- to light-hole band transition, and a weak tunable probe resonant between the heavy- and light-hole bands. For probe frequencies near the saturator frequency (within the homogeneous linewidth of the transition), the transmission of the probe beam is modified, analogous to the hole-burning effect in a low-pressure gas. Here, the measured values for the absorption coefficient of the probe vs photon energy of the probe yields information about the relaxation processes. The modulation of the probe transmission is due to the decrease in the initial hole states in the heavy-hole band due to saturation by the pump, and to an interference of the pump and probe in which the pump photons are frequency shifted in such a way as to match the probe beam's direction and frequency. In Chapter 5 values for the absorption coefficient of the probe are calculated and good agreement is found with experiment [25,26].

Since the absorption of light alters the distribution of free-holes, we expect a change in the sample conductivity upon illumination. The change depends on the density of free-holes and the intensity of the incident beam. Because the density of states in the heavy-hole

band is much greater than that in the light-hole band, the photoexcited holes primarily scatter into the high energy states in the heavy-hole band. Thus the dominant change in the distribution of hole states is an increase in the average energy of occupied states in this band. For temperatures and doping levels for which phonon scattering dominates the momentum relaxation, the conductivity decreases upon illumination because the rate of phonon scattering increases with increasing hole energy. For lower temperatures or higher doping levels where ionized impurity scattering dominates the momentum relaxation, the conductivity increases with illumination because ionized impurity scattering decreases with increasing hole energy. These photoconductive effects have been observed experimentally [27-32] and have been shown to influence the performance of p-Ge photon drag detectors [33-35]. In Chapter 6 we present a calculation of the photoconductive response of p-Ge upon illumination by 10.6 μm light as a function of doping level, temperature and light intensity.

II. OUTLINE OF THESIS

In Chapter 2, a theory is presented describing the laser-induced change in the dielectric constant of p-Ge resulting from the interaction with high-intensity infrared radiation. The imaginary part of the complex dielectric constant is related to the nonlinear absorption properties, and the real part is related to an intensity dependence in the index of refraction. These nonlinear properties in p-Ge are due to the

saturation of the heavy- to light-hole band transitions by the high intensity light. In order to calculate the intensity dependence of the complex dielectric constant, we first calculate the distribution of free-holes in the heavy- and light-hole bands as a function of the intensity of the light, allowing for the absorption by intervalence-band transitions and the hole relaxation by phonon, ionized impurity, and hole-hole scattering. Using the calculated values for the hole distribution, we relate the distribution to the absorption coefficient to determine the intensity dependence of the absorption coefficient. The intensity dependent absorption coefficient can be described to high accuracy by Eq. (2). Values of the saturation intensity are predicted as a function of the excitation wavelength and hole density and good agreement is found with the available experimental data with no adjustable parameters included in the theory.

Since the usefulness of p-Ge as a saturable absorber in CO_2 laser systems is determined by its saturation characteristics, it is of interest to be able to control the saturation behavior. We find

that the saturation behavior of p-Ge can be tuned by controlling the temperature of the sample due to the temperature dependence of the hole-phonon scattering rates. The saturation intensity is found to increase monotonically with increasing temperature due to the increase in the hole-phonon scattering rates, which allows the holes to re-route at a faster rate.

The distribution function is also related to the real part of the complex dielectric constant. Calculations of the nonlinear dispersive properties of p-Ge are performed at room temperature for light with a wavelength of 10.6 μm. The index of refraction is found to increase monotonically with increasing intensity due to the saturation of the heavy- to light-hole band transitions.

In Chapter 3, we examine the saturation characteristics of other p-type semiconductors to determine if other materials may be more promising for certain applications of saturable absorbers. For these materials the decrease in the absorption coefficient with increasing intensity is found to be closely approximated by an inhomogeneously broadened two-level model (Eq. 2), as well as for p-Ge. Values of the saturation intensity are predicted as a function of the excitation wavelength and temperature. In addition, a systematic analysis is presented for the dependence of the saturation intensity on the material parameters. The analysis of the saturation behavior of the different materials is divided into two categories: (1) materials with large spin-orbit splittings, (2) and materials with small spin-

orbit splittings. In the first case, only heavy- to light-hole band transitions are important and for the second case, the analysis is modified to also include heavy- to split-off hole band transitions and light- to split-off hole band transitions.

In Chapter 4, we present a theory to describe the enhanced transmission of a weak tunable probe laser with a wavelength near 3 μm in the presence of a high intensity saturating beam with a wavelength near 10 μm in p-Ge. The mechanism responsible for the increased transmission of the probe laser is the depletion of holes in the heavy-hole band by the 10 μm pump laser. Values of the absorption coefficient of the probe beam are predicted as a function of the intensity of the pump beam.

In Chapter 5, we consider the case of a high intensity pump in p-Ge which saturates the heavy- to light-hole band optical transition, and a weak tunable probe laser also resonant between the heavy- and light-hole bands. The transmission of the probe beam is altered due to the modification of the free-hole distribution function by the high-intensity pump laser. Values for the composite lineshape of the probe beam are predicted for a high-intensity beam of 10.6 μm and good agreement is found with experiment. Here, the values for the absorption coefficient of the probe as a function of the intensity of the pump yields information on the scattering processes and on the modification of the free-hole distribution by the pump laser.

We find that the sample conductivity in p-Ge is changed due to

the modification of the free-hole distribution by the absorption of CO_2 laser radiation. The change in the conductivity depends on the intensity of the excitation pulse and the free-hole density. This change in the sample conductivity allows an understanding of the response of p-Ge photon-drag detectors. In Chapter 6, the linear photoconductive response is predicted as a function of hole density and temperature for light with a wavelength of 10.6 μm. At higher light intensities, the effect of saturation of intervalence-band transitions is important, and the photoconductive response becomes a nonlinear function of the incident intensity. Values of the nonlinear photoconductive response are calculated as a function of hole density and excitation intensity for light with a wavelength of 10.6 μm and room temperature conditions.

III. SUMMARY OF MAIN RESULTS

Chapter 2

1. The distribution of free holes in the heavy- and light-hole bands is calculated as a function of the light intensity for p-Ge and light with a wavelength of 10.6 μm.
2. The nonlinear absorption of p-Ge in 9-11 μm region is found to be due to a depletion of hole states in the resonant region of the heavy-hole band. The absorption coefficient is found to decrease with intensity in a manner closely

approximated by an inhomogeneously broadened two-level model.

3. The saturation intensity is found to increase monotonically with increasing photon energy over the CO_2 laser spectrum.
4. The saturation intensity increases monotonically with increasing temperature for near room temperature conditions.
5. The saturation intensity is found to be independent of the hole concentration for hole densities less than about $3x10^{15}cm^{-3}$ and to increase montonically with increasing hole concentration for larger hole densities.
6. The saturation behavior is found to not vary significantly with the polarization of the CO_2 light.
7. The dispersive properties of p-Ge are also modified by the high intensity CO_2 laser radiation due to the saturation of the intervalence-band transitions.
8. The index of refraction is found to increase monotonically with increasing beam intensity. Values for the intensity dependence of the real part of the complex dielectric constant are given for unpolarized light, and light polarized along the [110] and [100] directions.

Chapter 3

1. Saturation of intervalence-band hole transitions is predicted for other materials as well as for p-Ge. The intensity dependence of the absorption coefficient is also found to be

fit to high accuracy by an inhomogeneously broadened two-level model.

2. The saturation intensities for the different p-type semiconductors are found to vary over about two orders of magnitude for the different materials. This variation is primarily due to the different hole mobilities and valence band structures for the different materials.
3. The saturation behavior for the different p-type semiconductors is predicted as a function of photon energy over the CO_2 laser spectrum and as a function of temperature for near room temperature conditions.
4. p-GaSb is predicted to saturate at lower light intensities than p-Ge and may be more important for the intended applications of saturable absorbers in the 9-11 μm region than p-Ge (which is the material most frequently examined experimentally).

Chapter 4

1. The transmission of weak tunable beam near 3 μm can be modulated by the presence of a high-intensity CO_2 beam near 10 μm. For this spectral region of the two beams, the direct intervalence-band transitions are coupled due to a sharing of common initial hole states in the heavy-hole band.
2. Values for absorption coefficient of the 3 μm probe are

predicted as a function of the intensity of the 10 μm pump.

3. This pump-and-probe method can be used to test band structure calculations for materials in which the cyclotron resonance parameters have not been accurately measured.

Chapter 5

1. The absorption of a weak tunable beam in the 9-11 μm region is found to be modified by the presence of a high-intensity beam at 10.6 μm. Values of the absorption coefficient of the probe beam are predicted as a function of the intensity of the pump beam.
2. The lineshape of the probe beam allows a means to examine the distribution of free-holes in the vicinity of the resonance of the pump beam.
3. A double-dip saturation spectrum is predicted for the probe which is not characteristic of a simple hole-burning model. In addition to the Lorentzian lineshape due to hole-burning, there exists another term in the probe absorption coefficient due to a coupling of the pump and probe beams, which allows pump photons to be scattered into the direction of the probe with the frequency of the probe and vice versa.
4. The composite lineshape of the probe beams in the presence of the high-intensity pump yields information on the scattering rates of the free holes.

Chapter 6

1. The conductivity of p-Ge is changed by light with a wavelength in the 8-25 μm region due to a modification of the free-hole distribution function.
2. The change in the conductivity allows an understanding of the response of photon-drag detectors. The linear photoconductive response is predicted for light with a wavelength of 10.6 μm as a function of the hole density at room temperature and as a function of temperature for fixed hole density.
3. The photoconductive response is also predicted for high light intensities where the effects of saturation of the intervalence-band transitions are important. This information allows an understanding of the nonlinear performance of p-Ge photon-drag detectors at high light intensities.

REFERENCES

1. See, for example, A. Yariv, Quantum Electronics, 2nd Ed. (Wiley, New York, N.Y., 1975), p. 327 ff.
   N. Bloembergen, Nonlinear Optics (Benjamin, Inc., New York, N.Y., 1965).
2. A. F. Gibson, C. A. Rosito, C. A. Raffo, and M. F. Kimmitt, Appl. Phys. Lett. 21, 356 (1972).
3. F. Keilmann, IEEE J. Quantum Electron. 12, 592 (1976).
4. C. R. Phipps, Jr. and S. J. Thomas, Opt. Lett. 1, 93 (1977).
5. R. L. Carlson, M. D. Montgomery, J. S. Ladish, and C. M. Lockhart, IEEE J. Quantum Electron. 13, 35D (1977).
6. E. M. Garmire and A. Yariv, IEEE J. Quantum Electron. QE-3, 222 (1967).
7. S. E. Schwarz and T. Y. Tan, Appl. Phys. Lett. 10, 4 (1967).
8. A. Yariv, Quantum Electronics, 2nd Ed. (Wiley, New York, N.Y. 1975), p. 277 ff.
9. B. J. Feldman and J. F. Figueria, Appl. Phys. Lett. 25, 301 (1974).
10. A. F. Gibson, M. F. Kimmitt, and B. Norris, Appl. Phys. Lett. 24, 306 (1974).
11. A. J. Alcock and A. C. Walker, Appl. Phys. Lett. 25, 299 (1974).
12. C. R. Phipps, Sr., S. J. Thomas, J. Ladish, J. J. Czuchlewski, and J. F. Figueira, IEEE J. Quantum Electron. 13, 360 (1977).
13. H. B. Briggs and R. C. Fletcher, Phys. Rev. 91, 1342 (1953).
14. A. H. Kahn, Phys. Rev. 97, 1647 (1955).

15. W. Kaiser, R. J. Collins, and H. Y. Fan, Phys. Rev. 91, 1342 (1953).

16. E. O. Kane, J. Phys. Chem. Solids 1, 82 (1956).

17. R. Braunstein and E. O. Kane, J. Phys. Chem. Solids 23, 1423 (1962).

18. J. W. Hodby, Proc. Phys. Soc. (London) 82, 324 (1963).

19. R. Braunstein, J. Phys. Chem. Solids 8, 280 (1959).

20. G. W. Gobeli and H. Y. Fan, Phys. Rev. 119, 613 (1960).

21. W. M. Becker, A. K. Ramdas, and H. Y. Fan, J. Appl. Phys. 32, 2094 (1961).

22. F. Matossi and F. Stern, Phys. Rev. 111, 472 (1958).

23. D. M. Brown and R. Bray, Phys. Rev. 127, 1593 (1962).

24. F. Keilmann and J. Kuhl, IEEE J. Quantum Electron. 14, 203 (1978).

25. F. Keilmann, Appl. Phys. 14, 29 (1977).

26. P. J. Bishop, A. F. Gibson, and M. F. Kimmitt, J. Phys. D9, L101 (1976).

27. A. M. Danishevskii, A. A. Kastal'skii, B. S. Ryvkin, S. M. Ryvkin, and I. D. Yaroshetskii, JETP Lett. 10, 302 (1969).

28. P. M. Valov, I. D. Yaroshetskii, and I. N. Yassievich, JETP Lett. 20, 204 (1974).

29. A. F. Gibson and P. N. D. Maggs, J. Phys. D.: Appl. Phys. 7, 292 (1974).

30. V. G. Agafonov, P. M. Valov, B. S. Ryvkin, and I. D. Yaroshetskii, Sov. Phys. Semicond. 9, 571 (1975).

31. H. Hattori, O. Fujitani, and M. Umeno, J. Phys. Soc. Japan 36, 485 (1974).

32. T. Grave and F. Keilmann, Z. Physik B32, 347 (1979).

33. A. F. Gibson, M. F. Kimmitt, P. N. D. Maggs, and B. Norris, J. Appl. Phys. 46, 1413 (1975).

34. P. J. Bishop, A. F. Gibson, and M. F. Kimmitt, IEEE J. of Quantum Electron. QE-9, 1007 (1973).

35. T. Kamibayashi, S. Yonemochi, and T. Miyakawa, Appl. Phys. Lett. 22, 119 (1973).

CHAPTER 2

I. INTRODUCTION

There exists considerable theoretical and experimental interest in nonlinear optical phenomena in semiconductors, particularly with those effects which are connected with the dependence of the complex dielectric constant on the intensity of the light. In this chapter we present a theory describing changes in the complex dielectric constant in p-type germanium due to the absorption of light with wavelength in the 9-11 μm region, which corresponds to the CO_2 laser spectrum.

In p-type germanium, direct free-hole transitions between the heavy- and light-hole bands are primarily responsible for the absorption of light at these wavelengths. At high light intensities, absorption due to these intervalence-band transitions has been found to saturate in p-Ge. [1-4] This saturation property allows a means of passively mode-locking a CO_2 laser by inserting a slice of p-Ge into the optical path of the cavity. Experiments have demonstrated that a CO_2 laser with p-Ge used as a saturable absorber can generate passively mode-locked pulses of subnanosecond duration [5-7]. In this chapter we present a theory of the saturation behavior of heavy-hole band to light-hole band transitions in p-type semiconductors at high light intensities. Detailed numerical results are presented for the intensity dependence of the absorption coefficient of p-Ge (the material in which the effect has been most frequently observed experimentally).

The theory is also used to describe the laser-induced change in the real part of the complex dielectric constant in p-Ge that results from saturation of the intervalence-band transitions.

In previous work, saturable absorption in p-type semiconductors has been described by modeling the valence bands as an ensemble of two-level systems whose level populations approach one another at high light intensities [2-4,8-9]. This two-level model predicts that the dependence of the absorption coefficient as a function of intensity is given by

$$\alpha(I,\omega) = \frac{\alpha_o(\omega)}{\sqrt{1 + I/I_s(\omega)}} \quad , \tag{1}$$

where $\alpha_o(\omega)$ is the absorption coefficient at low intensity, and $I_s(\omega)$ is the saturation intensity. The behavior described in Eq. (1) was found to be reasonably well satisfied experimentally, and values of $I_s(\omega)$ were determined [2-4]. However, attempts to calculate $I_s(\omega)$ as a function of photon energy using the two-level model and a multistep cascade relaxation [9] gave results that disagree with experiment [2]. A theoretical discussion of saturable absorption in p-type Ge based on a spherical parabolic band model has also been presented [10]. However, the results of that discussion are qualitatively different than that of Eq. (1) and are in disagreement with experiment.

In this chapter, we present a theoretical analysis of the saturable absorption by considering the initial and final hole states in the optical transition to form a continuum with the valence band structure determined by degenerate k • p perturbation theory[11-12]. This is the first time the saturable absorption properties have been discussed in a model which realistically accounts for the anisotropic and nonparabolic valence band. Our calculated results are in close agreement with Eq. (1), and the values of $I_s(\omega)$ deduced from the calculation are in good agreement with experiment. There are no adjustable parameters in the theory. We also determine the dependence of I_s on temperature and on the direction of the light polarization for polarization along certain symmetry directions. We present detailed results for p-Ge; however, the theory should be applicable to other semiconductors with the zincblende crystal structure as well.

The theory is also applied to describe a laser-induced change in the real part of the complex dielectric constant in p-type semiconductors at 10.6 μm due to the saturation of direct heavy- to light-hole band transitions. We find that the presence of a saturable beam alters the optical isotropy of p-Ge, where the changes in the dispersive properties depend on the intensity and polarization of the beam. A nonlinearity of this form manifests itself in a dependence of the index of refraction on the light intensity. This causes beam self-focusing (de-focusing) in regions where a beam "sees" a higher (lower) index of refraction at the center of the Gaussian beam profile

than at the tails. We report explicit values for the intensity dependence of the index of refraction for light at 10.6 μm and room temperature conditions.

II. THEORETICAL APPROACH

In semiconductors with the diamond or zincblende crystal structure, the valence band maximum occurs at the zone center. There are six bands (3 sets of 2-fold degenerate bands) near the valence maximum. Four of the bands are degenerate at k=0 and the other two bands (degenerate) are split-off to lower energy by the spin-orbit interaction. Away from the zone center, the bands degenerate at k=0 split into two 2-fold degenerate pairs, the heavy-hole and light-hole bands. In p-type semiconductors free holes occur primarily in the heavy-hole band.

Light with a wavelength near 10 μm can induce transitions between the heavy-hole band and the light-hole band in p-type semiconductors. In Ge (and several other materials), the spin-orbit splitting is greater than the photon energy for light with $\lambda \sim 10$ μm; thus transitions between the heavy-hole band and split-off band are not induced by light with this wavelength in these materials. The heavy- to light-hole transitions are the dominant absorption mechanism in p-Ge [13-16]. For example, at $\lambda = 10.6$ μm and room temperature the inter-valence-band absorption cross section in Ge is $6 \cdot 10^{-16} cm^2$ [15]. The

intravalence-band absorption cross section, estimated from Drude-Zener theory is about $10^{-17}cm^2$, and the absorption coefficient from multiphonon absorption is about $0.013\ cm^{-1}$ [17]. Thus, for hole concentrations in the $10^{15}cm^{-3}$ range intervalence-band absorption is 1 to 2 orders of magnitude greater than the other absorption processes.

Both energy and wavevector are conserved in the intervalence-band optical transitions. Thus, only holes in a narrow region of the heavy-hole band can directly participate in the absorption, and the absorption coefficient is governed by the population of these hole states. The optical transitions tend to deplete the population of the pertinent heavy-hole states. At low intensities, the population of the heavy-hole states involved in the optical transition is maintained close to the equilibrium value by various scattering processes. However, as the intensity becomes large, scattering cannot maintain the equilibrium population of the pertinent heavy-hole states, and they become depleted. As a result the absorption saturates at high intensity. To determine the saturation characteristics of the intervalence-band transitions, it is necessary to set up rate equations for the hole distribution function in the heavy- and light-hole bands.

For the hole concentrations and temperatures at which most saturable absorption measurements have been performed (room temperature and $N_h \lesssim 4x10^{15}cm^{-3}$), hole-phonon scattering is the dominant relaxation

mechanism. We first consider only hole-phonon scattering. (Later in this chapter, hole-impurity and hole-hole scattering are included so the theory can be applied to more heavily doped material). The system can then be described by the Hamiltonian

$$H = H_o + V + \gamma(t) \quad , \tag{2a}$$

where

$$H_o = H_\varepsilon + H_{ph} \quad , \tag{2b}$$

and

$$\gamma(t) = \frac{e}{mc} \underset{\sim}{A}(t) \cdot \underset{\sim}{P} \quad . \tag{2c}$$

Here H_ε describes the free holes, H_{ph} describes the phonon system, V is the hole-phonon interaction, and $\gamma(t)$ describes the interaction of the holes with the electromagnetic field. The electromagnetic field is described by the vector potential $\underset{\sim}{A}$; in the Coulomb gauge $\underset{\sim}{A}$ satisfies the wave equation

$$\nabla^2 \underset{\sim}{A} - \frac{\varepsilon_\infty}{c^2} \frac{\partial^2 \underset{\sim}{A}}{\partial t^2} = - \frac{4\pi}{c} \underset{\sim}{J} \tag{3}$$

where $\underset{\sim}{J}$ is the current density induced by the intervalence-band transitions

$$\underset{\sim}{J} = N_h \frac{e}{m} \mathrm{Tr}\,[\sigma \underset{\sim}{P'}] \quad , \tag{4}$$

Here N_h is the hole density, σ is the one-hole density matrix, and $\underset{\sim}{P'}$ is the off-diagonal (including only intervalence-band matrix elements) part of the hole momentum operator.

In Appendix A, we examine the time evolution of the density matrix σ. We find that σ is diagonal in wavevector and define

$$\langle b\underset{\sim}{k}|\sigma|b'\underset{\sim}{k}\rangle = \sigma_{bb'}(\underset{\sim}{k}) \quad , \tag{5}$$

where $\underset{\sim}{k}$ labels the wavevector, and b is the band index. The band index diagonal matrix elements of σ are determined by

$$\frac{d}{dt}\sigma_{bb}(\underset{\sim}{k},t) = -\frac{i}{\hbar}[\gamma(\underset{\sim}{k},t),\ \sigma(\underset{\sim}{k},t)]_{bb}$$

$$- \sum_{c\underset{\sim}{k}'} [R_{b\underset{\sim}{k}\to c\underset{\sim}{k}'}\ \sigma_{bb}(\underset{\sim}{k},t) - R_{c\underset{\sim}{k}'\to b\underset{\sim}{k}}\ \sigma_{cc}(\underset{\sim}{k}',t)] \quad , \tag{6a}$$

and the off-diagonal elements are determined by

$$\frac{d}{dt}\sigma_{bb'}(\underset{\sim}{k},t) = -\frac{i}{\hbar}[H_\varepsilon(\underset{\sim}{k}) + \gamma(\underset{\sim}{k},t),\ \sigma(\underset{\sim}{k},t)]_{bb'}$$

$$- \frac{1}{T_2(\underset{\sim}{k})}\sigma_{bb'}(\underset{\sim}{k},t) \quad , \tag{6b}$$

where

$$\frac{2}{T_2(\underset{\sim}{k})} = \sum_{c\underset{\sim}{k}'} \left[R_{h\underset{\sim}{k}\to c\underset{\sim}{k}'} + R_{\ell\underset{\sim}{k}\to c\underset{\sim}{k}'} \right] \quad . \tag{6c}$$

Here $R_{a\underset{\sim}{k}\to b\underset{\sim}{k}'}$ is the rate at which a hole in band a with wavevector $\underset{\sim}{k}$ is scattered into a state in band b with wavevector $\underset{\sim}{k}'$, $h(\ell)$ refers to the heavy- (light-) hole band, and $\gamma(\underset{\sim}{k})$ and $H_\varepsilon(\underset{\sim}{k})$ are defined analogous to Eq. (5).

Using the equations for the time evolution of σ, the current density owing to intervalence-band transitions is found (details in Appendix B) to be determined by

$$\frac{d^2}{dt^2}\underset{\sim}{J}(\underset{\sim}{k}) + \frac{2}{T_2(\underset{\sim}{k})}\frac{d}{dt}\underset{\sim}{J}(\underset{\sim}{k}) + \Omega^2(\underset{\sim}{k})\,\underset{\sim}{J}(\underset{\sim}{k})$$

$$= N_h \frac{e^2}{\hbar^2 m^2 c} \sum_{bc} f_b(\underset{\sim}{k})\,(E_c(\underset{\sim}{k}) - E_b(\underset{\sim}{k}))$$

$$\times\, (\underset{\sim}{A}\cdot\underset{\sim}{P}_{bc}(\underset{\sim}{k})\,\underset{\sim}{P}_{cb}(\underset{\sim}{k}) + \underset{\sim}{P}_{bc}\,\underset{\sim}{A}\cdot\underset{\sim}{P}_{cb}(\underset{\sim}{k})) \quad . \tag{7}$$

Here $E_b(\underset{\sim}{k})$ is the energy of a hole in band b with wavevector $\underset{\sim}{k}$, $\hbar\Omega(\underset{\sim}{k})$ is $(E_h(\underset{\sim}{k}) - E_\ell(\underset{\sim}{k}))$, we rename the diagonal elements of the hole density matrix $f_b(\underset{\sim}{k})$, and $\underset{\sim}{J}(\underset{\sim}{k})$ is the part of $\underset{\sim}{J}$ which includes only those terms in the trace with wavevector $\underset{\sim}{k}$ $(\sum_{\underset{\sim}{k}} \underset{\sim}{J}(\underset{\sim}{k}) = \underset{\sim}{J})$.

Eq. (7) is the basic equation describing the absorption and dispersion for the medium. We find that the current density acts as a

harmonic oscillator of frequency Ω driven by the electric field through a coupling coefficient proportional to the population difference for a given state with wavevector $\underset{\sim}{k}$. One important conclusion is that the ability of the vector potential to drive the current density is decreased as the probability of occupation of states in the heavy- and light-hole bands become more nearly equal. This constitutes the physical basis for the observed nonlinear absorption. Another important note is that in the absence of the applied interaction, the current density will be damped because of the internal dephasing of the individual dipoles through the interaction with the lattice, given by the constant T_2.

Assuming both $\underset{\sim}{A}$ and $\underset{\sim}{J}(\underset{\sim}{k})$ oscillate in time with angular frequency ω, we have

$$\underset{\sim}{J} = \frac{N_h e^2}{m^2 c\hbar} \sum_{\underset{\sim}{k}} (f_h(\underset{\sim}{k}) - f_\ell(\underset{\sim}{k})) \sum_{bc} \frac{\underset{\sim}{A}\cdot\underset{\sim}{P}_{bc}\underset{\sim}{P}_{cb} + \underset{\sim}{A}\cdot\underset{\sim}{P}_{cb}\underset{\sim}{P}_{bc}}{(\Omega^2(\underset{\sim}{k})-\omega^2) - i\,2\omega/T_2(\underset{\sim}{k})} \underset{\sim}{\Omega}(k) \,. \qquad (8)$$

Due to the peaked behavior of Eq. (8), the primary contribution to the current density is from states with an energy difference $\hbar\Omega(\underset{\sim}{k})$ which does not differ greatly from the photon energy $\hbar\omega$; thus, we write

$$\underset{\sim}{J} = \frac{N_h e^2}{2m^2 c\hbar} \Sigma (f_h(\underset{\sim}{k}) - f_\ell(\underset{\sim}{k})) \sum_{bc} \frac{\underset{\sim}{A}\cdot\underset{\sim}{P}_{bc}\underset{\sim}{P}_{cb} + \underset{\sim}{A}\cdot\underset{\sim}{P}_{cb}\underset{\sim}{P}_{bc}}{(\underset{\sim}{\Omega}(k) - \omega) - i/T_2(\underset{\sim}{k})} \,. \qquad (9)$$

Using Eq. (9), we write the susceptibility as a second-rank tensor given by

$$\underset{\approx}{\chi}(\omega,I) = \frac{N_h e^2}{2m^2\omega^2\hbar} \sum_{\underset{\sim}{k}} (f_h(\underset{\sim}{k}) - f_\ell(\underset{\sim}{k})) \sum_{bc} \frac{P_{\underset{\sim}{cb}}P_{\underset{\sim}{bc}} + P_{\underset{\sim}{bc}}P_{\underset{\sim}{cb}}}{(\Omega(\underset{\sim}{k}) - \omega) - i/T_2(\underset{\sim}{k})} . \quad (10)$$

The imaginary part of $\underset{\approx}{\chi}$ describes the changes in the absorptive properties of the semiconductor, and the real part of $\underset{\approx}{\chi}$ describes the changes in the dispersive properties. We define

$$\underset{\approx}{\chi} = \underset{\approx}{\chi}' + i\underset{\approx}{\chi}'' , \quad (11)$$

where χ' and χ'' are assumed to be real. Thus, we find

$$\underset{\approx}{\chi}'(\omega,I) = \frac{N_h e^2}{2m^2\omega^2\hbar} \Sigma(f_h(\underset{\sim}{k}) - f_\ell(\underset{\sim}{k})) \left(\sum_{bc} P_{\underset{\sim}{cb}}P_{\underset{\sim}{bc}} + c.c.\right) \frac{\Omega(\underset{\sim}{k}) - \omega}{(\Omega(\underset{\sim}{k}) - \omega)^2 + (1/T_2(\underset{\sim}{k}))^2} , \quad (12)$$

and

$$\underset{\approx}{\chi}''(\omega,I) = \frac{N_h e^2}{2m^2\omega^2\hbar} \Sigma(f_h(\underset{\sim}{k}) - f_\ell(\underset{\sim}{k})) \left(\sum_{bc} P_{\underset{\sim}{cb}}P_{\underset{\sim}{bc}} + c.c.\right) \frac{1/T_2(\underset{\sim}{k})}{(\Omega(\underset{\sim}{k}) - \omega)^2 + (1/T_2(\underset{\sim}{k}))^2} . \quad (13)$$

Here, the intensity dependence in the susceptibility is contained in

the distribution functions $f_h(\underset{\sim}{k})$ and $f_\ell(\underset{\sim}{k})$,

For a plane wave vector potential,

$$\underset{\sim}{A} = \underset{\sim}{A}_o \, e^{i(\underset{\sim}{K}\cdot\underset{\sim}{r} - \omega t)} \quad , \tag{14}$$

the complex propagation constant is given by [18-19]

$$K^2 = \frac{\varepsilon_\infty \omega}{c^2} \left[1 + \frac{4\pi}{\varepsilon_\infty \omega^2} \frac{N_h e^2}{3m^2 h} \right.$$

$$\left. \times \sum_{\underset{\sim}{k}} (f_h(\underset{\sim}{k}) - f_\ell(\underset{\sim}{k})) |P_{h\ell}(\underset{\sim}{k})|^2 \frac{(\Omega(\underset{\sim}{k})-\omega)+i/T_2(\underset{\sim}{k})}{(\Omega(\underset{\sim}{k})-\omega)^2+(1/T_2(\underset{\sim}{k}))^2} \right] , \tag{15}$$

where the squared momentum matrix element $|P_{h\ell}(\underset{\sim}{k})|^2$ is to be summed over the two degenerate states in both the heavy- and light-hole bands. Assuming that the second term in the square root in Eq. (15) is small compared to unity, the absorption coefficient is given by

$$\alpha(I,\omega) = 2\,\mathrm{Im}(K)$$

$$= \frac{4\pi^2}{\sqrt{\varepsilon_\infty}\, m^2\, \omega c} \frac{N_h e^2}{3}$$

$$\times \sum_{k} (f_h(\underset{\sim}{k}) - f_\ell(\underset{\sim}{k})) |P_{h\ell}(\underset{\sim}{k})|^2 \frac{1/(\hbar\pi\, T_2(\underset{\sim}{k}))}{(\Omega(\underset{\sim}{k})-\omega)^2+(1/T_2(\underset{\sim}{k}))^2} \quad . \tag{16}$$

Eq. (16) is the usual expression for the absorption coefficient except that a normalized Lorentzian replaces the usual energy conserving delta function. The absorption coefficient is a function of the light intensity because the interaction of the holes with the laser radiation alters the distribution in the heavy- and light-hole bands. We want to solve this equation as a function of intensity to determine the saturation characteristics.

In order to determine the absorption coefficient, we must calculate the distribution functions for free holes in the heavy- and light-hole bands. In the semiconductors of interest, the scattering rate for free holes occurs on a subpicosecond time scale. For a saturating laser operating with nanosecond pulse widths (the typical experimental situation), transient effects are damped out. Thus, we are interested in the steady state values of the distribution functions. Using Eqs. (6) the steady state distribution functions are found to solve (details in Appendix C) the rate equations

$$\beta(\underset{\sim}{k})\ (f_h(\underset{\sim}{k}) - f_\ell(\underset{\sim}{k})) = -\sum_{\underset{\sim}{ck}'} \left[R_{\underset{\sim}{hk}\to\underset{\sim}{ck}'} f_h(\underset{\sim}{k}) - R_{\underset{\sim}{ck}'\to\underset{\sim}{hk}}\ f_c(\underset{\sim}{k}')\right] , \quad (17a)$$

$$\beta(\underset{\sim}{k})\ (f_h(\underset{\sim}{k}) - f_\ell(\underset{\sim}{k})) = \sum_{\underset{\sim}{ck}'} \left[R_{\underset{\sim}{\ell k}\to\underset{\sim}{ck}'}\ f_\ell(\underset{\sim}{k}) - R_{\underset{\sim}{ck}'\to\underset{\sim}{\ell k}}\ f_c(\underset{\sim}{k}')\right] , \quad (17b)$$

where

$$\beta(\underset{\sim}{k}) = \frac{2\pi^2}{\sqrt{\varepsilon_\infty}\, m^2\, \omega c} \frac{e^2 I}{3\hbar\omega} |P_{\underset{\sim}{h\ell}}(\underset{\sim}{k})|^2 \frac{1/(\pi\hbar\, T_2(\underset{\sim}{k}))}{(\Omega(\underset{\sim}{k}) - \omega)^2 + (1/T_2(\underset{\sim}{k}))^2} \quad . \quad (17c)$$

These equations state that the rate of optical excitation out of (into) a given state is equal to the net rate of scattering into (out of) the state when steady state is attained. The lefthand sides of Eqs. (17a) and (17b) give the net rate of optical excitation out of a state with wavevector $\underset{\sim}{k}$ in the heavy-hole band into a state with wavevector $\underset{\sim}{k}$ in the light-hole band. The righthand side of Eq. (17a) gives the net rate of scattering into the state with wavevector $\underset{\sim}{k}$ in the heavy-hole band, and the righthand side of Eq. (17b) gives the net rate of scattering out of the state with wavevector $\underset{\sim}{k}$ in the light-hole band.

To calculate the absorption coefficient as a function of intensity, we first solve Eq. (17) for the distribution functions and then integrate Eq. (16). In solving Eq. (17), it is convenient to introduce the auxiliary functions defined by

$$\frac{1}{T_h(\underset{\sim}{k})} = \sum_{c\underset{\sim}{k}'} R_{h\underset{\sim}{k}\to c\underset{\sim}{k}'} \quad , \tag{18a}$$

$$\frac{1}{T_\ell(\underset{\sim}{k})} = \sum_{c\underset{\sim}{k}'} R_{\ell\underset{\sim}{k}\to c\underset{\sim}{k}'} \quad , \tag{18b}$$

$$F(\underset{\sim}{k}) = \sum_{c\underset{\sim}{k}'} R_{c\underset{\sim}{k}'\to h\underset{\sim}{k}}(f_c(\underset{\sim}{k}') - f_c^e(\underset{\sim}{k}')) \quad , \tag{18c}$$

and

$$G(\underset{\sim}{k}) = \sum_{c\underset{\sim}{k}'} R_{c\underset{\sim}{k}'\to \ell\underset{\sim}{k}}(f_c(\underset{\sim}{k}') - f_c^e(\underset{\sim}{k}')) \quad , \tag{18d}$$

where $f_c^e(\underset{\sim}{k})$ is the equilibrium value for the distribution function. The function $F(\underset{\sim}{k})$ is the difference in the feeding rate of free holes from the equilibrium feeding rate for the state with wavevector $\underset{\sim}{k}$ in the heavy-hole band. The function $G(\underset{\sim}{k})$ is analogously defined for the light-hole band. (Scattering into the light-hole band is small because of the small density of light-hole states. Thus the function $G(\underset{\sim}{k})$ is less important than $F(\underset{\sim}{k})$). In terms of the auxiliary functions, the distribution functions can be written as

$$f_h(\underset{\sim}{k}) = f_h^e(\underset{\sim}{k}) - \frac{\beta(\underset{\sim}{k})\, T_h(\underset{\sim}{k})\, (f_h^e(\underset{\sim}{k}) - f_\ell^e(\underset{\sim}{k}))}{1 + \beta(\underset{\sim}{k})\, (T_h(\underset{\sim}{k}) + T_\ell(\underset{\sim}{k}))}$$

$$+ \frac{F(\underset{\sim}{k})\, T_h(\underset{\sim}{k}) + \beta(\underset{\sim}{k})\, T_h(\underset{\sim}{k})\, T_\ell(\underset{\sim}{k})\, (F(\underset{\sim}{k}) + G(\underset{\sim}{k}))}{1 + \beta(\underset{\sim}{k})\, (T_h(\underset{\sim}{k}) + T_\ell(\underset{\sim}{k}))}, \qquad (19a)$$

and

$$f_\ell(\underset{\sim}{k}) = f_\ell^e(\underset{\sim}{k}) + \frac{\beta(\underset{\sim}{k})\, T_\ell(\underset{\sim}{k})\, (f_h^e(\underset{\sim}{k}) - f_\ell^e(\underset{\sim}{k}))}{1 + \beta(\underset{\sim}{k})\, (T_h(\underset{\sim}{k}) + T_\ell(\underset{\sim}{k}))}$$

$$+ \frac{G(\underset{\sim}{k})\, T_\ell(\underset{\sim}{k}) + \beta(\underset{\sim}{k})\, T_h(\underset{\sim}{k})\, T_\ell(\underset{\sim}{k})\, (F(\underset{\sim}{k}) + G(\underset{\sim}{k}))}{1 + \beta(\underset{\sim}{k})\, (T_h(\underset{\sim}{k}) + T_\ell(\underset{\sim}{k}))}. \qquad (19b)$$

The difference in occupation probabilities which appears in the expression for the absorption coefficient is given by

$$f_h(\underset{\sim}{k}) - f_\ell(\underset{\sim}{k}) = \frac{(f_h^e(\underset{\sim}{k}) - f_\ell^e(\underset{\sim}{k}))}{1 + \beta(\underset{\sim}{k})\ (T_h(\underset{\sim}{k}) + T_\ell(\underset{\sim}{k}))}$$

$$+ \frac{T_h(\underset{\sim}{k})\ F(\underset{\sim}{k}) - T_\ell(\underset{\sim}{k})\ G(\underset{\sim}{k})}{1 + \beta(\underset{\sim}{k})\ \ (T_h(\underset{\sim}{k}) + T_\ell(\underset{\sim}{k}))} \quad . \tag{20}$$

The first term in Eq. (20) gives the population difference that would occur for the states at $\underset{\sim}{k}$ if the populations of the states that feed those at $\underset{\sim}{k}$ were given by their equilibrium values. The second term in Eq. (17) accounts for the change in the population of the states that feed those at $\underset{\sim}{k}$. For those values of $\underset{\sim}{k}$ which are important in the integral in Eq. (16), the first term in Eq. (20) is found to be significantly greater than the second.

Using Eq. (17) and the definition of the auxiliary functions, one can write equations which determine $F(\underset{\sim}{k})$ and $G(\underset{\sim}{k})$. If there is no angular dependence in the phonon scattering matrix elements which go into the scattering rates, the functions $F(\underset{\sim}{k})$ and $G(\underset{\sim}{k})$ depend on $E_h(\underset{\sim}{k})$ and $E_\ell(\underset{\sim}{k})$, respectively. Thus, one-dimensional (rather than three-dimensional) equations must be solved to determine these functions. Our treatment of these functions is included in Appendix D.

III. CALCULATION OF VALENCE BAND STRUCTURE, MOMENTUM MATRIX ELEMENTS AND HOLE SCATTERING RATES

The free hole energies are determined by degenerate $\underset{\sim}{k}\cdot\underset{\sim}{p}$ perturbation theory by a method developed by Kane [11] based on measured values of the cyclotron resonance parameters. We present a short description of the method used to determine the one-hole energies for hole states with small wavevector k.

In a periodic lattice, the one-hole wave functions can be written as Bloch functions

$$\psi_{\underset{\sim}{k}} = e^{i\underset{\sim}{k}\cdot\underset{\sim}{r}} u_{\underset{\sim}{k}}(\underset{\sim}{r}) \tag{21}$$

where $u_{\underset{\sim}{k}}(\underset{\sim}{r})$ is cell periodic. The Schroedinger equation can then be written as

$$[(p^2/2m) + V + \frac{\hbar}{m}(\underset{\sim}{k}\cdot\underset{\sim}{p})]\, u_{\underset{\sim}{k}}(\underset{\sim}{r}) = [E_{\underset{\sim}{k}} - \frac{\hbar^2 k^2}{2m}]\, u_{\underset{\sim}{k}}(\underset{\sim}{r}) \tag{22}$$

The term $(\frac{\hbar}{m}\,\underset{\sim}{k}\cdot\underset{\sim}{p})$ is treated as a perturbation for determining $u_{\underset{\sim}{k}}$ and $E_{\underset{\sim}{k}}$ in the vicinity of k=0 in terms of the complete set of cell periodic wave functions and energy eigenvalues at k=0, which are assumed known. It is convenient to define $E'_{\underset{\sim}{k}}$ as

$$E'_{\underset{\sim}{k}} = E_{\underset{\sim}{k}} - \frac{\hbar^2 k^2}{2m} \quad . \tag{23}$$

In a lattice where the inversion is a symmetry operation (as for diamond structure), the first-order matrix elements of the $\underset{\sim}{k}\cdot\underset{\sim}{p}$ perturbation vanish when the zero-order wave functions are taken at $k = 0$, and second-order perturbation theory must be used to describe the energy surfaces.

Following Ref. (20), we take three degenerate states at k=0 to transform as $\varepsilon_1^+ \sim yz$, $\varepsilon_2^+ \sim zx$ and $\varepsilon_3^+ \sim xy$. We now construct by perturbation theory three functions $u^i_{\underset{\sim}{k}}(\underset{\sim}{r})\, e^{i\underset{\sim}{k}\cdot\underset{\sim}{r}}$ which are eigenfunctions of the crystal translation operator, but which are not eigenfunctions to first-order in $\underset{\sim}{k}$ of the Hamiltonian. However, linear combinations of $u^i_{\underset{\sim}{k}}$ diagonalize the Hamilton to first-order in $\underset{\sim}{k}$; thus,

$$u^i_{\underset{\sim}{k}}(\underset{\sim}{r}) = \varepsilon^+_i + \frac{\hbar}{m}\,\underset{\sim}{k}\cdot\sum_{\ell\alpha j}\frac{|\ell\alpha j><\ell\alpha j|p|i+>}{E_o - E_{\ell\alpha}} \quad , \tag{24}$$

where $\ell\alpha j$ denotes the state j belonging to the representation α in the band ℓ, and E_ℓ is the energy of the ℓ^{th} band at $\underset{\sim}{k}=0$. Neglecting spin, the perturbation matrix to be diagonalized is of the form [20]

$$\begin{bmatrix} Lk_x^2+M(k_y^2+k_z^2) & Nk_xk_y & Nk_xk_z \\ Nk_xk_y & Lk_y^2+M(k_x^2+k_z^2) & Nk_yk_z \\ Nk_xk_z & Nk_yk_z & Lk_z^2+M(k_x^2+k_y^2) \end{bmatrix} = 0 \quad . \tag{25}$$

Here, symmetry arguments have been used to replace the sums over momentum matrix elements by the three constant L, M, and N. The quantities L, M, and N can be determined from cyclotron resonance

measurements,

The effects of spin-orbit coupling are most easily considered by regarding the spin-orbit interaction H_{so} as a perturbation. The perturbation is written in the following form as an operator on the cell periodic function $u_{\underset{\sim}{k}}$.

$$H_{so} = \frac{\hbar}{4m^2c^2}[\nabla V \times \underset{\sim}{p}]\cdot\underset{\sim}{\sigma} \quad . \tag{26}$$

The coupling is k independent and analogous to an atomic spin-orbit splitting term. When spin-orbit effects are considered we take the basis functions to be $|\varepsilon_1^+\uparrow\rangle$, $|\varepsilon_2^+\uparrow\rangle$, $|\varepsilon_3^+\uparrow\rangle$, $|\varepsilon_1^+\downarrow\rangle$, $|\varepsilon_2^+\downarrow\rangle$ and $|\varepsilon_3^+\downarrow\rangle$, where $\uparrow$ and $\downarrow$ designate the spin functions, spin-up and spin-down. The $\underset{\sim}{k}\cdot\underset{\sim}{p}$ Hamiltonian including spin then becomes a 6x6 matrix as written in Ref. (11), where the eigenvalues can be determined numerically.

We calculate the valence band structure of germanium in this manner using the measured cyclotron resonance parameters of Ref. (21). A spin-orbit splitting of 0.295 eV [22] is used in the calculation. The results for the one-hole energies for $\underset{\sim}{k}$ in the [100], [110], [111] and [γ] directions are shown in Fig. (2) of Chapter 1. We note that there exist six bands (three sets of two-fold degenerate bands). For a given direction in $\underset{\sim}{k}$-space, the heavy-hole band may be taken as parabolic, the light-hole band effective mass increases with increasing energy and the split-off hole band effective mass decreases with increasing energy. The constant energy surfaces are warped and depend on the particular direction in $\underset{\sim}{k}$-space.

The optical absorption coefficient for transitions between the heavy- and light-hole bands is proportional to the matrix elements $|\langle u_h|\underset{\sim}{A}\cdot\underset{\sim}{p}|u_\ell\rangle|^2$, where $\underset{\sim}{A}$ is the vector potential of the light inducing the transitions, and u_h (u_ℓ) is the cell periodic wave function for the heavy- (light-) hole band. At k=0, parity is a good quantum number in a cubic crystal. The $\underset{\sim}{k}\cdot\underset{\sim}{p}$ perturbation brings in a first-order correction to the wave function of parity opposite to the k=0 parity of the band. The operator $\underset{\sim}{A}\cdot\underset{\sim}{p}$ then has a matrix element between bands of like parity which is proportional to k. The periodic part of the wave function correct to first order in the perturbation is given by

$$u = u_{oi} + \sum_J \left(\frac{\hbar}{m}\right) \frac{\langle u_{oJ}|\underset{\sim}{k}\cdot\underset{\sim}{p}|u_{oi}\rangle}{E_i^o - E_J^o}\, u_{oJ} \quad . \tag{27}$$

The $\underset{\sim}{A}\cdot\underset{\sim}{p}$ matrix elements between bands h and ℓ is

$$\langle u_h|\underset{\sim}{A}\cdot\underset{\sim}{p}|u_\ell\rangle = \frac{\hbar}{m} \sum_J \frac{\langle u_{oh}|\underset{\sim}{k}\cdot\underset{\sim}{p}|u_{oJ}\rangle\langle u_{oJ}|\underset{\sim}{A}\cdot\underset{\sim}{p}|u_{o\ell}\rangle + \langle u_{oJ}|\underset{\sim}{k}\cdot\underset{\sim}{p}|u_{o\ell}\rangle\langle u_{oh}|\underset{\sim}{A}\cdot\underset{\sim}{p}|u_{oJ}\rangle}{E_i^o - E_J^o} \tag{28}$$

The righthand side of Eq. (28) is identical in form to the second order $\underset{\sim}{k}\cdot\underset{\sim}{p}$ energy. The $\underset{\sim}{A}\cdot\underset{\sim}{p}$ matrix elements can be conveniently obtained by using the $\underset{\sim}{k}\cdot\underset{\sim}{p}$ part of the Hamiltonian matrix (without a spin-orbit splitting) and substituting $(k_\ell A_m + A_\ell k_m)$ for $k_\ell k_m$ [11]. The resulting matrix is then transformed by the unitary matrix which diagonalizes the Hamiltonian. The $\underset{\sim}{A}\cdot\underset{\sim}{p}$ matrix elements are independent of the direction of $\underset{\sim}{A}$ if we average the equivalent cubic directions.

In order to calculate the distribution of free holes as a function of intensity, it is necessary to know the hole scattering rates, in addition to the hole energies and momentum matrix elements. We consider the region of temperature and impurity densities for which hole-phonon is the dominant scattering mechanism. (This condition is relaxed in a later section to also include the effect of hole-impurity and hole-hole scattering). Optical phonon scattering is the dominant energy relaxation mechanism. The optical phonon spectrum is relatively flat for small k with an average energy of 0.037 eV. For the small k region in which we are interested, the acoustic phonon energy is quite small, and we neglect it. Although acoustic phonon scattering does not contribute significantly to energy relaxation, it can change the wavevector of the hole. The valence bands of Ge are rather anisotropic and an acoustic phonon scattering event can take a hole from a region in which $\beta(k)$ is small to one in which it is large. Thus, although acoustic phonon scattering is less important than optical phonon scattering in determining the distribution functions, it is not negligible because of the anisotropy of the valence bands. We take the scattering rates to be given by

$$R_{\underset{\sim}{a}\underset{\sim}{k}\to\underset{\sim}{b}\underset{\sim}{k}'} = \frac{2\pi}{\hbar}|M_{op}^{+}|^2\,\delta(E_a(\underset{\sim}{k}) - E_b(\underset{\sim}{k}') + \hbar\omega_o)$$

$$+ \frac{2\pi}{\hbar}|M_{op}^{-}|^2\,\delta(E_a(\underset{\sim}{k}) - E_b(\underset{\sim}{k}') - \hbar\omega_o) \qquad (29)$$

$$+ \frac{2\pi}{\hbar}|M_{ac}|^2\,\delta(E_a(\underset{\sim}{k}) - E_b(\underset{\sim}{k}))\quad .$$

Here $|M_{op}^{+}|^2$ is the squared matrix element for optical phonon emission, $|M_{op}^{-}|^2$ is the squared matrix element for optical phonon absorption, and $|M_{ac}|^2$ is the squared acoustic phonon scattering matrix element (summed over both absorption and emission processes).

We consider the case of deformation potential scattering. The central idea of the deformation potential scattering is that the matrix element is approximately equal to that obtained by replacing the perturbation energy by the shift δE_v of the band edge energy that would be produced by a homogeneous strain of magnitude equal to the local strain at $\underset{\sim}{r}$ induced by the mode $\underset{\sim}{q}$.

For spherical energy surfaces and acoustic mode scattering, the shift of the band edge is given by

$$\delta E_v = E_{ac} (e_{xx} + e_{yy} + e_{zz}) \equiv E_{ac}\Delta \quad , \tag{30}$$

where the e_{ii} are the diagonal components of the strain tensor, their sum being equal to the dilatation Δ, and E_{ac} is the shift of the band edge per unit dilatation. One obtains after some calculation that only longitudinal lattice waves scatter the holes with the matrix element given by [23]

$$|M_{ac}|^2 = \frac{E_{ac}^2 k_B T}{2V\rho u_\ell^2} \quad . \tag{31}$$

Here, T is the temperature, V is the sample volume, ρ is the material density, and u_ℓ is the longitudinal sound velocity.

For nonpolar crystals (as Ge) and spherical energy surfaces, the hole-optical phonon scattering can also be described by a deformation potential approach. In this case, the optical strain is proportional to the displacement of the sublattice containing one type of atom with respect to the sublattice containing the other, where the displacement is induced by the optical mode. Integration over the electron coordinates and lattice oscillator coordinates gives [23]

$$|M_{op}^{+}|^2 = \frac{E_{op}^2 \hbar\omega_o}{2V\rho u_\ell^2} \left[N_q + 1\right] , \tag{32a}$$

and

$$|M_{op}^{-}|^2 = \frac{E_{op}^2 \hbar\omega_o}{2V\rho u_\ell^2} N_q , \tag{32b}$$

where E_{op} is the deformation potential for optical phonon scattering, $\hbar\omega_o$ is the zero-center optical phonon energy, and N_q is the optical phonon Bose factor defined by

$$N_q = \frac{1}{\exp\left(\frac{\hbar\omega_o}{k_B T}\right) - 1} , \tag{33}$$

Following Ref. (23), we have neglected angular dependence in the phonon scattering matrix element and taken the scattering rates to be the same for the heavy- and light-hole bands. The numerical value for

the constants appearing in the squared matrix elements were taken from the mobility fits of Ref. (24), where E_{ac} was taken to be 3.5 eV and E_{op} to be 6.8 eV. The scattering times $T_2(\underset{\sim}{k})$, $T_h(\underset{\sim}{k})$ and $T_\ell(\underset{\sim}{k})$ are computed from Eqs. (6c) and (18a,b) using these scattering rates. Optical phonon scattering (primarily emission) dominates in the results for $T_2(\underset{\sim}{k})$ and $T_\ell(\underset{\sim}{k})$ for the states of interest. For states in the resonant region of the heavy-hole band, optical phonon emission is typically not possible and acoustic phonon scattering makes a significant contribution to $T_h(\underset{\sim}{k})$.

IV. CALCULATION OF THE HOLE DISTRIBUTION

We calculate the distribution of holes in $\underset{\sim}{k}$-space allowing the holes to interact with the laser excitation and the phonon system. The calculation of the hole distribution for states in the resonant region can be simplified as discussed in the following section. To describe the hole states outside of the resonant region, we must numerically compute the auxiliary functions $F(\underset{\sim}{k})$ and $G(\underset{\sim}{k})$ as discussed in Appendix D.

a) First Approximation for $(f_h(\underset{\sim}{k}) - f_\ell(\underset{\sim}{k}))$

As a first approximation for the population difference $(f_h(\underset{\sim}{k})-f_\ell(\underset{\sim}{k}))$, we neglect the auxiliary functions $F(\underset{\sim}{k})$ and $G(\underset{\sim}{k})$ and include only the first term in Eq. (20). This approximation is equivalent to assuming that the rate at which free holes are scattered into the states involved in the optical transition is given by the equilibrium value. For optical

phonon scattering, the energy of the initial hole state in the scattering event differs from that of the final hole by the optical phonon energy. As a result, hole states that can scatter into a resonant optical transition region by optical phonon scattering are, for the most part, themselves out of the resonant region. Thus, the population of these states is not directly depleted by the optical transitions. The population of these states is indirectly depleted by the optical transition because there is a decrease in the feeding rate of these states owing to the decrease in population of hole states in the resonant region. However, this decreased feeding from the resonant region is partially compensated for by an increased feeding from the re-routing of optically excited holes. For acoustical phonon scattering, the energy of the initial-hole state in the scattering event is essentially the same as that of the final hole state. As a result, hole states that can scatter into a resonant optical transition region by acoustic phonon scattering are, for the most part, in the resonant region themselves. Thus, the population of these states is directly depleted by the optical transitions. Including only the first term in Eq. (20) therefore overestimates the importance of acoustic phonon scattering. At this level of approximation, it is better to ignore acoustic phonon scattering. We will see that this first approximation for $(f_h(\underset{\sim}{k}) - f_\ell(\underset{\sim}{k}))$ ignoring acoustic phonon scattering produces results close to that of our more complete calculation.

Using only the first term in Eq. (20) to determine the population difference, the absorption coefficient becomes

$$\alpha^1(I,\omega) = \frac{4\pi^2}{\sqrt{\epsilon_\infty}\, m^2\, \omega c}\, \frac{N_h e^2}{3} \sum_{\underset{\sim}{k}} (f_h^e(\underset{\sim}{k}) - f_\ell^e(\underset{\sim}{k}))\, |P_{h\ell}(\underset{\sim}{k})|^2$$

$$\times \frac{1/(\hbar\pi\, T_2(\underset{\sim}{k}))}{(\Omega(\underset{\sim}{k})-\omega)^2 + \left(\frac{1}{T_2(\underset{\sim}{k})}\right)^2 \left[1 + I/\ell(\underset{\sim}{k})\right]}\,, \tag{34}$$

where

$$\ell(\underset{\sim}{k}) = \frac{3\hbar^2 c\, \sqrt{\epsilon_\infty}\, m^2\, \omega^2}{(T_h(\underset{\sim}{k}) + T_\ell(\underset{\sim}{k}))\, T_2(\underset{\sim}{k})\, 2\pi\, e^2 |P_{h\ell}(\underset{\sim}{k})|^2}\,. \tag{35}$$

Transforming to an integration over surfaces of constant $\Omega(\underset{\sim}{k})$, and assuming that the power-broadened Lorentzian is sharply peaked, Eq. (35) can be written as

$$\alpha^1(I,\omega) = \frac{4\pi^2}{\sqrt{\epsilon_\infty}\, m^2\, \omega c}\, \frac{N_h e^2}{3\hbar} \left(\frac{1}{2\pi}\right)^3 \tag{36}$$

$$\int_{\Omega(\underset{\sim}{k})=\omega} \frac{ds}{|\nabla_{\underset{\sim}{k}} \Omega(\underset{\sim}{k})|}\, \frac{|P_{h\ell}(\underset{\sim}{k})|^2\, (f_h^e(\underset{\sim}{k}) - f_\ell^e(\underset{\sim}{k}))}{\sqrt{1 + I/\ell(\underset{\sim}{k})}}\,.$$

Here the integral is over a surface of constant $\Omega(\underset{\sim}{k})$. Integrating Eq. (36) numerically, we find that the absorption coefficient satisfies Eq. (1) to high accuracy. Indeed, if $\ell(\underset{\sim}{k})$ were independent of $\underset{\sim}{k}$ over

the region of the surface integral, Eq. (36) would reduce to Eq. (1) exactly.

b) Higher-order Approximation for $(f_h(\underset{\sim}{k}) - f_\ell(\underset{\sim}{k}))$

The auxiliary functions $F(\underset{\sim}{k})$ and $G(\underset{\sim}{k})$ are computed numerically as discussed in Appendix D. The distribution function computed from these auxiliary functions for $\underset{\sim}{k}$ in the [111] and [100] directions together with their equilibrium values are shown in Fig. (1). The dominant dip in the heavy-hole distribution function and corresponding peak in the light-hole distribution function is due to direct optical transitions. Additional dips in the heavy-hole distribution function occur because of the discrete energy of the optical phonons. The increase in the heavy-hole distribution compared to the equilibrium value at large values of k is due to scattering of the photoexcited holes in the light-hole band into the heavy-hole band.

Figure 1. Calculated hole distribution functions in p-Ge as a function of k^2 for $\underset{\sim}{k}$ in the [111] and [100] directions. The calculations were performed for λ = 10.6 μm, T = 300°K and I = 30 MW/cm^2. The equilibrium distribution functions are shown for comparison. N_c is the effective density of states.

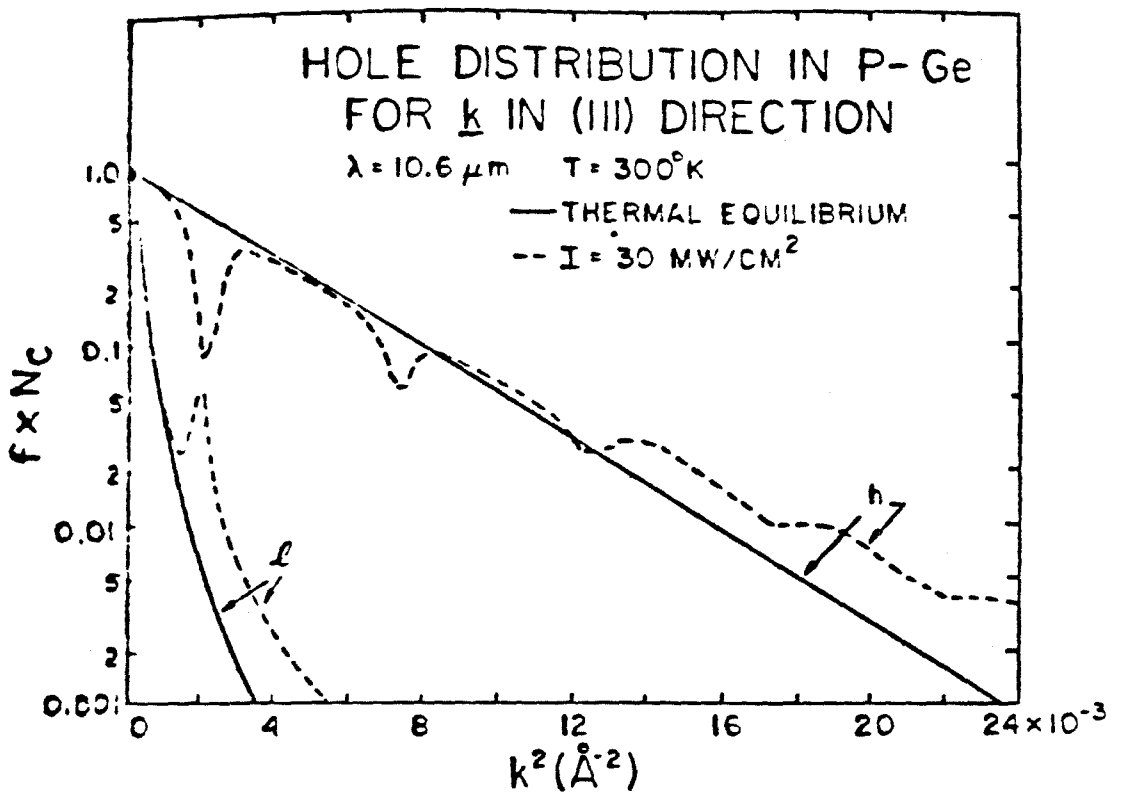
HOLE DISTRIBUTION IN P-Ge
FOR k IN (111) DIRECTION
λ = 10.6 μm T = 300°K
—THERMAL EQUILIBRIUM
-- I = 30 MW/CM²
f x Nc
1.0
5
2
0.1
5
2
0.01
5
2
0.001
h
ℓ
0
4
8
12
16
20
24×10⁻³
k² (Å⁻²)

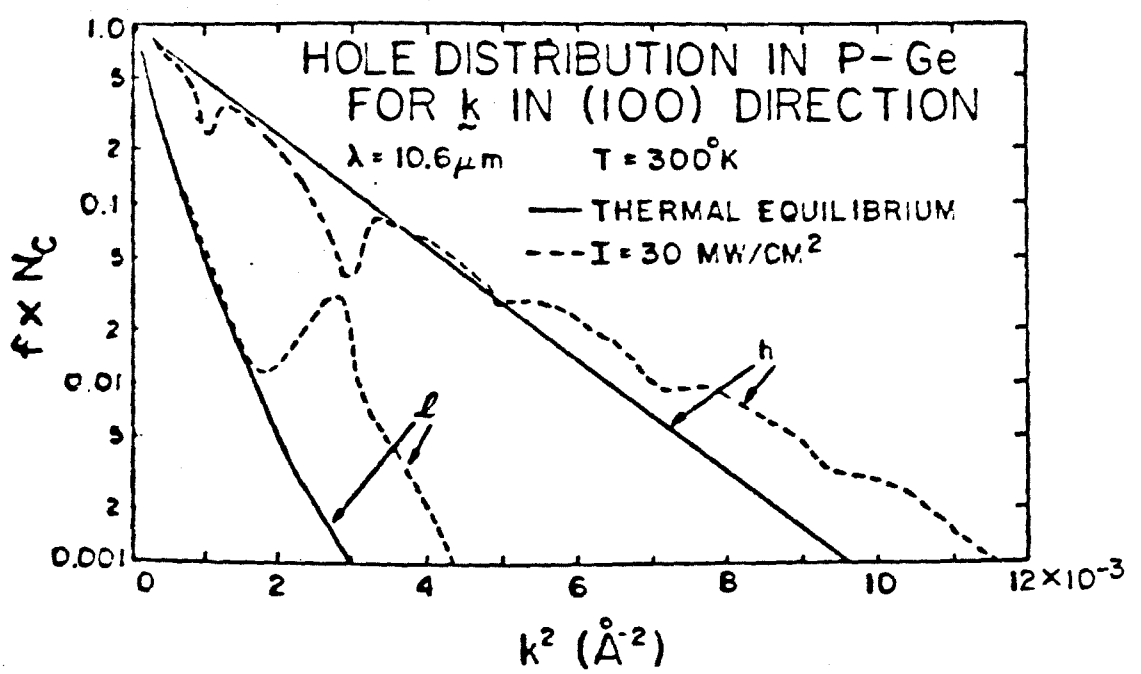
HOLE DISTRIBUTION IN P-Ge
FOR k IN (100) DIRECTION
λ = 10.6μm T = 300°K
— THERMAL EQUILIBRIUM
---I = 30 MW/CM²
f x Nc
1.0
5
2
0.1
5
2
0.01
5
2
0.001
h
ℓ
0
2
4
6
8
10
12×10⁻³
k² (Å⁻²)

V. INTENSITY DEPENDENCE OF THE ABSORPTION PROPERTIES OF p-Ge

The absorption coefficient is calculated numerically. The calculated result for $\lambda = 10.6\ \mu m$ and $T = 295^{\circ}K$ is compared with the expression in Eq. (1) in Fig. (2). The value of I_s used in Eq. (1) was determined by fitting the calculated result for $\alpha(I,\omega)$. The numerical results could be fit to an accuracy of about 5% for intensities less than 25 times I_s. (This is the range of intensities which has been most frequently explored experimentally.) If only the first term in Eq. (20) is retained, the calculated $\alpha(I,\omega)$ has almost exactly the form of Eq. (1). The second term in Eq. (20) is smaller than the first and leads to the small deviations seen in Fig. (2).

Measurements of the saturable absorption in p-type Ge have been interpreted in terms of the inhomogeneously broadened two-level model which produces Eq. (1), and the values of $I_s(\omega)$ have been reported. In Fig. (3), we compare measured values of $I_s(\omega)$ at room temperature as a function of photon energy with our theoretical values. The theoretical values of $I_s(\omega)$ are determined by fitting the expression in Eq. (1) to the calculated results for $\alpha(I,\omega)$ for intensities between zero and 100 MW/cm^2. In the range of photon energies considered, $I_s(\omega)$ was found to increase monotonically with photon energy. There is good agreement between theory and experiment. There are no adjustable parameters in the theory.

Figure 2. Calculated absorption coefficient normalized to its low intensity value as a function of intensity for p-Ge. The calculations were performed for λ = 10.6 μm and T = 295°K. The inhomogeneously broadened two-level model result with I_s = 4.1 MW/cm^2 is also shown.

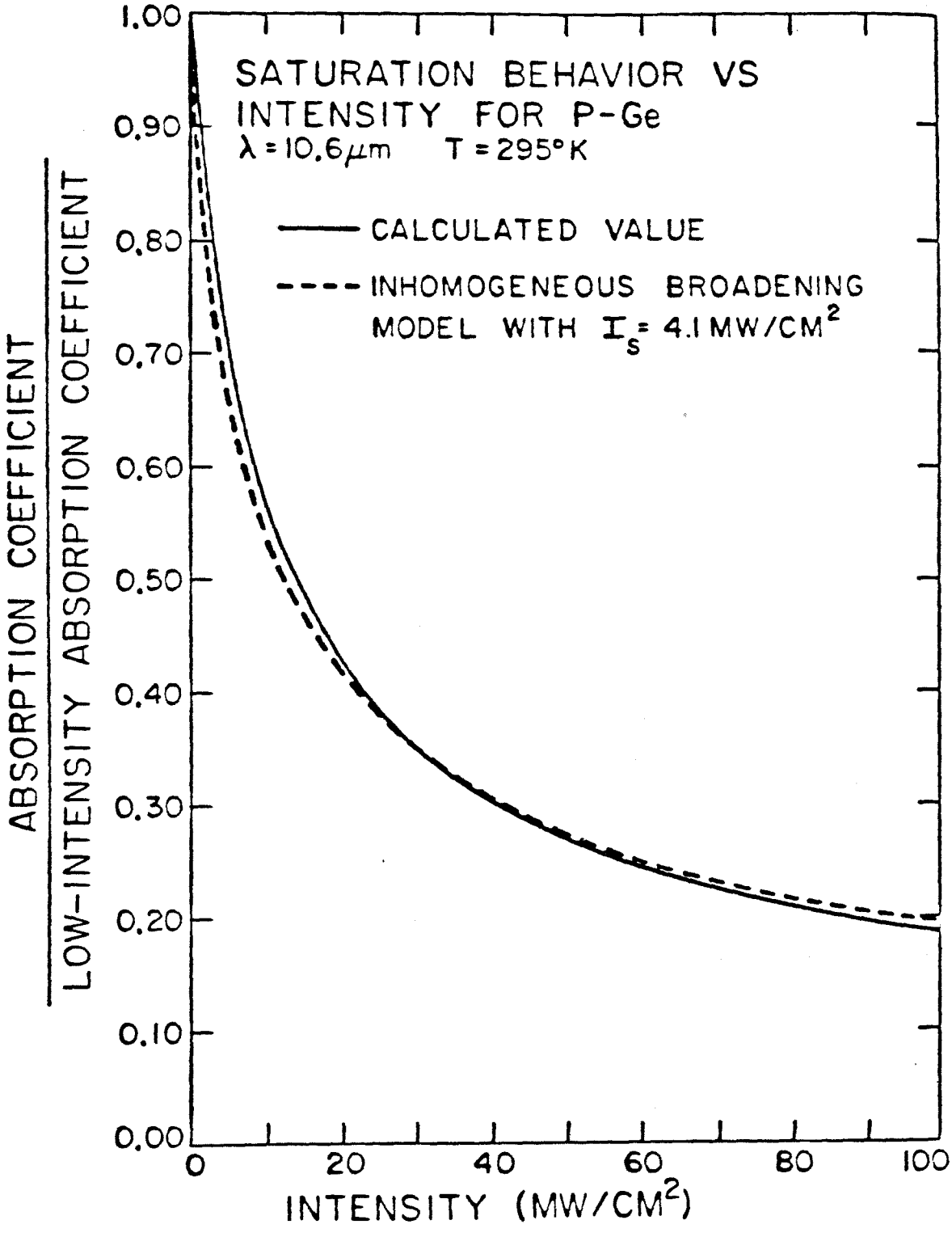
SATURATION BEHAVIOR VS
INTENSITY FOR P-Ge
λ = 10.6μm T = 295°K
CALCULATED VALUE
INHOMOGENEOUS BROADENING
MODEL WITH I_s = 4.1 MW/CM^2
ABSORPTION COEFFICIENT
LOW-INTENSITY ABSORPTION COEFFICIENT
1.00
0.90
0.80
0.70
0.60
0.50
0.40
0.30
0.20
0.10
0.00
0
20
40
60
80
100
INTENSITY (MW/CM^2)

Figure 3. Calculated saturation intensity as a function of photon energy for p-Ge at 295^{o}K. The experimental results are from Refs. (2), (3) and (4). Error bars are only given in Ref. (2).

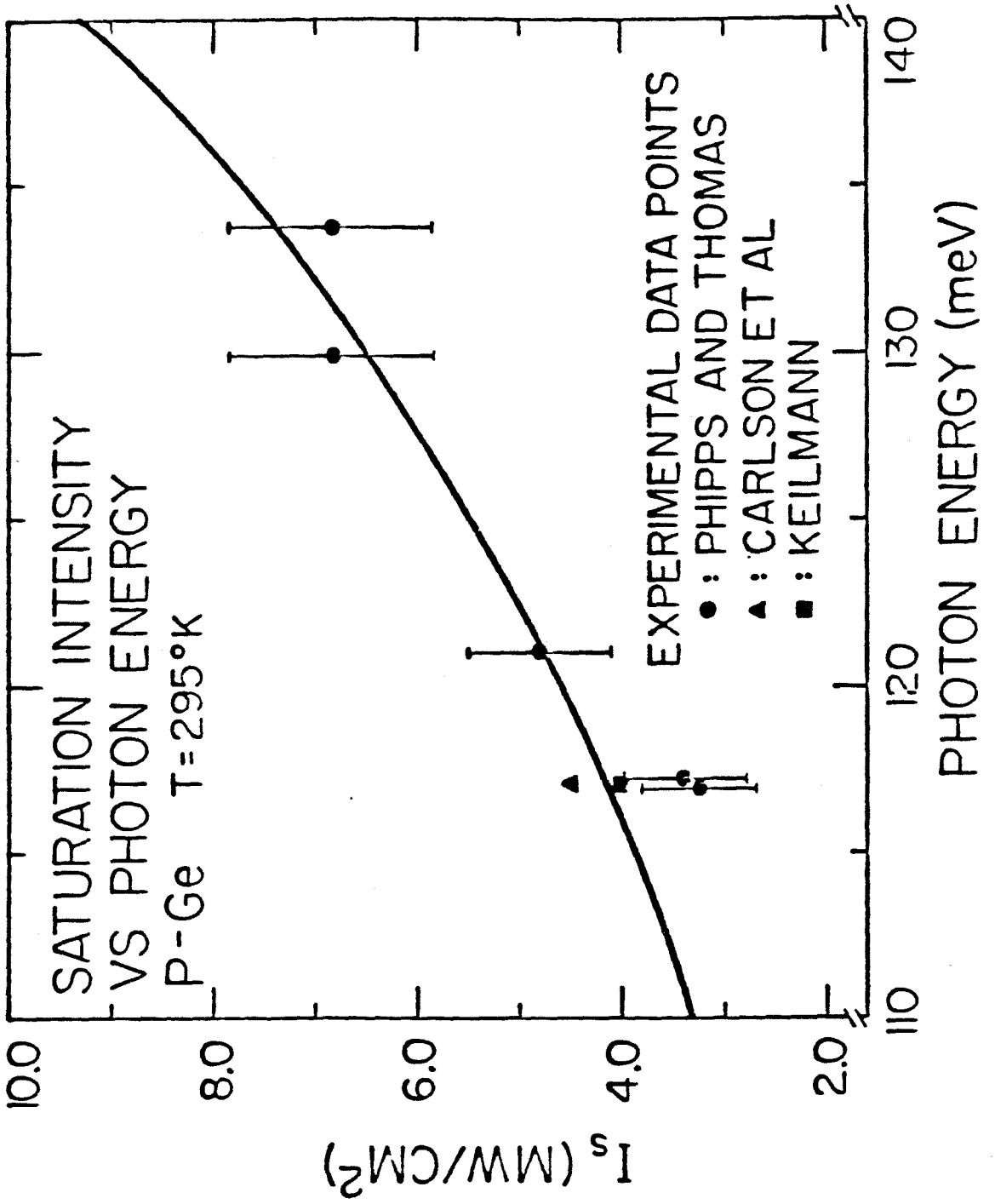
SATURATION INTENSITY
VS PHOTON ENERGY
P-Ge T=295°K
EXPERIMENTAL DATA POINTS
●: PHIPPS AND THOMAS
▲: CARLSON ET AL
■: KEILMANN
I_s (MW/CM^2)
10.0
8.0
6.0
4.0
2.0
110
120
130
140
PHOTON ENERGY (meV)

The calculated results shown in Fig. (3) were attained using the higher order approximation for $(f_h(\underset{\sim}{k}) - f_\ell(\underset{\sim}{k}))$. The results for the first order approximation are qualitatively similar to those of the more complete calculation; the numerical values of the two calculations differ by an approximately constant factor. At $\lambda = 10.6$ μm and T = 295K, the more complete calculation gives a value of I_s of 4.1 MW/cm^2, the first order calculation including acoustic phonon scattering gives a result of 5.8 MW/cm^2, and the first order calcultion neglecting acoustic phonon scattering gives a result of 3.5 MW/cm^2. Thus the first order calculation neglecting acoustic phonon scattering is within about 15% of the more complete calculation. This result is interesting because the first order calculation is much easier and less expensive to perform than the more complete calculation.

The increase in $I_s(\omega)$ with increasing ω is due both to the behavior of the scattering rates and the optical matrix elements. The relative contribution of the scattering rates and the optical matrix elements can be most easily seen in the first order calculation. At this level of approximation, $I_s(\omega)$ is given by a weighted average of $\ell(\underset{\sim}{k})$ (see Eq. (34)). The values of $\ell(\underset{\sim}{k})$ are proportional to: ω^2, $T_2^{-1}(\underset{\sim}{k})$, $(T_h(\underset{\sim}{k}) + T_\ell(\underset{\sim}{k}))$ and $|P_{h\ell}(\underset{\sim}{k})|^{-2}$. In Fig. (4), the variation of these factors is illustrated as a function of photon energy for $\underset{\sim}{k}$ in the [100] and [111] directions.

Since the usefulness of p-Ge as a saturable absorber in CO_2 laser systems is determined by its saturation characteristics, it is of

Figure 4. Variation of the factors which contribute to the photon energy dependence of $I_s(\omega)$ in our first approximation for the absorption coefficient in p-Ge. The values of the factors are normalized to their value at $\hbar\omega$ = 117 meV (λ = 10.6 μm). The factors were computed for T = 295^{o}K.

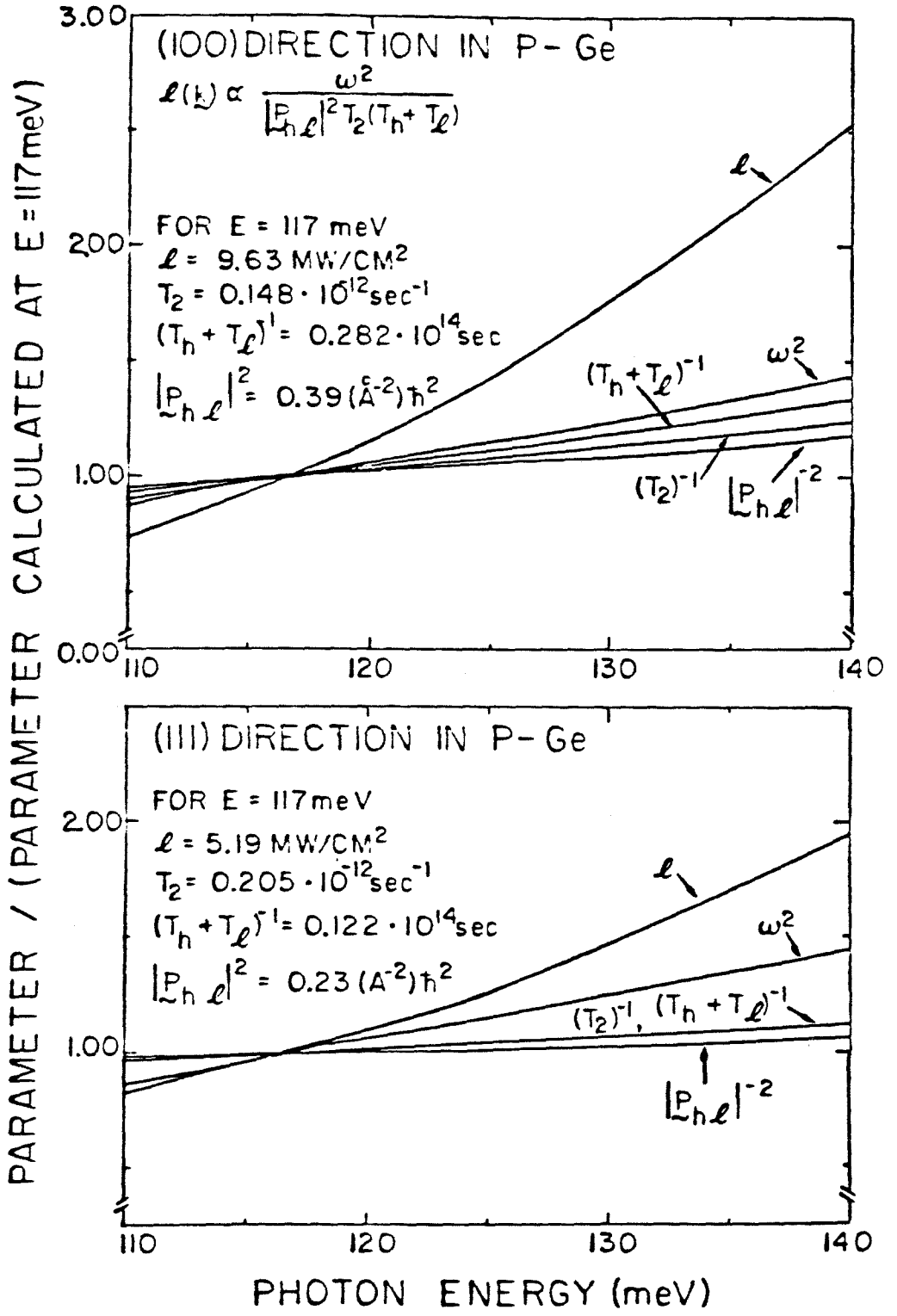
(100) DIRECTION IN P-Ge
$\ell(\omega) \propto \frac{\omega^2}{|P_{h\ell}|^2 T_2 (T_h + T_\ell)}$
FOR E = 117 meV
ℓ = 9.63 MW/CM^2
$T_2 = 0.148 \cdot 10^{12}$ sec^{-1}
$(T_h + T_\ell)^{-1} = 0.282 \cdot 10^{14}$ sec
$|P_{h\ell}|^2 = 0.39 (\text{Å}^{-2})\hbar^2$
ℓ
ω^2
$(T_h + T_\ell)^{-1}$
$(T_2)^{-1}$
$|P_{h\ell}|^{-2}$
3.00
2.00
1.00
0.00
110
120
130
140
(111) DIRECTION IN P-Ge
FOR E = 117 meV
ℓ = 5.19 MW/CM^2
$T_2 = 0.205 \cdot 10^{12}$ sec^{-1}
$(T_h + T_\ell)^{-1} = 0.122 \cdot 10^{14}$ sec
$|P_{h\ell}|^2 = 0.23 (\text{Å}^{-2})\hbar^2$
ℓ
ω^2
$(T_2)^{-1}$, $(T_h + T_\ell)^{-1}$
$|P_{h\ell}|^{-2}$
2.00
1.00
110
120
130
140
PARAMETER / (PARAMETER CALCULATED AT E = 117 meV)
PHOTON ENERGY (meV)

interest to be able to control the saturation behavior. Since optical phonon scattering is the dominant relaxation mechanism, and the optical phonon occupation is temperature dependent, it is clear that $I_s(\omega)$ will depend on temperature. In Fig. (5), we present the results of a calculation of the temperature dependence of $I_s(\omega)$ in p-Ge for a light with a wavelength of 10.6 μm. $I_s(\omega)$ increases monotonically with temperature. This increase is due to the increased rate of phonon scattering at higher temperatures. Because of the rather strong dependence of $I_s(\omega)$ on temperature, it should be possible to tune the saturation behavior of p-Ge with temperature.

We now consider the orientational dependence of the sample on the saturation characterisitics. This behavior would predict a dependence of the saturation intensity on the direction of the light polarization. Here, the dependence of the saturation intensity on the direction of the light polarization is contained in the momentum matrix elements. Using the first-order approximation for the hole distribution, we numerically calculate $\alpha(I)$ for light polarization along the [100], [110] and [111] directions. Values of I_s for the different directions of polarization and for the case of unpolarized light are given in Table (1). The experimental results of Ref. (2) indicate no significant variation of I_s with crystal orientation, which is consistent with our calculations in consideration of the uncertainty in the reported data.

Figure 5. Calculated saturation intensity as a function of temperature for p-Ge and light with a wavelength of 10.6 μm.

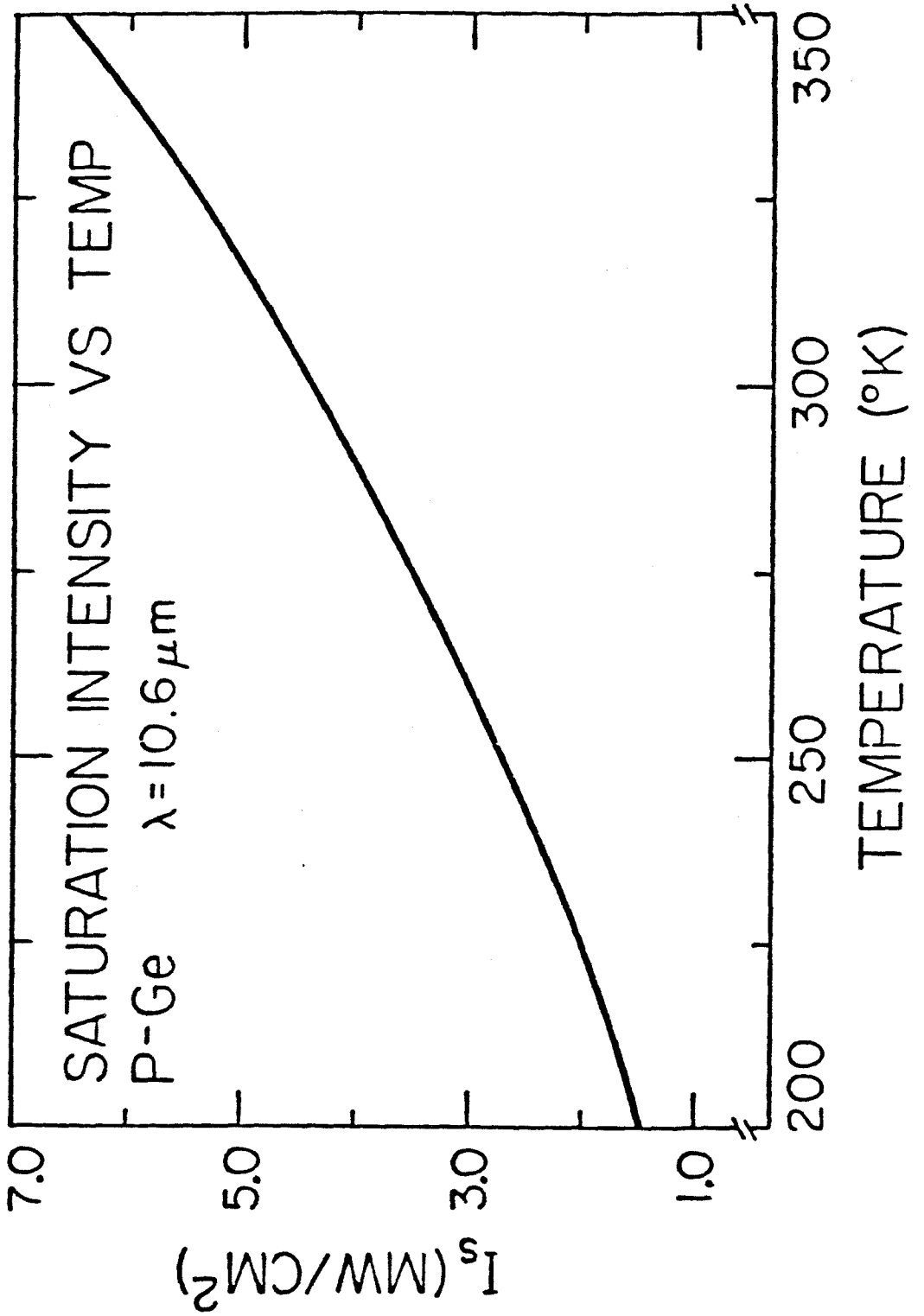
SATURATION INTENSITY VS TEMP
P-Ge λ=10.6μm
I_s (MW/CM²)
7.0
5.0
3.0
1.0
200
250
300
350
TEMPERATURE (°K)

TABLE (1). Values of the saturation intensity for the laser excitation polarized only the [100], [110] and [111] directions. Also shown is the value of I_s for the case of unpolarized light. All values are for lightly doped p-Ge (doping concentration less than about $3.0 \times 10^{15} cm^{-3}$) and room temperature conditions.

Direction of Light Polarization	I_s (MW/cm^2)
[100]	3.2
[110]	3.4
[111]	3.3
unpolarized	3.5

VI. HOLE-IONIZED IMPURITY AND HOLE-HOLE SCATTERING

For those temperatures and hole densities for which hole-impurity and hole-hole scattering is small compared to phonon scattering, the calculated I_s is independent of hole concentration. At room temperature, I_s has been found experimentally to be independent of hole concentration for concentrations less than about $4 \cdot 10^{15} cm^{-3}$ (1). We now extend the range of doping concentrations for which the theory is valid by including the effects of hole-impurity and hole-hole scattering. We consider only uncompensated samples of p-type germanium where the acceptors are all shallow and ionized at room temperature conditions.

The scattering rate for a hole with energy ε by singly ionized impurities is given by

$$V_I = \frac{\pi e^4}{K^2 \sqrt{2m^*}\, \varepsilon^{3/2}} N_I \left[\ell n(1+\beta^2) - \frac{\beta^2}{1+\beta^2} \right] , \tag{35a}$$

where

$$\beta^2 = \frac{2Km^* k_B T}{\pi N_I e^2 \hbar^2}\, \varepsilon , \tag{35b}$$

K is the dielectric constant, m^* is the free-carrier effective mass, k_B is the Boltzmann constant, and N_I is the total concentration of ionized impurities (26).

Following Ref. (27), the rate of hole-hole scattering for a hole

with energy ε is given by

$$V_{hh} = \frac{2\sqrt{2}\ \pi\ N_h e^4 \lambda}{K^2\ \varepsilon^{3/2}\sqrt{m^*}} \tag{36a}$$

where

$$\lambda = 1 + \ell n \left(\frac{\varepsilon}{2h} \left(\frac{K\ m^*}{2\pi N_h e^2} \right)^{1/2} \right) \quad . \tag{36b}$$

The calculation of the saturation intensity I_s at different impurity concentrations is performed using the first-order approximation to $(f_h(\underset{\sim}{k}) - f_\ell(\underset{\sim}{k}))$, where the calculation of scattering rates is modified to include hole-impurity and hole-hole scattering in addition to carrier-phonon scattering [28]. The inclusion of hole scattering by ionized impurities and other holes causes an increase in the scattering rate of the free holes and introduces a concentration dependence in the saturation intensity. The result of increasing the scattering rates is that higher intensities are required to reduce the free-hole population in the heavy-hole band at the resonant region, since the excited holes can re-route at a faster rate.

The calculated values of I_s as a function of the impurity concentration are given in Fig. (6) for 250, 300 and 350°K. We note that I_s is substantially independent of the hole concentration for concentrations less than about $3\times10^{15}cm^{-3}$, that is, in the region where the hole-phonon scattering mechanism is dominant. For hole concentrations greater than about $3\times10^{15}cm^{-3}$, the saturation intensity begins to

Figure 6. Calculated values of the saturation intensity I_s vs the hole concentration for p-Ge with light having a wavelength of 10.59 μm. Values of I_s vs N_h are shown for 250, 300 and 350°K. The dashed line in the figure represents a calculation of I_s assuming hole-impurity and hole-hole scattering to be negligible compared to hole-phonon scattering. The solid line in the figure represents a calculation of I_s which includes hole-impurity, hole-hole, and hole-phonon scattering mechanisms.

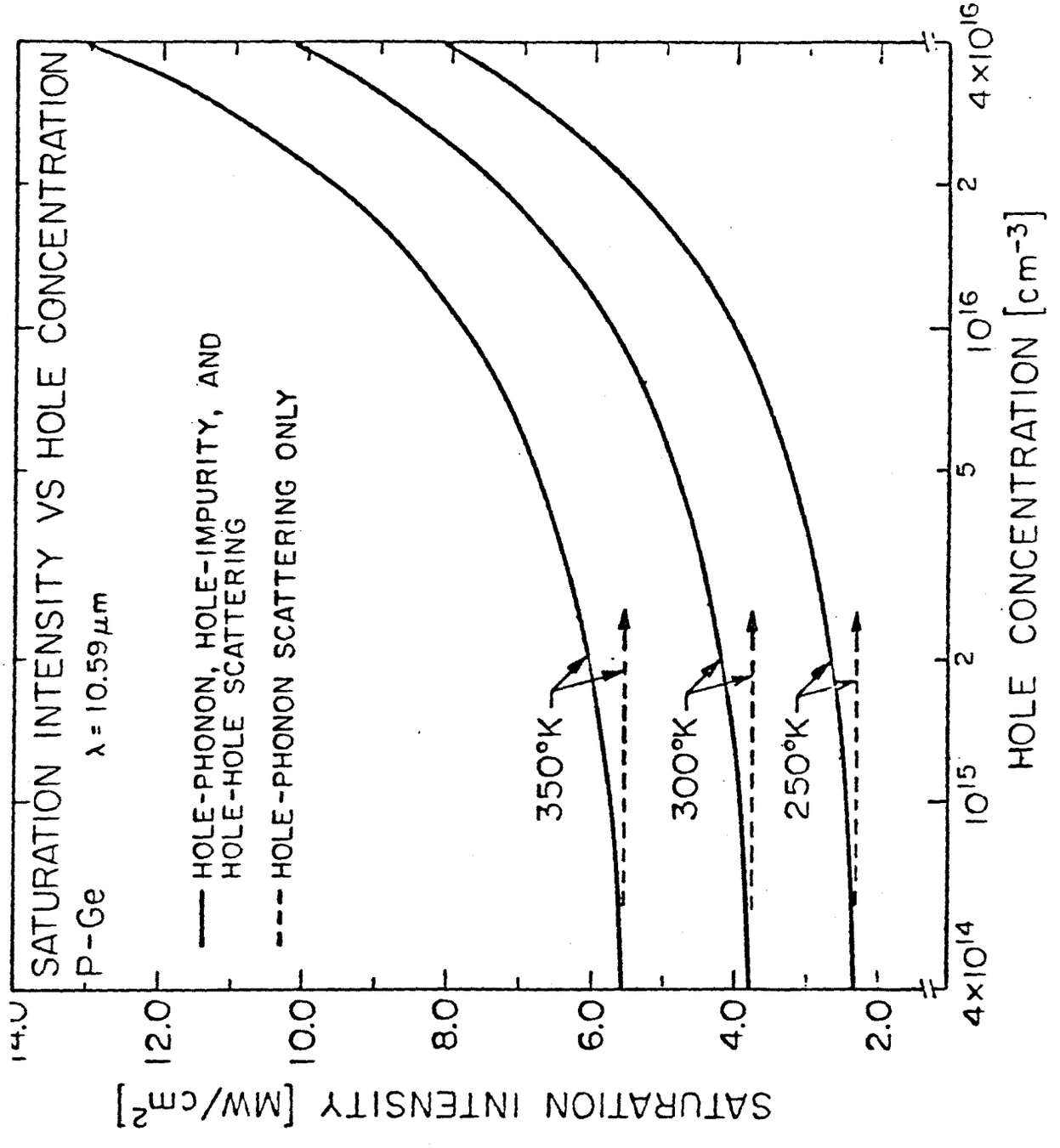
SATURATION INTENSITY VS HOLE CONCENTRATION
P-Ge
λ = 10.59 μm
HOLE-PHONON, HOLE-IMPURITY, AND HOLE-HOLE SCATTERING
HOLE-PHONON SCATTERING ONLY
350°K
300°K
250°K
SATURATION INTENSITY [MW/cm²]
HOLE CONCENTRATION [cm⁻³]
14.0
12.0
10.0
8.0
6.0
4.0
2.0
4×10¹⁴
10¹⁵
2
5
10¹⁶
2
4×10¹⁶

increase monotonically with increasing hole concentration due to the increased scattering rate of the free holes participating in the optical interaction. For hole concentrations less than about $3.5 \times 10^{15} cm^{-3}$, measured values of I_s at room temperature have been found to be independent of hole concentrations [1] with a value of about 4 MW/cm^2, [2-4] which is consistent with our calculation.

For a fixed impurity density, we find that I_s increases with increasing temperature. This increase is predominantly due to the increase in the hole-phonon scattering rate at the higher temperatures. The fractional increase in I_s with increasing impurity density is smaller for the larger temperatures. The decrease in the impurity concentration dependence at higher temperatures occurs because the hole-impurity and hole-hole scattering mechanisms become less important compared to hole-phonon scattering as the temperature is increased.

Thus, depending on the intended application of the saturable absorber, we predict that at a fixed temperature one can control the saturation characteristics by controlling the doping concentration. In addition, knowledge of the effect of the doping concentration on the saturation intensity is useful in interpreting independent experimental results where the transmission experiments are performed in samples of different resistivities.

We finally consider the case in which the intensity is sufficiently high that the effect of residual absorption becomes important in determining the absorption properties. In this case we expect $\alpha(I)/\alpha(I=0)$ to more strongly deviate from the functional form given in

Eq. (1). This deviation may be significant for $I >> I_s$ owing to the decrease in the direct intervalence-band absorption compared to the nonsaturable absorption. The important residual (nonsaturable) absorption mechanisms are lattice absorption and indirect free-hole transitions.

Lattice absorption for wavelengths near 10 μm requires the co-operation of at least three optical phonons to conserve energy. Measured values of the lattice absorption in Ge yield an absorption coefficient of $\alpha_p = 0.013\ cm^{-1}$ at room temperature. Similar measurements of the lattice absorption for other Groups IV and III-V semiconductors yield small absorption coefficients at these wavelengths.

The absorption coefficient $\alpha_I(\omega)$ due to indirect free-hole transitions is approximated by

$$\alpha_I(\omega) = \frac{4\pi}{nc} \frac{N_h e^2 \tau}{m^*(1+\omega^2\tau^2)} \quad , \tag{37}$$

where ω is the frequency of the light, n is the refractive index, and τ is the average scattering time of the carriers determined by mobility data [14]. The intravalence-band absorption cross section estimated from Eq. (37) is about $10^{-17}\ cm^2$, which is small compared to the direct intervalence-band cross section of about $6.0 \times 10^{-16} cm^2$.

The total absorption coefficient at 10.59 μm can be written as:

$$\alpha(I) = \alpha_p + \alpha_I + \frac{\alpha_o}{\sqrt{1+I/I_s}} \quad , \tag{38}$$

where I_s has a calculated value of about 4 MW/cm^2 for a hole concentration of $2x10^{15}cm^2$. The effect of a nonzero α_p and α_I in Eq. (38) is illustrated in Fig. (7) for $N_h = 2x10^{15}cm^{-3}$, where values of $\alpha(I)/\alpha(I=0)$ are plotted as a function of intensity. Values of $\alpha(I)/\alpha(I=0)$ are shown for intensities ranging up to 1 GW/cm^2, which corresponds to the estimated optical damage threshold [3]. For this value of N_h, $\alpha_o = 1.20\ cm^{-1}$, $\alpha_I = 0.02\ cm^{-1}$, and $\alpha_p = 0.013\ cm^{-1}$. The values of $\alpha(I)/\alpha(I=0)$ for $\alpha_p = \alpha_I = 0$ are also shown for comparison. The inclusion of residual absorption effects becomes important for $I >> I_s$ and produces significant deviations of $\alpha(I)/\alpha(I=0)$ from the form of Eq. (1). A deviation has been measured for $I \gtrsim 200\ MW/cm^2$, which is consistent with our predictions; however, other effects may also be contributing to the deviation. That is, we have found that if only the first term of Eq. (20) is retained, the calculated $\alpha(I,\omega)$ has precisely the form of Eq. (1). The second term of Eq. (20), which is not included in the first-order approximation, is smaller than the first term and leads to small deviations of the calculated form of $\alpha(I,\omega)$ from the expression of Eq. (1). And since the magnitudes of the nonsaturable absorption and the second term of Eq. (20) become more important as the intensity is increased, we expect a measurable deviation of $\alpha(I,\omega)$ from the form of Eq. (1) for $I >> I_s$, as has been experimentally verified for $I \gtrsim 50$ times I_s.

Figure 7. Calculated values of the absorption coefficient $\alpha(I)/\alpha(I=0)$ vs intensity for a hole concentration of $2x10^{15}cm^{-3}$ and light having a wavelength of 10.59 μm. The solid line in the figure represents the calculated values assuming no residual absorption. The dashed line in the figure represents the calculated values assuming a residual (non-saturable) absorption due to lattice absorption and indirect free-hole transitions. The upper curves show values of $\alpha(I)/\alpha(I=0)$ for intensities in the range of 1 - 100 MW/cm^2, and the lower curves are for intensities ranging from 100-1000 MW/cm^2.

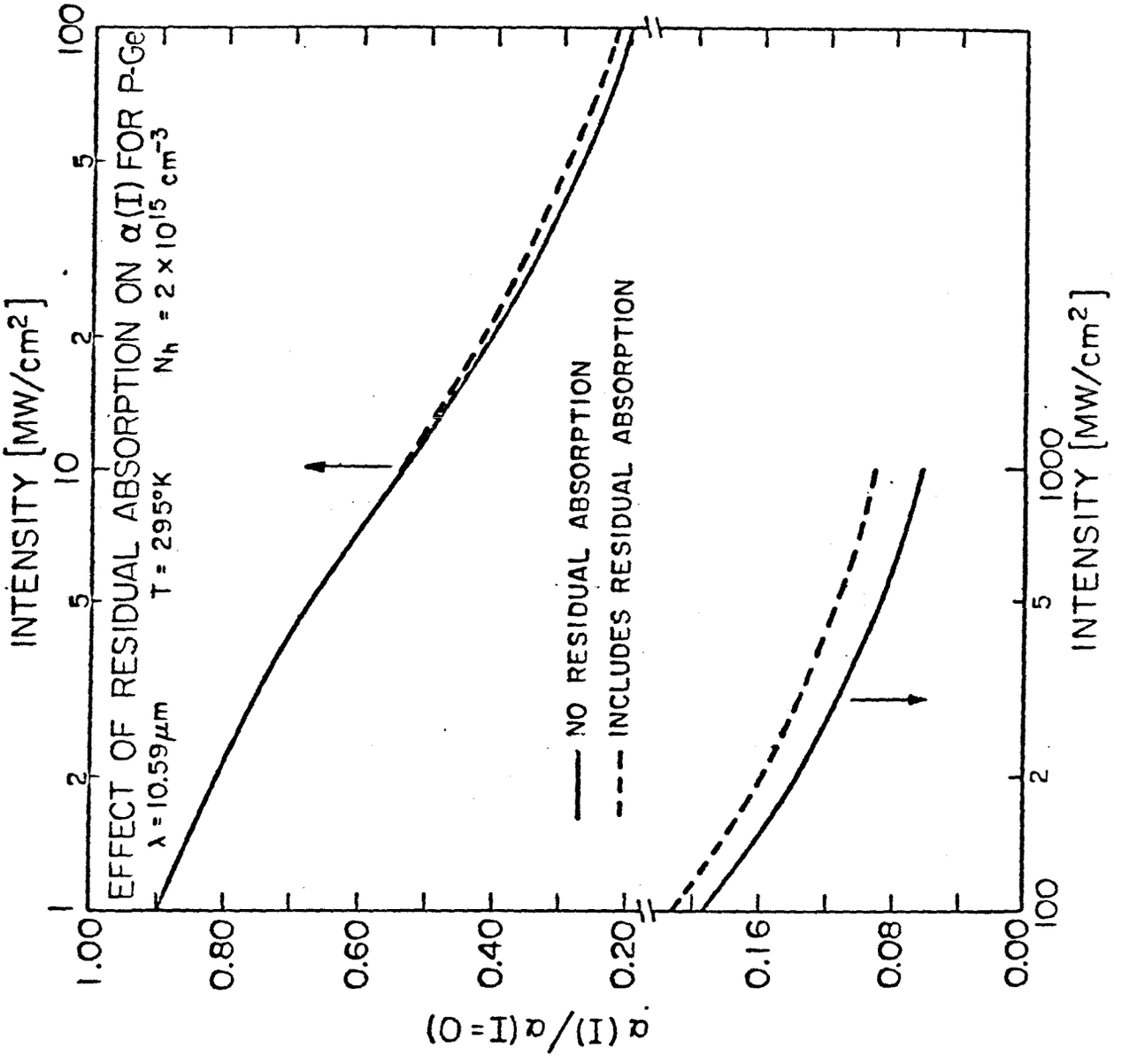
EFFECT OF RESIDUAL ABSORPTION ON α(I) FOR P-Ge
λ = 10.59μm
T = 295°K
$N_h = 2 \times 10^{15}$ cm^{-3}
NO RESIDUAL ABSORPTION
INCLUDES RESIDUAL ABSORPTION
INTENSITY [MW/cm^2]
INTENSITY [MW/cm^2]
α (I)/α (I = 0)
1.00
0.80
0.60
0.40
0.20
0.16
0.08
0.00
1
2
5
10
100
1000

VII. INTENSITY DEPENDENCE OF THE DISPERSIVE PROPERTIES OF p-Ge

There is also an intensity dependence in the real part of the dielectric constant associated with the saturation of the intervalence-band transitions. These laser-induced changes in the real part of the dielectric constant alter the dispersive properties of the media and thus modify the spatial and temporal behavior of the laser pulse. Since the laser pulse shape is important in many applications of CO_2 laser systems, one needs to understand the changes in the dispersive properties induced by the high-intensity beam. An intensity dependence of the real part of the dielectric constant can be exploited for phase conjugation. Phase conjugation in the CO_2 laser frequency regime using Ge as the nonlinear medium is of current interest [29].

For light with a wavelength near 10 μm, the dominant absorption mechanism in p-Ge is due to direct free-hole transitions between the heavy- and light-hole bands. These resonant transitions also contribute to the index of refraction. At high light intensities, the absorption due to these transitions saturates [1-4] owing to a modification of the free-hole distribution function. This intensity dependent modification of the distribution function also changes the contribution of the free-hole transitions to the index of refraction. In addition to the intensity dependence of the index of refraction from the resonant intervalence-band transitions, there is an intrinsic contribution due to a field modification of the virtual electron-hole

pair creation processes [30]. The magnitude of the resonant intervalence-band contribution depends on the doping level. Both contributions lead to an increase in the index of refraction with increasing intensity. We find that the magnitude of the resonant intervalence-band contribution to the first order modification of the index of refraction equals measured values [31] of the intrinsic contribution at a doping level of about $3\times10^{15}cm^{-3}$. In this section I present a calculation of the resonant intervalence-band contribution to the intensity dependence of the real part of the dielectric constant in p-Ge for light with a wavelength of 10.6 μm.

In Section IV, we presented a calculation of the hole distribution in p-Ge as a function of the CO_2 laser intensity. Using the calculated distribution function, the intensity dependence of the absorption coefficient was determined. Good agreement with the available experimental data was found. Here we use the calculated distribution function to determine the intensity dependence of the real part of the dielectric constant owing to resonant intervalence-band transitions.

Using the equation for the current density owing to the intervalence-band transitions, the real part of the susceptibility is given by (Eq. 12 of Section IV),

$$\underset{\sim}{\chi}'(\omega,I) = \frac{N_h e^2}{2m^2\omega^2\hbar}\sum_{\underset{\sim}{k}}(f_h(\underset{\sim}{k})-f_\ell(\underset{\sim}{k}))\sum_{\substack{b\ in\ h\\ c\ in\ \ell}}(\underset{\sim}{P}_{cb}\underset{\sim}{P}_{bc}+\underset{\sim}{P}_{bc}\underset{\sim}{P}_{cb})\frac{\Omega(k)-\omega}{(\Omega(\underset{\sim}{k})-\omega)^2+(1/T_2(\underset{\sim}{k}))^2}\cdot \tag{39}$$

Here, the intensity dependence is contained in the distribution functions $f_h(\underset{\sim}{k})$ and $f_\ell(\underset{\sim}{k})$. At low light intensities, $\underset{\approx}{\chi}$ is a scalar because of the cubic symmetry of Ge. For high intensity polarized light, the cubic symmetry is reduced and $\underset{\approx}{\chi}$ is described by a second-rank tensor. Using the results of Section IV, the steady-state difference in the occupation probabilities which appear in the expression for $\underset{\approx}{\chi}'(\omega,I)$ is given by

$$f_h(\underset{\sim}{k})-f_\ell(\underset{\sim}{k}) = \frac{f_h^e(\underset{\sim}{k})-f_\ell^e(\underset{\sim}{k})}{1+\beta(\underset{\sim}{k})(T_h(\underset{\sim}{k})+T_\ell(\underset{\sim}{k}))} + \frac{T_h(k)F(k)-T_\ell(k)G(k)}{1+\beta(\underset{\sim}{k})(T_h(\underset{\sim}{k})+T_\ell(\underset{\sim}{k}))} \quad , \tag{40}$$

where the auxiliary functions $T_h(\underset{\sim}{k})$, $T_\ell(\underset{\sim}{k})$, $F(\underset{\sim}{k})$ and $G(\underset{\sim}{k})$ are defined in Eqs. (18a), (18b), (18c) and (18d). The function $\beta(\underset{\sim}{k})$ is defined as

$$\beta(\underset{\sim}{k}) = \frac{2\pi^2}{\sqrt{\varepsilon_o}m^2\omega c}\frac{e^2 I}{\hbar\omega}\sum_{\substack{b \text{ in } h \\ c \text{ in } \ell}}|\underset{\sim}{\eta}\cdot\underset{\sim}{P}_{bc}(\underset{\sim}{k})|^2\frac{1/(\pi\hbar T_2(\underset{\sim}{k}))}{(\Omega(\underset{\sim}{k})-\omega)^2+(1/T_2(\underset{\sim}{k}))^2} \quad , \tag{41}$$

where I is the light intensity, $\underset{\sim}{\eta}$ is the polarization of the light, and ε_o is the intrinsic material dielectric constant. The definition of $\beta(\underset{\sim}{k})$ in Eq. (41) differs slightly from that of Eq. (17c) because we have not averaged over polarizations. As a result the distribution function which we calculate here depends on the polarization of the light and does not have cubic symmetry. The calculational approach however is the same as that of Section IV. Some of the results we present here are for unpolarized light. In this case we average Eq. (41) over polarizations as in Section IV.

We calculate the intensity dependence of the real part of the susceptibility due to resonant intervalence-band transitions. The results quoted in this section for $\Delta n(I)$ or $\Delta\varepsilon(I)$ refer to only this contribution. There is an additional intrinsic contribution which is to be added to our results. There may also be heating effects in any particular experiment. One can determine the contribution from thermal effects using measured values of $\frac{dn}{dT}$. The thermal effects can be eliminated by using short laser pulses.

In order to calculate the occupation probability that a hole state is occupied, it is necessary to know the free-hole scattering rates. For the hole concentrations and temperatures at which most saturable absorption experiments have been performed, phonon scattering is the dominant scattering mechanism. The phonon scattering rates were treated in the manner of Section IV. The one-hole energies and momentum matrix elements are determined by degenerate $\underset{\sim}{k}\cdot\underset{\sim}{p}$ perturbation theory as previously discussed. The cyclotron resonance parameters of Hensel and Suzuki [21] were used. Using the steady-state solution for the difference in the occupation probabilities, we integrate Eq. (39) to determine the laser-induced changes in the real part of the susceptibility.

The real part of the susceptibility is calculated numerically for λ=10.6 μm and T = 300 K. Using Eq. (39) we can calculate $\underset{\approx}{\chi}'(I)$ for any polarization of the light. Explicit values of $\underset{\approx}{\chi}'(I)$ are calculated for the case of unpolarized light, and for the polarization along the [100] and [110] directions.

For unpolarized light the second-rank tensor $\underset{\approx}{\chi}'$ becomes a scalar, since any orientational dependence has been averaged out when we averaged over the directions of the vector potential [19]. We find that values of $\chi'(I)$ increase monotonically with increasing intensity due to changes in the distribution of free-holes. Room temperature values of $\chi'(I)/\chi'(I=0)$ are given in Fig. (8) for intensities between 0 and 60 MW/cm^2. At low intensities $(\chi'(I=0)/N_h)$ is equal to 1.4×10^{-20}cm^3 ($\chi'(I=0)$ is proportional to N_h).

Laser-induced changes in $\chi'(\omega)$ can be measured by observing changes in the real part of the dielectric constant, which determine the dispersive properties of the medium. The real part of the complex dielectric constant $\underset{\approx}{\varepsilon}$ is given by

$$\underset{\approx}{\varepsilon} = \varepsilon_o + 4\pi\underset{\approx}{\chi}' \quad . \tag{42}$$

Values for the change in ε can be measured by studying threshold values for self-focusing (for $\frac{d\varepsilon}{dI}$ positive). In Fig. (9) we show the calculated results for $\Delta\varepsilon$ and the corresponding results for the change in the index of refraction, Δn, for unpolarized light with a wavelength of 10.6 μm at 300 K. The changes in ε and in n are directly proportional to the free-hole density. We find that ε and n are increasing functions of intensity.

The intrinsic contribution to dn/dI in Ge has recently been measured to be about 1×10^{-6}cm^2/MW [31]. The resonant intervalence-

Figure 8. Calculated values of $\chi'(I)/\chi'(I=0)$ as a function of intensity for unpolarized light in p-Ge. The calculation was done for light with a wavelength of 10.6 μm and a temperature of 300 K.

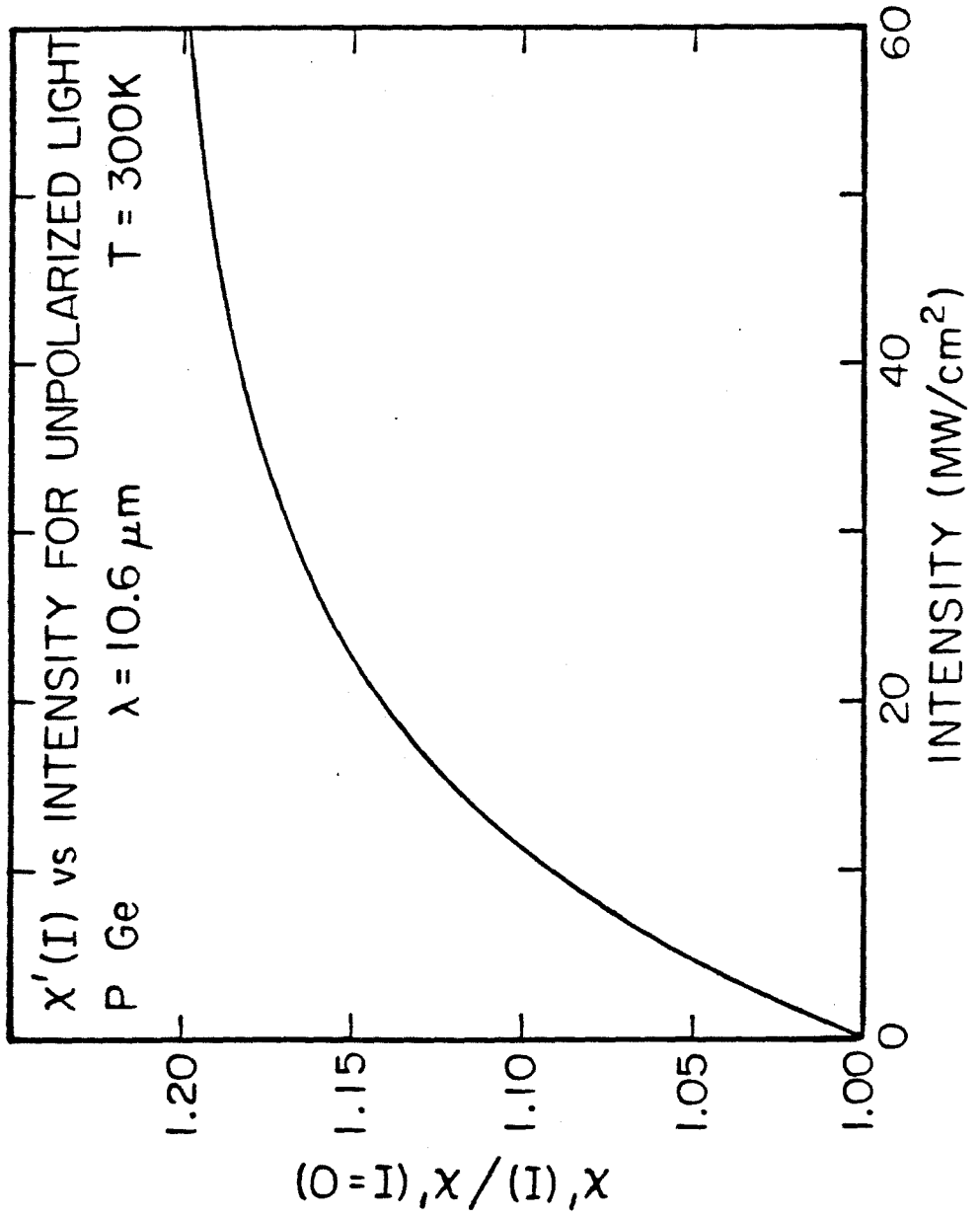
χ'(I) vs INTENSITY FOR UNPOLARIZED LIGHT
P Ge
λ = 10.6 μm
T = 300K
χ'(I)/χ'(I=0)
1.20
1.15
1.10
1.05
1.00
0
20
40
60
INTENSITY (MW/cm²)

Figure 9. The top panel gives the calculated values of the change in the real part of the dielectric constant (divided by the density of free-holes) as a function of intensity for p-Ge at λ = 10.6 μm, T = 300 K, and for unpolarized light. The corresponding values for the change in the index of refraction are given in the lower panel,

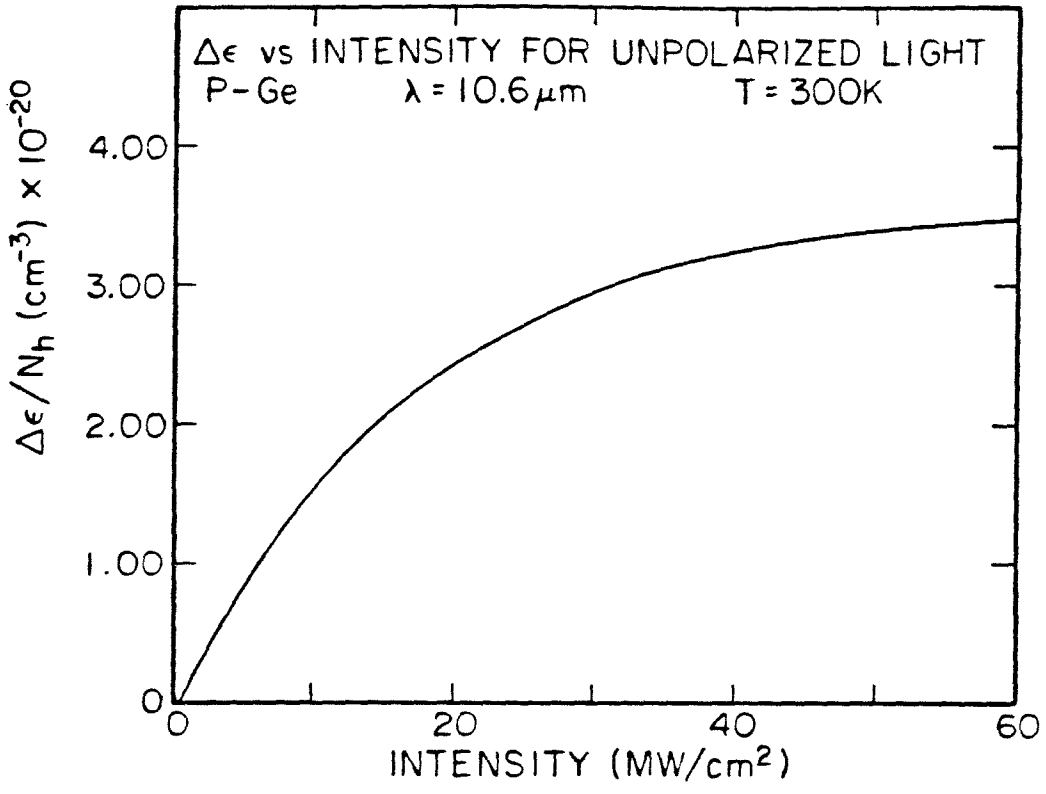
Δε vs INTENSITY FOR UNPOLARIZED LIGHT
P-Ge λ = 10.6μm T = 300K
Δε/N_h (cm^-3) x 10^-20
4.00
3.00
2.00
1.00
0
0
20
40
60
INTENSITY (MW/cm^2)

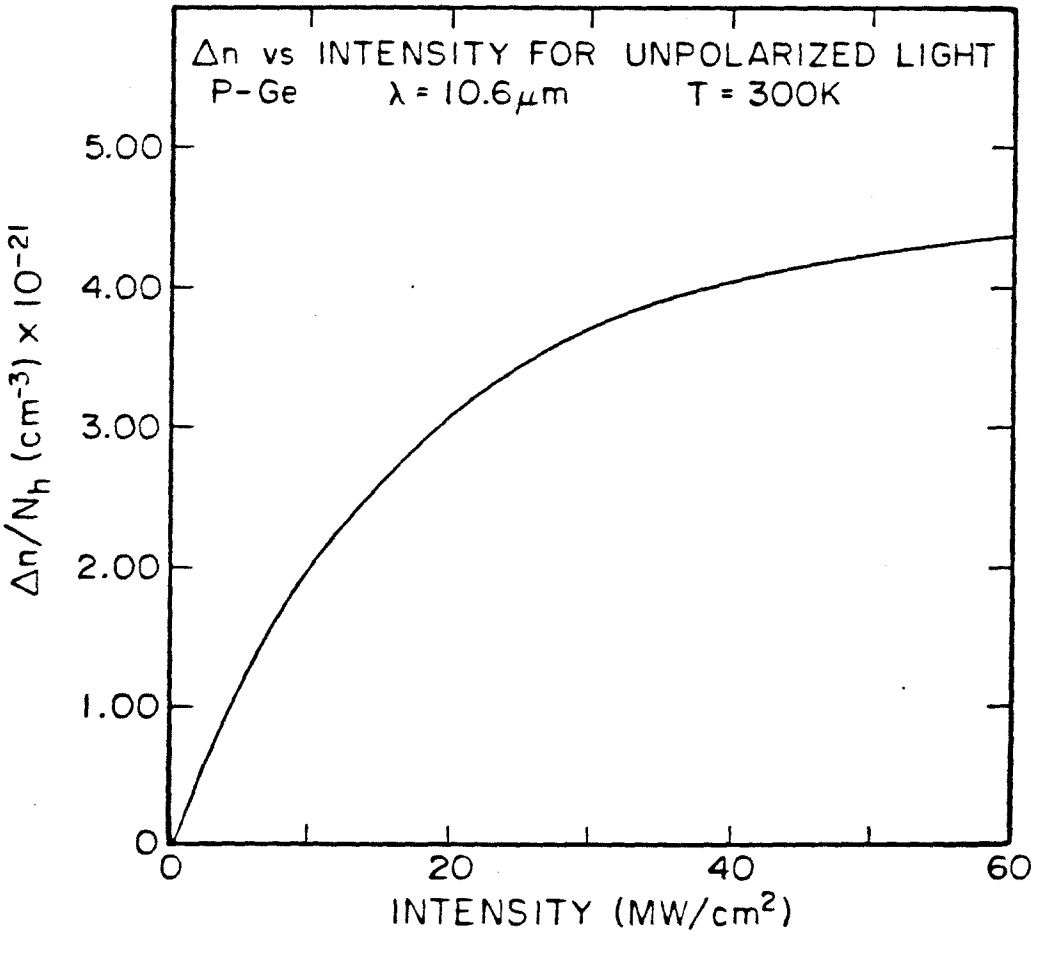
Δn vs INTENSITY FOR UNPOLARIZED LIGHT
P-Ge λ = 10.6μm T = 300K
Δn/N_h (cm^-3) x 10^-21
5.00
4.00
3.00
2.00
1.00
0
0
20
40
60
INTENSITY (MW/cm^2)

band contribution to dn/dI is intensity dependent. In the lower intensity region the change in n is linear in I. For hole densities greater than about $3\times10^{15}cm^{-3}$, the resonant intervalence-band contribution is larger than the intrinsic contribution at the lower intensities.

In Fig. (10) we show the calculated results for the diagonal components of $(\Delta\underset{\sim}{\varepsilon}/N_h)$ as a function of intensity for light polarized in the [100] and [110] directions. For the case of [100] polarization the coordinate axes are chosen to be the crystal axis of the sample. In this coordinate system, the off-diagonal components of $\underset{\approx}{\varepsilon}$ vanish as at low intensities. There is a small difference in the values of ε_{xx} and ε_{zz} ($\varepsilon_{yy} = \varepsilon_{zz}$ in this case) due to the polarization dependence of $\beta(\underset{\sim}{k})$ in determining the distribution of holes in the heavy- and light-hole bands. For the case of [110] polarization, the X axis is taken in the [110] direction, the Y axis in the $[1\bar{1}0]$ direction and the Z axis in the [001] direction. In this coordinate system $\underset{\approx}{\varepsilon}$ is diagonal. There is a small difference in the values of the three diagonal components. Overall, from Fig. (10), we see that the effects of polarization on $\Delta\underset{\approx}{\varepsilon}$ are rather small.

The change in $\underset{\approx}{\varepsilon}$ with intensity is due to the change in the distribution of hole states. We find that the diagonal components of increase monotonically with increasing intensity. From Eq. (39), we see that values of $\underset{\sim}{k}$ for which $\Omega(\underset{\sim}{k}) < \omega$ lead to a positive contribution to $\underset{\approx}{\chi}'$ and thus to $\underset{\approx}{\varepsilon}$, whereas values of $\underset{\sim}{k}$ for which $\Omega(\underset{\sim}{k}) < \omega$ lead to a

Figure 10. Calculated values of the diagonal elements of $\underset{\approx}{\Delta\varepsilon}$ (divided by the free-hole density) as a function of intensity in p-Ge at 300 K for light with a wavelength of 10.6 μm. In the top panel the result for [100] polarization is shown. The coordinate system is chosen to be the crystal axis; $\underset{\approx}{\varepsilon}$ is diagonal in this coordinate system. In the lower panel the result for [110] polarization is shown. For this panel, the X axis is in the [110] direction, the Y axis is in the $[1\bar{1}0]$ direction and the Z axis is in the [001] direction. In this coordinate system $\underset{\approx}{\varepsilon}$ is diagonal.

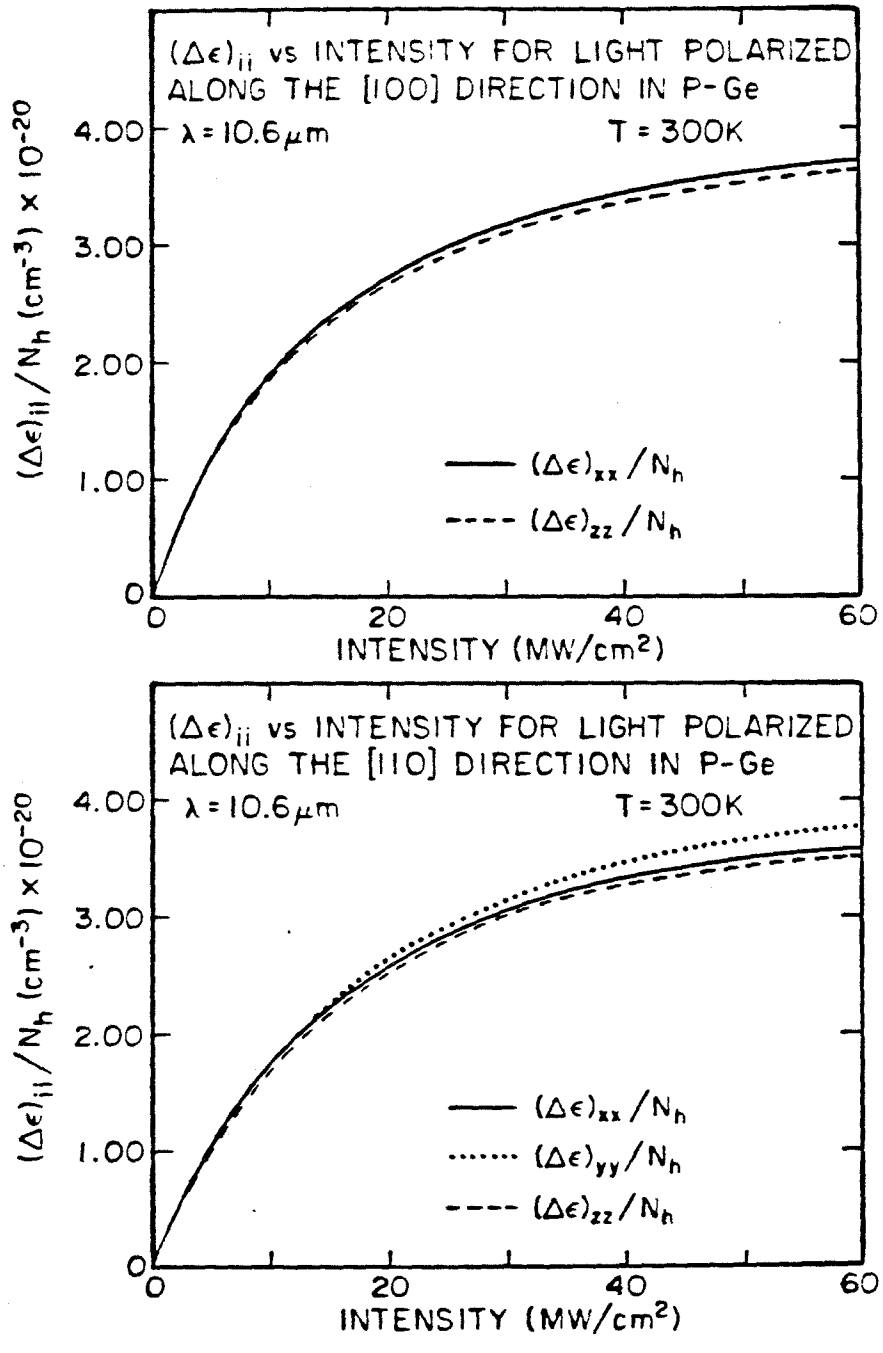
$(\Delta\epsilon)_{ii}$ vs INTENSITY FOR LIGHT POLARIZED ALONG THE [100] DIRECTION IN P-Ge
λ = 10.6μm
T = 300K
$(\Delta\epsilon)_{ii}/N_h$ (cm^{-3}) x 10^{-20}
4.00
3.00
2.00
1.00
0
0
20
40
60
INTENSITY (MW/cm^2)
$(\Delta\epsilon)_{xx}/N_h$
$(\Delta\epsilon)_{zz}/N_h$
$(\Delta\epsilon)_{ii}$ vs INTENSITY FOR LIGHT POLARIZED ALONG THE [110] DIRECTION IN P-Ge
λ = 10.6μm
T = 300K
$(\Delta\epsilon)_{ii}/N_h$ (cm^{-3}) x 10^{-20}
4.00
3.00
2.00
1.00
0
0
20
40
60
INTENSITY (MW/cm^2)
$(\Delta\epsilon)_{xx}/N_h$
$(\Delta\epsilon)_{yy}/N_h$
$(\Delta\epsilon)_{zz}/N_h$

negative contribution to $\underset{\approx}{\chi}'$. Under optical excitation, the holes occupy higher energy states than in equilibrium. Thus for the higher energy states with $\Omega(\underset{\sim}{k}) > \omega$ the difference in occupation probabilities $(f_h(\underset{\sim}{k})-f_\ell(\underset{\sim}{k}))$ is on the average enhanced compared to the equilibrium value, whereas for states with $\Omega(\underset{\sim}{k}) < \omega$ the difference in occupation probabilities is decreased compared to the equilibrium value. Hence the positive contributions to $\underset{\approx}{\varepsilon}$ from terms with $\Omega(\underset{\sim}{k}) > \omega$ is increased by illumination, and the magnitude of the negative contribution to $\underset{\approx}{\varepsilon}$ from terms with $\Omega(\underset{\sim}{k}) < \omega$ is decreased by illumination. Consequently, $\underset{\approx}{\varepsilon}$ monotonically increases with increasing intensity. As the intensity increases, the increase in $\underset{\approx}{\varepsilon}$ is slower than linear due to saturation of the intervalence-band transitions.

From the results for $\Delta\underset{\approx}{\varepsilon}(I)$, together with the intrinsic contribution, one can determine the effect of self-focusing actions in nonlinear optics experiments using p-Ge. The importance of self-focusing in any given experimental situation must be independently analyzed since it depends on the doping level, the intensity range, the sample thickness and the beam profile.

For two laser beams incident on a Ge sample, as in a pump-probe experiment, the light intensity is modulated in space and time due to the interference of the two beams. Since the index of refraction is a function of intensity, it is modulated by the oscillating intensity. The periodic variation of the index of refraction leads to a coupling of the two beams. This coupling can influence the

transmission of the beams which may be important in the analysis of a pump-probe experiment.

Many semiconductors have a valence band structure which is similar to that of Ge and an intensity dependence in $\underset{\sim}{\chi}'$ should be present in these materials. The theory presented here should apply for these materials as well as for Ge.

VII. SUMMARY AND CONCLUSIONS

We have presented a theory of saturation of heavy- to light-hole band transitions in p-type semiconductors with the diamond or zincblende crystal structure. Detailed calculations have been presented for p-type Ge and light in the 9-11 μm region. We found that the intensity dependence of the absorption coefficient is closely approximated by an inhomogeneously broadened two-level model. For the temperature and concentration range where hole-phonon scattering dominates hole-impurity and hole-hole scattering, I_s is found to be independent of hole density. For larger hole densities where hole impurity and hole-hole scattering are important, the saturation intensity increases monotonically with increasing hole concentration. This behavior is consistent with experimental results. The dependence of the saturation intensity on photon energy has been computed and compared with available experimental results. Good agreement between theory and experiment was found. We have predicted the dependence of the saturation intensity on temperature.

We have also used the theory to describe the intensity dependence of the real part of the dielectric constant in p-Ge due to modifications of the free-hole distribution function by the high intensity CO_2 laser light. We find that the high intensity light alters the optical isotropy, and the susceptibility becomes a second-rank tensor with elements which depend on both the intensity and the polarization of the saturable beam. These changes in the susceptibility are directly proportional to the concentration of free-holes in the sample. We find that the diagonal components of the susceptibility increase monotonically with increasing intensity. At high light intensities, the increase in χ' is slower than linear due to saturation of the intervalence-band transitions. The magnitude of the resonant intervalence-band contribution to the first-order modification of n equals measured values of the intrinsic contribution at a doping level of about $3 \times 10^{15} cm^{-3}$.

APPENDIX A: THE FREE-HOLE DENSITY MATRIX

In this appendix we outline the derivation of Eqs. (6) for the hole density matrix. We consider the low-hole density limit and take the Hamiltonian to be given by Eq. (2). The density matrix $\rho(t)$ satisfies

$$\frac{d\rho}{dt} = \frac{-i}{\hbar} [H,\rho] \quad . \tag{A1}$$

We are interested in the electronic part of the problem. The lattice can be considered as a surrounding medium and regarded as large and dissipative. In general, to calculate the time evolution of physical observables, we would need to know the density matrix of the whole system $\rho(t)$. But since the effects of the interaction on the free-holes are quickly dissipated by the lattice, and since the lattice (which acts as a heat bath) is not significantly heated over the duration of the interaction, we write the density matrix $\rho(t)$ as the product of an operator $\sigma(t)$ describing the free-hole density matrix and an operator P_L describing the lattice in equilibrium. Then $\rho(t) \simeq \sigma(t)P_L$. Using standard approximations [32], one finds

$$\frac{d\sigma_I(t)}{dt} \simeq \frac{-i}{\hbar} \left[\gamma_I(t),\, \sigma_I(t)\right] - \frac{1}{\hbar^2} \int_0^\infty dt'\, Tr_L \left[V_I(t), \left[V_I(t'),\, \sigma_I(t)\, P_L\right]\right] . \tag{A2}$$

Here the subscript I signifies that an operator is in the interaction representation, and Tr_L signifies a trace over lattice modes.

From Eq. (A2), one can see that $\sigma(t)$ is diagonal in wavevector. Prior to laser excitation, $\sigma(t)$ has the equilibrium value which is diagonal in wavevector. Taking matrix elements of Eq. (A2), we see that the time derivative of any matrix element of $d\sigma_I(t)/dt$ which is off-diagonal in $\underset{\sim}{k}$ is equal to a sum of terms, all of which are proportional to a matrix element of $\sigma_I(t)$ which is off-diagonal in $\underset{\sim}{k}$. Thus when the equation is integrated in time, all off-diagonal in $\underset{\sim}{k}$ matrix elements of $\sigma_I(t)$ vanish. This result is to be expected since the electromagnetic field leads to transitions between states with the same wavevector. Taking matrix elements of Eq. (A2), dropping non-resonant terms and returning to the Schrödinger representation gives Eq. (6).

APPENDIX B: EQUATIONS OF MOTION FOR $\underset{\sim}{J}(\underset{\sim}{k})$

In this appendix we derive Eq. (7). Multiplying Eq. (6b) on $\underset{\sim}{P}'$, taking the time derivative and tracing over bands gives

$$\frac{d^2}{dt^2}\left(Tr_b(\sigma(\underset{\sim}{k},t)\ \underset{\sim}{P}')\right) + \frac{1}{T_2(\underset{\sim}{k})}\ \frac{d}{dt}\ Tr_b(\sigma(\underset{\sim}{k},t)\ \underset{\sim}{P}')$$

$$= -\frac{i}{\hbar}\ Tr_b\left(\frac{d\sigma(\underset{\sim}{k},t)}{dt}[\underset{\sim}{P}', H_\varepsilon]\right) \quad . \tag{B1}$$

We have used the facts that σ, $\underset{\sim}{P}'$, γ, and H_ε are all diagonal in $\underset{\sim}{k}$ and hence can be cyclically permitted in the trace on bands and that $[\underset{\sim}{P}', \gamma]$ vanishes. Using Eq. (6b), we can write

$$\frac{1}{\hbar}\ Tr_b\left(\frac{d\sigma(\underset{\sim}{k},t)}{dt}[\underset{\sim}{P}', H_\varepsilon]\right)$$

$$= -\frac{i}{\hbar^2}\ Tr_b(\sigma(\underset{\sim}{k},t)\ [(H_\varepsilon + \gamma)\ ,\ [H_\varepsilon,\ \underset{\sim}{P}']])$$

$$-\frac{i}{T_2(\underset{\sim}{k})}\ \frac{d}{dt}\ Tr_b\ (\sigma(\underset{\sim}{k},t)\ \underset{\sim}{P}') - \frac{i}{(T_2(\underset{\sim}{k}))^2}\ Tr_b(\sigma(\underset{\sim}{k},t)\underset{\sim}{P}'). \tag{B2}$$

Thus Eq. (B1) becomes

$$\frac{d^2}{dt^2}\left(Tr_b(\sigma(\underset{\sim}{k},t)\underset{\sim}{P}')\right) + \frac{2}{T_2(\underset{\sim}{k})}\ \frac{d}{dt}\ \left(Tr_b(\sigma(\underset{\sim}{k},t)\underset{\sim}{P}')\right)$$

$$+ \left(\frac{1}{T_2(\underset{\sim}{k})}\right)^2 Tr_b(\sigma(\underset{\sim}{k},t)\ \underset{\sim}{P}')$$

$$= -\frac{1}{\hbar^2}\ Tr_b(\sigma(\underset{\sim}{k},t)\ [(H_\varepsilon+\gamma),\ [H_\varepsilon,\underset{\sim}{P}']]) \quad . \tag{B3}$$

Evaluating the trace on the righthand side, multiplying by $(N_h e/m)$ and neglecting $(1/T_2(\underset{\sim}{k}))^2$ compared with $\Omega(\underset{\sim}{k})^2$ gives Eq. (7). We find that $(1/T_2(\underset{\sim}{k}))^2$ is about three orders of magnitude smaller than $(\Omega(\underset{\sim}{k}))^2$ for wavelengths in the 9-11 μm region. Physically, this corresponds to the fact that the frequency linewidth of the transition is small compared to the resonant frequency.

APPENDIX C: EQUATIONS OF MOTION FOR THE DISTRIBUTION FUNCTIONS

In this appendix we derive equations for the distribution functions $f_h(\underset{\sim}{k})$ and $f_\ell(\underset{\sim}{k})$. Multiplying Eq. (6b) by $(N_h e\underset{\sim}{P}'/m)$ and taking the trace over bands gives

$$i\ \frac{d}{dt}\ \underset{\sim}{J}(\underset{\sim}{k}) + \frac{i}{T_2(\underset{\sim}{k})}\ \underset{\sim}{J}(\underset{\sim}{k}) =$$

$$\frac{N_h e}{m}\ \Omega(\underset{\sim}{k}) \sum_{\substack{b \text{ in } h \\ b' \text{ in } \ell}} \left[\sigma_{bb'}(\underset{\sim}{k},t)\ \underset{\sim}{P}_{b'b}(\underset{\sim}{k}) - \sigma_{b'b}(\underset{\sim}{k},t)\ \underset{\sim}{P}_{bb'}(\underset{\sim}{k})\right] . \qquad (C1)$$

Using Eq. (C1) and neglecting $(1/T_2(\underset{\sim}{k}))$ compared with ω, Eq. (6a) can be written as (with b in the heavy-hole band)

$$\frac{df_h(\underset{\sim}{k},t)}{dt} = -\frac{1}{2N_h c\hbar\Omega(\underset{\sim}{k})}\ (\frac{d}{dt}\ \underset{\sim}{J}(\underset{\sim}{k})\ \cdot \underset{\sim}{A})$$

$$- \sum_{c\underset{\sim}{k}'} [R_{h\underset{\sim}{k}\to c\underset{\sim}{k}'}\ f_h(\underset{\sim}{k},t) - R_{c\underset{\sim}{k}'\to h\underset{\sim}{k}}\ f_c(\underset{\sim}{k}',t)] . \qquad (C2)$$

With b in the light-hole band, Eq. (6a) can be written as

$$\frac{df_\ell(\underset{\sim}{k},t)}{dt} = \frac{1}{2N_h c\hbar\Omega(\underset{\sim}{k})}\ (\frac{d}{dt}\ \underset{\sim}{J}(\underset{\sim}{k})\ \cdot \underset{\sim}{A})$$

$$- \sum_{c\underset{\sim}{k}'} [R_{\ell\underset{\sim}{k}\to c\underset{\sim}{k}'}\ f_\ell(\underset{\sim}{k},t) - R_{c\underset{\sim}{k}'\to \ell\underset{\sim}{k}}\ f_c(\underset{\sim}{k}',t)] . \qquad (C3)$$

Assuming $\underset{\sim}{J}(k)$ and $\underset{\sim}{A}$ have sinusoidal time dependence and averaging over many cycles, one gets the steady rate equations of Eq. (17).

APPENDIX D: THE AUXILIARY FUNCTIONS $F(\underset{\sim}{k})$ AND $G(\underset{\sim}{k})$

In this appendix we describe our treatment of the auxiliary functions $F(\underset{\sim}{k})$ and $G(\underset{\sim}{k})$. From the definition of these functions, we see that when the phonon scattering matrix elements are approximated as independent of the scattering angle, $F(\underset{\sim}{k})$ depends on $E_h(\underset{\sim}{k})$, and $G(\underset{\sim}{k})$ depends on $E_\ell(\underset{\sim}{k})$. Using the definitions of $F(\underset{\sim}{k})$ and $G(\underset{\sim}{k})$ and Eqs. (17) for the distribution functions, $F(E_h(\underset{\sim}{k}))$ is seen to be determined by

$$F(E_h(\underset{\sim}{k})) = \sum_{\underset{\sim}{k}} (-R_{h\underset{\sim}{k}'\to h\underset{\sim}{k}}\, T_h(\underset{\sim}{k}') + R_{\ell\underset{\sim}{k}'\to h\underset{\sim}{k}}\, T_\ell(\underset{\sim}{k}'))$$

$$\times \left[(f_h^e(\underset{\sim}{k}') - f_\ell^e(\underset{\sim}{k}')) + F(E_h(\underset{\sim}{k}'))\, T_h(\underset{\sim}{k}') - G(E_\ell(\underset{\sim}{k}'))\, T_\ell(\underset{\sim}{k}') \right]$$

$$\times \frac{\beta(\underset{\sim}{k}')}{\beta(\underset{\sim}{k}')\,(T_h(\underset{\sim}{k}') + T_\ell(\underset{\sim}{k}')) + 1} \qquad \text{(D1)}$$

$$+ \sum_{\underset{\sim}{k}'} R_{h\underset{\sim}{k}'\to h\underset{\sim}{k}}\, F(E_h(\underset{\sim}{k}'))\, T_h(\underset{\sim}{k}') + \sum_{\underset{\sim}{k}'} R_{\ell\underset{\sim}{k}'\to h\underset{\sim}{k}}\, G(E_\ell(\underset{\sim}{k}))\, T_\ell(\underset{\sim}{k}') \quad ,$$

and $G(E_\ell(\underset{\sim}{k}))$ is determined by a similar equation where $(h\underset{\sim}{k})$ in the scattering rates is replaced by $(\ell\underset{\sim}{k})$. The function $G(\underset{\sim}{k})$ describes the increased (from the equilibrium value) scattering into the light-hole band states. Because of the small density of light-hole band states, the magnitude of this function is much smaller than that of $F(\underset{\sim}{k})$. In addition $T_h(\underset{\sim}{k})$ is much greater than $T_\ell(\underset{\sim}{k})$. Thus in Eq.

(D1), we neglect $T_\ell(\underset{\sim}{k})\ G(\underset{\sim}{k})$ compared with $T_h(\underset{\sim}{k})\ F(\underset{\sim}{k})$. We have explicitly checked the self-consistency of this approximation at the end of the calculation.

Eq. (D1) is an inhomogeneous, linear integral equation. Because of the energy conserving delta functions in the phonon scattering rates, it reduces to algebraic equations relating $F(E_h(k))$ at different values of $E_h(k)$. The term proportional to $R_{\ell\underset{\sim}{k}'\to h\underset{\sim}{k}}\ F(E_h(\underset{\sim}{k}'))$, however, is responsible for coupling the equation for $F(E_h(\underset{\sim}{k}))$ to those for all other values of $E_h(\underset{\sim}{k}')$. (In the other terms, the equation for $F(E_h(\underset{\sim}{k}))$ is only coupled to those for $F(E_h(\underset{\sim}{k})+\hbar\omega_o)$ and $F(E_h(k)-\hbar\omega_o)$). To overcome this difficulty, we approximate the first term on the righthand side of Eq. (D1), which can be written as

$$\sum_{\underset{\sim}{k}'} \left(-R_{h\underset{\sim}{k}'\to h\underset{\sim}{k}}\ T_h(\underset{\sim}{k}') + R_{\ell\underset{\sim}{k}'\to h\underset{\sim}{k}}\ T_\ell(\underset{\sim}{k}')\right) \times \beta(\underset{\sim}{k}')\ (f_h(\underset{\sim}{k}') - f_\ell(\underset{\sim}{k}'))\ ,$$

by

$$X \sum_{\underset{\sim}{k}'} \left(-R_{h\underset{\sim}{k}'\to h\underset{\sim}{k}}\ T_h(\underset{\sim}{k}') + R_{\ell\underset{\sim}{k}'\to h\underset{\sim}{k}}\ T_\ell(\underset{\sim}{k}')\right) \times \beta(\underset{\sim}{k}')\ (f_h(\underset{\sim}{k}') - f_\ell(\underset{\sim}{k}'))^1\ , \qquad (D2)$$

where $(f_h(\underset{\sim}{k}') - f_\ell(\underset{\sim}{k}'))^1$ is the first approximation to $(f_h(\underset{\sim}{k}')-f_\ell(\underset{\sim}{k}'))$; that is, the first term in Eq. (20). Here X is a function of $\hbar\omega$, T and I, but is assumed independent of $E_h(k)$. We determine X by requiring

$$\sum_{\underset{\sim}{k}'} \beta(\underset{\sim}{k}') \; (f_h(\underset{\sim}{k}') - f_\ell(\underset{\sim}{k}')) = X \sum_{\underset{\sim}{k}'} \beta(\underset{\sim}{k}') \; (f_h(\underset{\sim}{k}') - f_\ell(\underset{\sim}{k}'))^1 \quad . \tag{D3}$$

Since scattering to the light-hole band is much slower than scattering to the heavy-hole band (owing to the small density of states in the light-hole band)

$$\sum_{\underset{\sim}{k}} R_{h\underset{\sim}{k}' \to h\underset{\sim}{k}} \; T_h(\underset{\sim}{k}') \simeq \sum_{\underset{\sim}{k}} R_{\ell\underset{\sim}{k}' \to h\underset{\sim}{k}} \; T_\ell(\underset{\sim}{k}') \simeq 1. \tag{D4}$$

Thus Eq. (D3) assures that the integral of the positive and negative parts of Eq. (D2) are separately satisfied. We solve the equations

$$\begin{aligned} F(E_h(\underset{\sim}{k})) = X \sum_{\underset{\sim}{k}'} & [-R_{h\underset{\sim}{k}' \to h\underset{\sim}{k}} \; T_h(\underset{\sim}{k}') + R_{\ell\underset{\sim}{k}' \to h\underset{\sim}{k}} \; T_\ell(\underset{\sim}{k}')] \\ & \times \beta(\underset{\sim}{k}') \; (f_h(\underset{\sim}{k}') - f_\ell(\underset{\sim}{k}'))^1 \\ & + \sum_{\underset{\sim}{k}'} R_{h\underset{\sim}{k}' \to h\underset{\sim}{k}} \; F(E_h(\underset{\sim}{k}')) \; T_h(\underset{\sim}{k}') \quad . \end{aligned} \tag{D5}$$

This is a series of inhomogeneous linear algebraic equations. We truncate the series for $E_h(\underset{\sim}{k}) > 400$ meV. ($F(E_h(\underset{\sim}{k}))$ is negligible for these high energies.) We first find the solution for $X = 1$. Calling the result of this calculation F', F is given by XF'. We determine X from Eq. (D3) which reduces to

$$X = 1 + X\left[\int_{\Omega(\underset{\sim}{k})=\omega} \frac{ds \quad |P_{h\ell}(\underset{\sim}{k})|^2 \, T_h(k) \, F^1(E_h(\underset{\sim}{k}))}{|\nabla_{\underset{\sim}{k}}\Omega(\underset{\sim}{k})|\sqrt{1 + I/\ell(\underset{\sim}{k})}}\right] \Bigg/ \left[\int_{\Omega(\underset{\sim}{k})=\omega} \frac{ds \quad (f_h^e(\underset{\sim}{k}) - f_\ell^e(\underset{\sim}{k})) \, |P_{h\ell}(\underset{\sim}{k})|^2}{|\nabla_{\underset{\sim}{k}}\Omega(\underset{\sim}{k})| \sqrt{1 + I/\ell(\underset{\sim}{k})}}\right] . \tag{D6}$$

In order to limit the numerical expense, we approximate the surface integrals in Eq. (D6) using the four point prescription suggested by Kane [11].

From Eqs. (16) and (D3), we see that the function X relates the absorption coefficient calculated in the first approximation to the result of the more complete calculation by

$$\alpha(I,\omega) = X \, \alpha^1(I,\omega) \quad , \tag{D7}$$

where $\alpha^1(I,\omega)$ is given by Eq. (34).

REFERENCES

1. A. F. Gibson, C. A. Rosito, C. A. Raffo, and M. F. Kimmitt, Appl. Phys. Lett. 21, 356 (1972).
2. C. R. Phipps, Jr., and S. J. Thomas, Opt. Lett. 1, 93 (1977).
3. R. L. Carlson, M. D. Montgomery, J. S. Ladish, and C. M. Lockhart, IEEE J. Quantum Electron. 13, 35D (1977).
4. F. Keilmann, IEEE J. Quantum Electron. 12, 592 (1976).
5. A. J. Alcock and A. C. Walker, Appl. Phys. Lett. 25, 299 (1974).
6. B. J. Feldman and J. F. Figueira, Appl. Phys. Lett. 25, 301 (1974).
7. A. F. Gibson, M. F. Kimmitt, and B. Norris, Appl. Phys. Lett. 24, 306 (1974).
8. M. Kawai and T. Miyakawa, Jap. J. of Appl. Phys., to be published.
9. M. Sargent III, Opt. Commun. 20, 298 (1977).
10. V. L. Komolov, I. D. Yaroshetskii, and I. N. Yassievich, Fiz. Tekh. Poluprovodn. 11, 85 (1977) [Sov. Phys. Semicond. 11, 48 (1977)].
11. E. O. Kane, J. Phys. Chem. Solids 1, 82 (1956).
12. W. Fawcett, Proc. Phys. Soc. 85, 931 (1965).
13. H. B. Briggs and R. C. Fletcher, Phys. Rev. 91, 1342 (1953).
14. A. H. Kahn, Phys. Rev. 97, 1647 (1955).
15. W. Kaiser, R. J. Collins, and H. Y. Fan, Phys. Rev. 91, 1342 (1953).
16. R. Braunstein, J. Phys. Chem. Solids 8, 280 (1959).
17. A. J. Bishop and A. F. Gibson, Appl. Optics 12, 2549 (1973).

18. We neglect off-diagonal terms that can appear in the nonlinear susceptibility tensor for polarized light, and we average over polarizations. That is, we consider the case of unpolarized light.

19. We average the vector potential over all angles.

20. G. Dresselhaus, A. F. Kip, and C. Kittel, Phys. Rev. 98, 368 (1955).

21. J. C. Hensel and K. Suzuki, Phys. Rev. B9, 4219 (1974).

22. P. Lawaetz, Phys. Rev. B4, 3460 (1971).

23. E. Conwell, J. Phys. Chem. Solids 8, 236 (1959).

24. D. M. Brown and R. Bray, Phys. Rev. 127, 1593 (1962).

25. J. D. Wiley, Solid State Commun. 8, 1865 (1970).

26. H. Brooks, Advances in Electronics and Electron Physics (L. Marton, ed.), Vol. 7, p. 85. Academic Press, New York (1955).

27. I. N. Yassievich, and I. D. Yaroshetskii, Fiz. Tekh. Poluprovodn. 9, 857 (1975). [Sov. Phys. Semicond. 9, 565 (1975)].

28. We use the first-order approximation discussed in Section III of this chapter. This approximation was shown to produce results for I_s within 15% of the more complete calculation.

29. See, for example, E. Bergmann, I. Bigio, B. Feldman, and R. Fisher, Opt. Lett. 3, 82 (1978).

30. J. Wynne, Phys. Rev. 178, 1295 (1969).

31. D. E. Watkins, C. R. Phipps, Jr., and S. J. Thomas, Opt. Lett. 5, 248 (1980).

32. See, for example, A. Abragam, The Principles of Nuclear Magnetism (Oxford: Clarendon Press, 1961) p. 272ff.

CHAPTER 3

I. INTRODUCTION

There is active theoretical and experimental interest in saturable absorbers in the 9-11 μm region due to their practical use in CO_2 laser systems [1-4]. The attempts have been to find a material with a large low-intensity absorption coefficient and which saturates at high intensities. The material must be integrable in a beam transport system and should have a high material damage threshold. Several p-type semiconductors should exhibit these desirable properties and in addition have some distinct advantages over gaseous saturable absorbers, such as a picosecond recovery time and a broadband performance under saturation conditions. Most experimental studies on saturable absorption in p-type semiconductors have used samples of p-Ge [4-6,8]. These measurements indicate that p-Ge satisfies the above criteria over the CO_2 laser spectrum; however, other materials should also exhibit similar behavior and may be more promising for certain applications. In this chapter we analyze the systematic dependence of the saturation characteristics on the material parameters and report values of the saturation intensity for the materials considered.

Measurements of the saturable absorption in p-type Ge have been interpreted by fitting the decrease in the absorption coefficient with increasing intensity to the functional form:

$$\alpha(I,\omega) = \frac{\alpha_o(\omega)}{\sqrt{1 + I/I_s(\omega)}} \quad , \tag{1}$$

where $\alpha_o(\omega)$ is the absorption coefficient at low intensity, and $I_s(\omega)$ is the saturation intensity.

In this chapter, we consider the saturation characteristics for two different types of materials: semiconductors with a spin-orbit splitting large compared to the photon energy of the CO_2 laser (as is the case for Ge), and semiconductors with a small spin-orbit splitting compared to the photon energy (as Si). In the first case the split-off hole band is not involved in the optical excitation process. For materials with small spin-orbit splittings, the theory must be modified to include transitions between the heavy- and light-hole bands, the light- and split-off hole bands, and the heavy- and split-off hole bands.

We first present a calculation describing the saturation behavior of materials with spin-orbit splittings large compared to the energy of the incident radiation. Thus, the split-off band is not involved in the optical transition and can be ignored. Some of the materials with large spin-orbit splitting include p-type Ge, GaAs, GaSb, AlSb, InAs, and AlAs. Results for p-Ge have been presented in Chapter 2. The dominant absorption mechanism in each material is assumed to be direct free-hole transitions in which a hole in the heavy-hole band is optically excited into the light-hole band by the absorption of a photon [7]. The absorption due to this mechanism has been shown to saturate at high light intensities for p-Ge [4-6,8]. Other absorption processes at room temperature include lattice absorption, the photoionization

of impurities, and indirect free-carrier transitions. Absorption due to these mechanisms is significantly smaller than direct free-hole absorption for p-Ge [9], p-GaAs[10], p-GaSb[11], p-AlSb[12] and p-InAs [13]. Due to the strong similiarities of AlAs with the other materials considered, we consider the absorption in p-AlAs at 9-11 μm to also be determined by direct heavy- to light-hole band transitions.

The chapter is organized in the following way: In Sec. II we present the results for the absorption saturation of p-GaAs, in Sec. III we present the calculational approach for the other materials with large spin-orbit splittings, in Sec. IV we present the results of the calculation, in Sec. V we modify the calculational approach to understand the saturation behavior of materials with small spin-orbit splittings, in Sec. VI we present the results for these materials with small Δ, and in Sec. VII we summarize our conclusions.

The absorption of light by direct intervalence-band transitions in a volume element of $\underset{\sim}{k}$-space depends on the distribution of holes in the heavy-hole band which can absorb a photon and make a vertical transition to states in the light-hole band. Thus only holes in a narrow region of the heavy-hole band can directly participate in the absorption. Since the high intensity light decreases the population of the free holes in the resonant region of the heavy-hole band, the absorption coefficient is reduced. An expression for the absorption coefficient as a function of the light intensity is given by Eq. (16) of Chapter 2. We first examine the saturation behavior for p-GaAs

since there exists experimental information for this material. A detailed calculation is presented for p-GaAs; later in this chapter, the theory is modified to analyze the saturation characteristics of several other p-type semiconductors.

II. RESULTS AND DISCUSSION FOR p-GaAs

We use the cyclotron resonance parameters of Lawaetz [14] to determine the GaAs valence band structure. (We neglect the small terms linear in k which appear in the $\underset{\sim}{k}\cdot\underset{\sim}{p}$ perturbation theory for zinc-blende crystals.) Hole-phonon scattering is described as in Ge; E_{ac} is taken to be 3.6 eV [15] and E_{op} to be 6.5 eV [15]. The input parameters that we use for GaAs are not as accurately known as those for Ge.

Our calculations of the intensity dependence of the absorption coefficient give a result that is numerically close to the inhomogeneously broadened two-level model result of Eq. (1). In Fig. (1), we compare the calculated result for λ = 10.6 μm and T = 295°K with Eq. (1). As for Ge, the small difference between the calculated result and inhomogeneously broadened two-level model result comes from the second term in Eq. (20) of Chapter 2.

In Fig. (2), we show the theoretical results for $I_s(\omega)$ as a function of photon energy at room temperature. The theoretical results are determined by fitting the expression in Eq. (1) to the calculated

results for $\alpha(I,\omega)$ for intensities between zero and 100 MW/cm^2. The results for $I_s(\omega)$ are qualitatively similar to those for Ge except that $I_s(\omega)$ is uniformly larger in GaAs than in Ge. The values of $I_s(\omega)$ are larger in GaAs than in Ge primarily because the hole-phonon scattering times are shorter in GaAs. The scattering times are shorter in GaAs because the heavy-hole effective mass is larger in GaAs, and as a result the density of final scattering states is larger in GaAs.

Saturation of intervalence-band absorption in p-GaAs has been observed in one experiment in p-GaAs [16]. A saturation intensity of $I_s = 20\pm5$ MW/cm^2 at $\lambda = 10.6$ μm and room temperature was reported. However, these measurements were performed over a relatively small range of incident intensities and were interpreted in terms of a homogeneously (rather than an inhomogeneously) broadened two-level model. If the results had been interpreted in terms of the inhomogeneously broadened two-level model (which we believe would have been more correct), a smaller value of I_s would most likely have been attained.

In Fig. (3), we present the results of a calculation of the temperature dependence of the saturation intensity at $\lambda = 10.6$ μm in p-GaAs. As for Ge, I_s is an increasing function of temperature owing to the increased phonon scattering rates at higher temperature.

Figure 1. Calculated absorption coefficient normalized to its low intensity value as a function of intensity for p-GaAs. The calculations were performed for λ = 10.6 μm and T = 295^{o}K. The inhomogeneously broadened two-level model result with I_s = 22 MW/cm^2 is also shown.

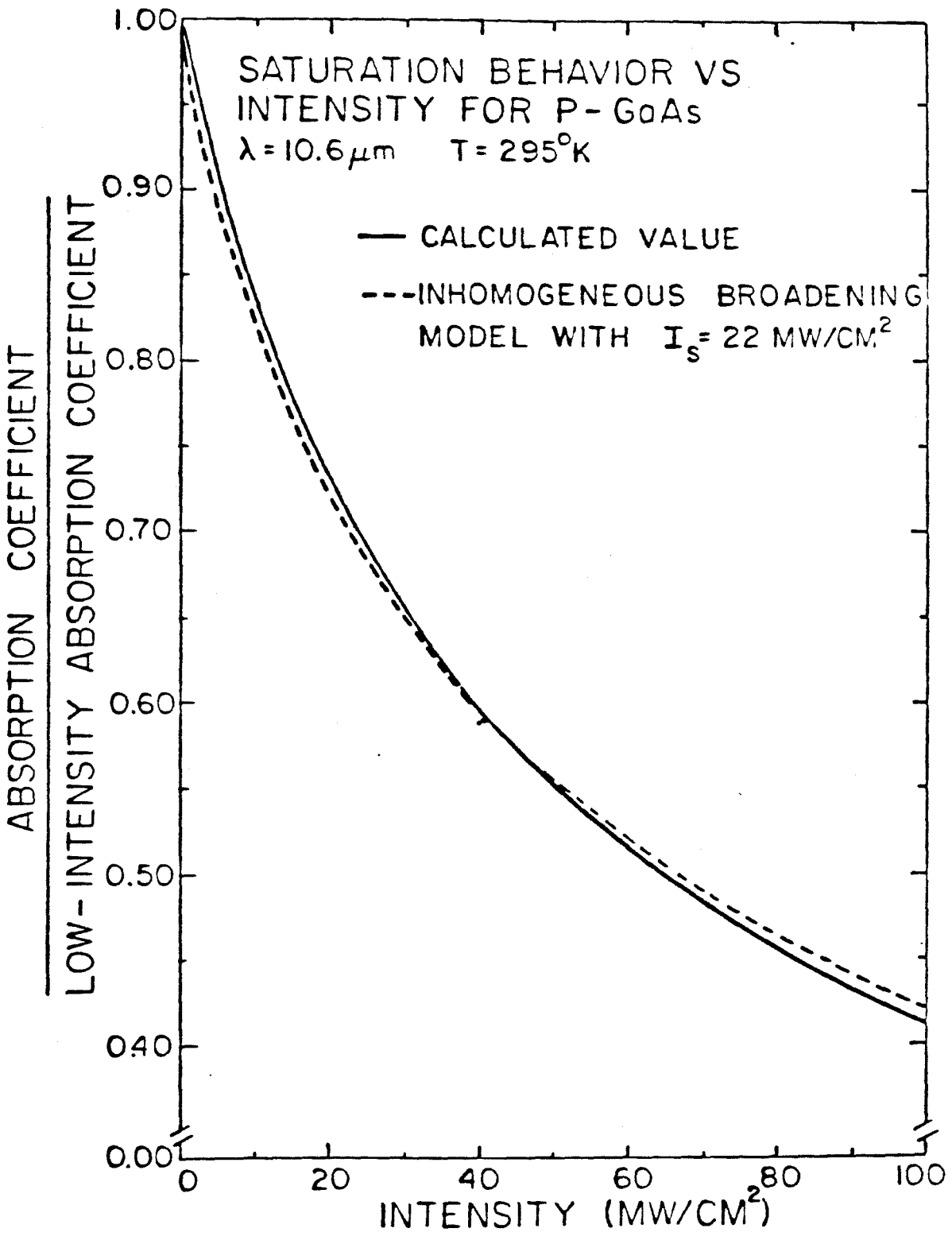
SATURATION BEHAVIOR VS
INTENSITY FOR P-GaAs
λ = 10.6 μm T = 295°K
— CALCULATED VALUE
---INHOMOGENEOUS BROADENING
MODEL WITH I_s = 22 MW/CM.^{2}
ABSORPTION COEFFICIENT
LOW-INTENSITY ABSORPTION COEFFICIENT
1.00
0.90
0.80
0.70
0.60
0.50
0.40
0.00
0
20
40
60
80
100
INTENSITY (MW/CM^2)

Figure 2. Calculated saturation intensity as a function of photon energy for p-GaAs at 295^{o}K.

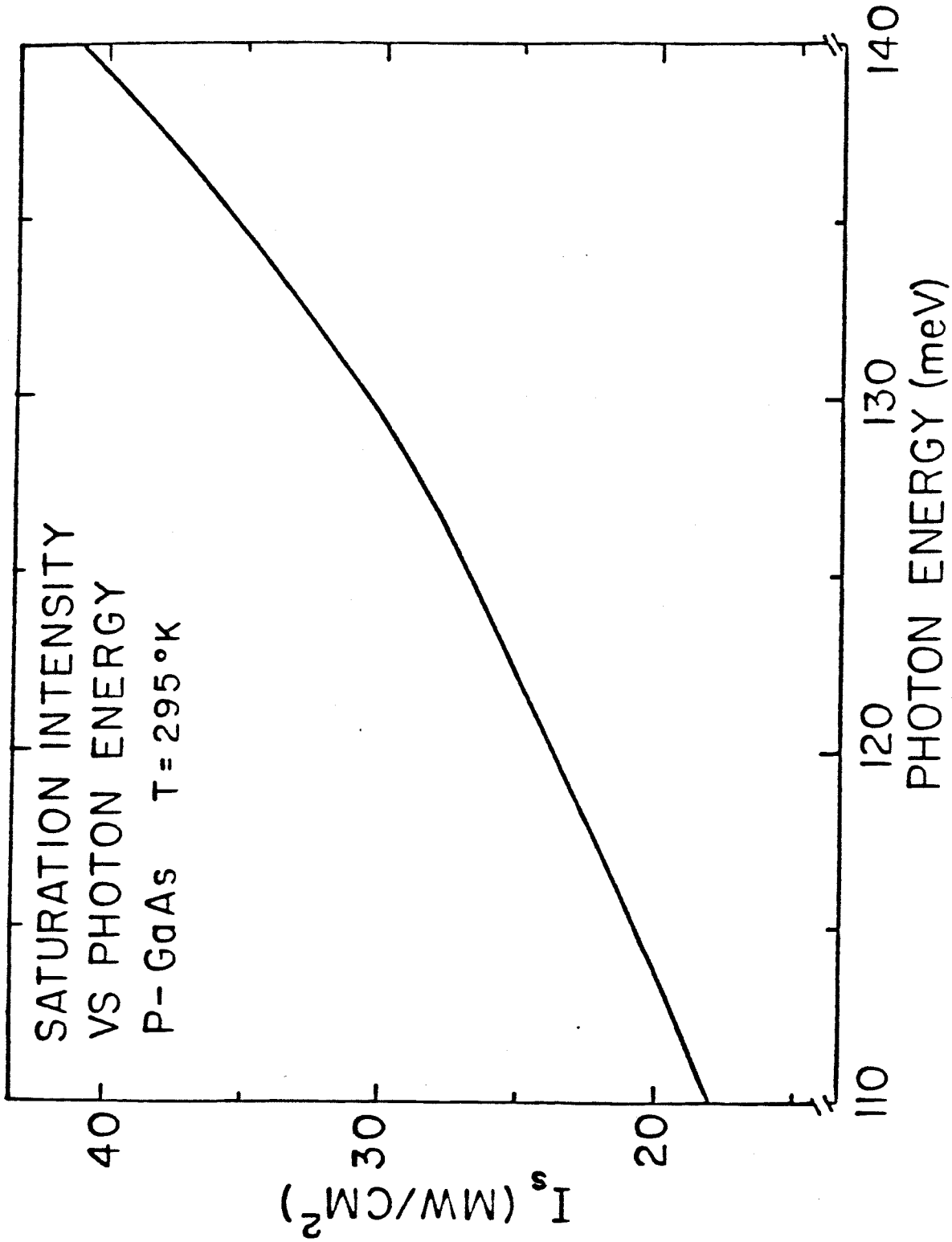
SATURATION INTENSITY
VS PHOTON ENERGY
P-GaAs T=295°K
I_s (MW/CM^2)
40
30
20
110
120
130
140
PHOTON ENERGY (meV)

Figure 3. Calculated saturation intensity as a function of temperature for p-GaAs and light with a wavelength of 10.6 μm.

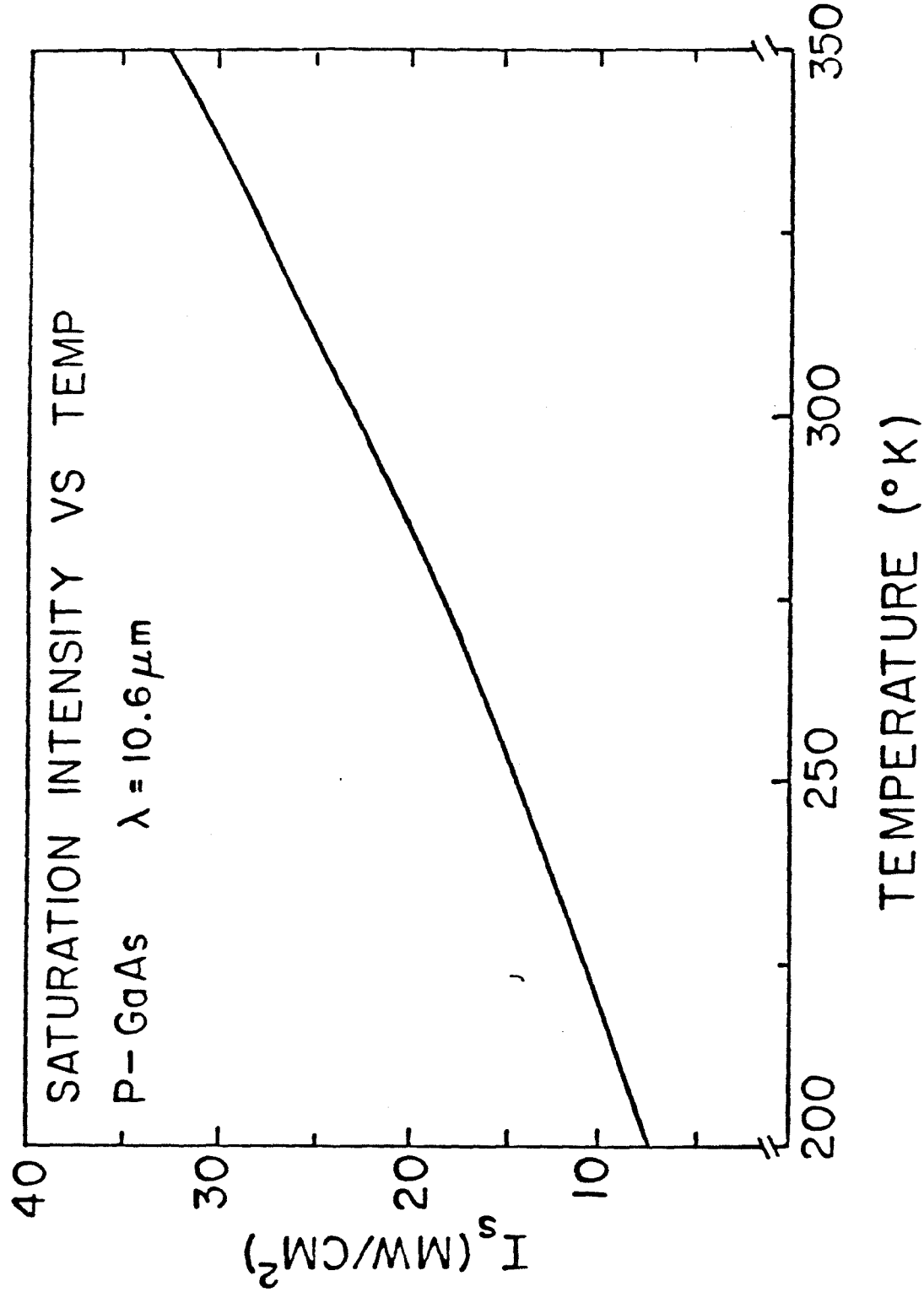
SATURATION INTENSITY VS TEMP
P-GaAs λ = 10.6μm
I_s (MW/CM²)
40
30
20
10
200
250
300
350
TEMPERATURE (°K)

III. CALCULATIONAL APPROACH FOR MATERIALS WITH LARGE SPIN-ORBIT SPLITTINGS

We are not aware of any experimental measurements for p-type GaSb, AlSb, AlAs, or InAs; however, due to the similarities with p-Ge and p-GaAs, we also expect the absorption in these materials to saturate. In order to limit the numerical expense involved in the calculation, we use the first-order calculation for the distribution of hole states in the resonant region of the heavy- and light-hole bands. The first-order calculation which neglects acoustical phonon scattering produces results which are within 15% of the more complex calculation of the saturation intensity for p-Ge and p-GaAs. In this approximation (discussed in Sec. III of Chapter 2), we find that the absorption coefficient as a function of intensity is given by:

$$\alpha(I,\omega) = \frac{4\pi^2}{\sqrt{\epsilon_\infty}\, m^2 \omega c} \frac{N e^2}{3\hbar} \left(\frac{1}{2\pi}\right)^3 \int_{\Omega(\underset{\sim}{k})=\omega} \frac{dS}{|\nabla_{\underset{\sim}{k}} \Omega(\underset{\sim}{k})|} \frac{|P_{h\ell}(\underset{\sim}{k})|^2 (f_h^e(\underset{\sim}{k}) - f_\ell^e(\underset{\sim}{k}))}{\sqrt{1 + 1/\ell(\underset{\sim}{k})}}, \tag{4}$$

where all symbols have previously been defined in Eqs. (6c), (18a), (18b) and (35) of Chapter 2.

In order to calculate the intensity dependence of the absorption coefficient, we must know the scattering rates of the free holes. We consider hole concentrations such that hole-phonon scattering is the dominant scattering mechanism. Following the results of Wiley and DiDomenico [17], we assume the mobility data for the p-type group IV

and III-V semiconductors can be explained by acoustic and non-polar optical scattering. The deformation potential parameters are chosen so that the temperature dependence of the mobility agrees with the experimental results [17-18]. Following Ref. (18), we neglect the angular dependence in the phonon scattering matrix elements and take the scattering rates to be the same function of energy for the heavy- and light-hole bands.

The total mobility is given by

$$\mu = (N_h\mu_h + N_\ell\mu_\ell)/(N_h + N_\ell) \tag{5}$$

where N_h (N_ℓ) is the density of holes in the heavy- (light-) hole band. Following Conwell [19], the scattering rates for acoustical and non-polar optical phonon scattering are given by:

$$\frac{1}{\tau_{ac}} = \frac{2^{1/2}(m_h^*)^{3/2}(k_BT)^{3/2} \times 1/2\ \xi}{\pi\hbar^4} \quad , \tag{6}$$

and

$$\frac{1}{\tau_{op}} = \frac{1}{\tau_{ac}} \{C\,[\,(1 + \frac{\theta}{k_BT})^{1/2} + e^{\theta/T}(1 - \frac{\theta}{k_BT})^{1/2}]\} \quad , \tag{7}$$

where

$$\xi = E_{ac}{}^2/\rho\bar{u}^2 \quad , \tag{8a}$$

$$x = \varepsilon/k_BT \quad , \tag{8b}$$

$$C = 1/2\ \eta(\theta/T)\ (e^{\theta/T} - 1)^{-1} \quad , \tag{8c}$$

and

$$\eta = (E_{op}/E_{ac})^2 \quad . \tag{8d}$$

Here E_{ac} and E_{op} are the deformation potentials for the acoustic and non-polar optical modes, $k_B\theta_L$ is the energy of the zone-center longitudinal optical phonon, ρ is the material density, and $\bar{u}$ is the average sound velocity. Using the results of Ref. (17), we write

$$\mu = \frac{2^{3/2}\pi^{1/2}e\hbar^4}{3m_o^{5/2}k_B^{3/2}}\left(\frac{r+r^{3/2}}{1+r^{3/2}}\right)((m_h^*/m_o)^{5/2}\xi)^{-1}\ S(\theta,\eta,T)\ T^{-3/2} \quad , \tag{9}$$

where

$$r = m_h^*/m_\ell^* \quad , \tag{10a}$$

and

$$S(\theta,\eta,T) = \int_o^\infty \frac{xe^{-x}\,dx}{1 + C\ \ (1+\frac{\theta}{xT})^{1/2} + e^{\theta/T}(1-\theta/xT)^{1/2}} \quad . \tag{10b}$$

In Table I we list the parameters used in calculating the hole scattering rates for the materials considered. In calculating the scattering rates, we follow Ref. (17) and assume $\eta = 4$ in all the materials. By fitting the magnitude of μ at $T = 300^oK$, we obtain ξ

:

as given in Table I. The average effective masses used in determining ξ are given in the table. Using the parameters determined from the fits of the temperature dependence of the mobility, we determine the hole-phonon scattering rate.

IV. RESULTS AND DISCUSSION FOR MATERIALS WITH LARGE SPIN-ORBIT SPLITTINGS

The calculated values of the saturation intensity at room temperature and a photon energy of 117 meV (λ=10.6 μm) for the materials considered are given in Table II. We find that the dependence of I_s on temperature and incident photon energy are qualitatively similar to those for Ge and GaAs. This smooth behavior of I_s near room temperature and over the CO_2 laser spectrum allows one to characterize the saturation behavior by I_s (at E_o = 117 meV and $T_o = 295^oK$) and the slopes $(\partial I_s/\partial E)\big|_{E_o}$ and $(\partial I_s/\partial T)\big|_{T_o}$. Values of the derivative of I_s with respect to photon energy and temperature are given in Table II. For completeness, we include the results for Ge and GaAs.

From Table II, we note a large variation of the saturation intensity for the materials. This large variation of the saturation intensity I_s is due to two factors: (1) the deformation potential parameters and (2) the valence band structures. We discuss the effect on the calculation of I_s on each of the two factors separately.

Using Eq. (6) to determine $1/\tau_{ac}$, we note that large values of $(m_h^*)^{3/2}\xi$ (see Table I) indicate that the coupling of the free holes to

TABLE I. Parameters used in determining the hole-phonon scattering rates. The hole mobility is given at room temperature in units of $[\frac{cm^2}{V\text{-}sec}]$. Values of ξ are given in units of $[\frac{eV^2\text{-}cm\text{-}sec^2}{gm}]$. All symbols are defined in the text.

Material	θ_L (°K)	m_h^*/m_o	m_ℓ^*/m_o	μ	$\xi(\times 10^{-11})$	$\left(\frac{m_h^*}{m_o}\right)^{3/2}\xi(\times 10^{-11})$
GaSb	347 [a]	0.49 [b]	0.046 [b]	1400 [c]	0.94	0.32
AlAs	578 [a]	0.76 [b]	0.15 [b]	200 [d]	3.08	2.04
AlSb	480 [a]	0.94 [b]	0.14 [b]	420 [c]	0.74	0.67
InAs	350 [a]	0.60 [b]	0.027 [b]	460 [c]	1.64	0.76

a. W. Richter, Springer Tracts in Modern Physics 78, Solid-State Physics, ed. by G. Höhler (Springer-Verlag, Berlin 1976), p. 174.

b. P. Lawaetz, Phys. Rev. B4, 3460 (1971).

c. Helmut F. Wolf, Semiconductors (Pergamon Press, Oxford, England, 1971).

d. J. D. Wiley, Semiconductors and Semimetals, ed. by R. K. Willardson and A. C. Beer (Academic Press, New York, 1975), p. 141.

the lattice by acoustical interactions is strong; hence, the scattering rates of the free holes with acoustical phonons is large. A large value of $1/\tau_{ac}$ also indicates a large value of $1/\tau_{op}$ (Eq. (7)) since $1/\tau_{op} \propto 1/\tau_{ac}$. The result of an increase in the scattering rates on the saturation intensity is that higher intensities are required to reduce the free-hole population in the heavy-hole band at the resonant region since the free holes re-route at a faster rate. Consequently, high values of the hole mobility yields small values for the saturation intensity. A comparison of the mobility data at room temperature with I_s can be made using Tables I and II.

One can also present qualitative interpretations of the effect of the valence band structure on the saturation intensity. Small values of I_s are produced when the resonant transition between the heavy- and light-hole bands occurs for small values of k. That is, we predict smaller values of I_s for cases when the heavy- and light-hole band are more split apart in energy for a fixed wavevector $\underset{\sim}{k}$. The reason for this behavior is that intervalence-band resonances for smaller values of k yield smaller values of the hole energies in the two bands at the resonant region. The smaller values for the hole energies involved in the optical excitation yield a smaller density of states for the holes and consequently a smaller scattering rate due to lattice events. The increase in the scattering rates with increasing hole energies is clear from Eqs. (6) and (7).

The effect of the heavy- and light-hole bands on the saturation

TABLE II. Saturation Intensity as a Function of Photon Energy and Temperature. Also included are the band parameters used in the calculation, where Δ is the spin-orbit splitting. Values of I_s are given for $T_o = 295^oK$ and $E_o = 117$ meV.

Material	$m_o(1/m_\ell^* - 1/m_h^*)$	I_s (MW/cm^2)	$\left.\frac{\partial I_s}{\partial E}\right\|_{E_o}$ $\left[\frac{MW}{cm^2}\frac{1}{meV}\right]$	$\left.\frac{\partial I_s}{\partial T}\right\|_{T_o}$ $\left[\frac{MW}{cm^2}\frac{1}{^oK}\right]$	Cyclotron Resonance Parameters	Δ(meV)
Ge	20.4 [d]	3.5 [a]	0.1 [a]	0.03 [a]	Ref. (b)	295. [c]
GaAs	11.9 [d]	18. [a]	0.5 [a]	0.2 [a]	Ref. (d)	340. [e]
GaSb	19.7 [d]	1.8	0.03	0.02	Ref. (d)	770. [e]
AlAs	5.4 [d]	400	9	4	Ref. (d)	280. [f]
AlSb	6.1 [d]	24.	0.4	0.2	Ref. (d)	750. [g]
InAs	35.4 [d]	5.1	0.1	0.05	Ref. (d)	380. [h]

a. Values for Ge and GaAs are taken from Chapters 1 and 2.

b. J. C. Hensel and K. Suzuki, Phys. Rev. B9, 4219 (1974).

c. J. B. Arthur, A. C. Caynham, W. Fawcett, and E. G. S. Paige, Phys. Rev. 152, 740 (1966).

d. P. Lawaetz, Phys. Rev. B4, 3460 (1971).

e. M. Cardona, K. L. Shaklee, and F. H. Pollack, Phys. Rev. 154, 696 (1967).

f. A. Onton, Proc. of the Tenth International Conf. on the Physics of Semiconductors, Cambridge (U. S. Atomic Energy Commission, Springfield, Va., 1970), p. 107.

g. R. Braunstein and E. O. Kane, J. Phys. Chem. Solids 23, 1423 (1962).

h. C. R. Pidgeon, S. H. Groves, and J. Femleib, Solid State Comm. 5, 677 (1967).

characteristics is most easily analyzed by considering the average effective masses for the heavy- and light-hole bands. Smaller values of the saturation intensity are predicted for the larger heavy-hole masses and smaller light-hole masses. That is, for a large heavy-hole mass and a small light-hole mass, the two bands split apart much faster with increasing k, and I_s should be small. This behavior is shown in Table II where we compare calculated values of I_s with $(1/m_\ell^* - 1/m_h^*)$.

The two extreme cases for the saturation intensity are p-GaSb and p-AlAs. GaSb has high hole mobility and a large value of $(1/m_\ell^* - 1/m_h^*)$, both of which contribute to low values of I_s. On the other hand, AlAs has low hole mobility and a low value of $(1/m_\ell^* - 1/m^*)$, both of which contribute to high values of I_s.

The predicted results indicate that the saturation characteristics vary considerably between the different materials considered. Depending on the intended application of the saturable absorber, one has a wide variation on the saturation behavior for a given incident intensity under room temperature conditions. In addition, we predict that one can control the saturation characteristics for a given incident intensity by controlling the temperature of the material.

The theory presented is applicable over a wide range of circumstances for the materials examined. We consider temperatures of the saturable absorber to be about room temperature. The assumption that direct intervalence-band hole transitions dominate the absorption process puts a lower limit on the free-hole concentrations. And the

assumption that hole-impurity and hole-hole scattering rates are small compared to the hole-phonon scattering puts an upper limit on the free-hole concentrations. At present, most saturable absorption experiments on p-type semiconductors are within these limitations. Values of the saturation intensity for carrier concentrations such that hole-impurity and hole-hole scattering mechanisms are comparable to hole-phonon scattering can be calculated using the theory presented in Chapter 2.

The calculations of the saturation intensity require knowledge of the cyclotron resonance parameters and deformation potentials for the materials considered. These input parameters are known much more accurately for Ge than for the other materials. Thus there is larger uncertainty in the predicted values of I_s for these other materials. However, the qualitative dependence of the calculated values of I_s on material parameters should be valid.

V. CALCULATIONAL APPROACH FOR MATERIALS WITH SMALL SPIN-ORBIT SPLITTINGS

In the previous sections we presented the results of a theory describing the saturable absorption of several p-type semiconductors for light having a wavelength in the 9-11 μm region, which corresponds

to the CO_2 laser spectrum. The dominant absorption mechanism is intervalence-band transitions where a free-hole in the heavy-hole band absorbs a photon and makes a direct transition to the light-hole band. Results of the theory have been presented for most of the Group IV and III-V semiconductors for which the spin-orbit splitting was large compared to the energy of the incident photon. However, for materials, such as Si, where the spin-orbit splitting is less than the photon energy, one must generalize the theory to include transitions from the heavy-hole to light-hole band, the heavy-hole to split-off band, and the light-hole to split-off band. In this section,we consider the saturation properties of Si and InP, GaP, and AlP which also have small spin-orbit splittings.

The absorption coefficient for these materials in the 9-11 μm region can be written as

$$\alpha = \alpha_p + \alpha_{h\to\ell} + \alpha_{h\to s} + \alpha_{\ell\to s} \quad , \tag{11}$$

where α_p is the residual absorption due to phonons, $\alpha_{h\to\ell}(\alpha_{h\to s})$ is the absorption coefficient due to direct heavy-hole to light-hole (split-off) band transitions, and $\alpha_{\ell\to s}$ is the absorption coefficient due to direct light-hole to split-off band transitions. The effect of lattice absorption depends on the wavelength of the light and the temperature of the material. Lattice absorption at 9.6 μm requires the cooperation of at least three phonons to conserve energy and is therefore small. In Si, two-phonon absorption is energetically possible for a wavelength

of 10.6 μm. The absorption of light by the creation of phonons can be included in a straightforward way, since this process is nonsaturable and just adds a residual absorption term. In this section, we analyze the saturable absorption due to the direct intervalence-band transitions.

In Section IV of this chapter we have given an expression to determine the decrease in the absorption coefficient with increasing intensity when only the heavy-hole and light-hole bands were involved in the optical transition. Analogous expressions can be written for direct transitions between the heavy-hole and split-off bands and between the light-hole and split-off bands. In order to numerically integrate the expressions for $\alpha_{h\to\ell}$, $\alpha_{h\to s}$ and $\alpha_{\ell\to s}$, we must calculate the steady-state distribution functions in each band as a function of intensity for each wavevector $\underset{\sim}{k}$. If we assume that the three direct optical transitions are uncoupled, then the absorption due to each resonant transition can be independently analyzed. That is, we can determine the saturation characteristics for $\alpha_{h\to\ell}$, $\alpha_{h\to s}$ and $\alpha_{\ell\to s}$ independently using Eq. (4) for $\alpha_{h\to\ell}$ and the analogous expressions for $\alpha_{h\to s}$ and $\alpha_{\ell\to s}$. Here, we assume that the modification in the distribution function of free-holes due to one particular resonant transition between two valence bands in $\underset{\sim}{k}$-space does not strongly affect the distribution of free-holes in the resonant regions for the other transitions. This assumption is made in order to limit the numerical expense involved in the calculation of the distribution functions for each band; however, a more exact calculation can be performed

provided new experimental evidence becomes available to justify the additional complexity in the calculation. We present the calculation to qualitatively characterize the saturation behavior of these materials and determine if the saturation properties are of sufficient interest to warrant additional experimental investigation. The method used for determining the momentum matrix elements $|p_{\sim h\ell}(\underset{\sim}{k})|^2$, $|p_{\sim hs}(\underset{\sim}{k})|^2$, and $|p_{\sim \ell s}(\underset{\sim}{k})|^2$ is described by Kane [20]. The one-hole energies are determined by degenerate $\underset{\sim}{k}\cdot\underset{\sim}{p}$ perturbation theory [20].

The dominant scattering mechanism is hole-phonon scattering for the hole densities we consider. Using the results of Section (III) of the chapter, we choose the deformation potential parameters so that the temperature dependence of the mobility agrees with the experimental results. The values of ξ defined in Eq. (8a) for the materials considered are given in Table III. The values are obtained by assuming $\eta=4$ and fitting the magnitude of the mobility at room temperature [17]. Given the values for the deformation potential parameters, we can write expressions for the scattering rates for acoustical and non-polar optical phonon scattering following Conwell [19]. For the case of lightly doped material near room temperature, ionized impurity scattering and hole-hole scattering can be neglected. For heavier doped material, the effect of these scattering mechanisms can be included in analogy with the results of Section (III) of Chapter 2.

TABLE III. Parameters used in determining the valence band deformation potential parameters. The hole mobility is given at room temperature in units of $\frac{cm^2}{V\text{-}sec}$. Values of ξ are given in units of $\frac{cV^2\text{-}cm\text{-}sec^2}{gm}$.

Material	μ	m_h^*/m_o	m_ℓ^*/m_o	θ	Cyclotron Resonance Parameters	Δ(meV)	$\xi(\times 10^{-11})$
Si	480 [a]	0.53 [b]	0.16 [b]	730 [c]	Ref. (b)	44. [d]	3.71
InP	154 [e]	0.85 [b]	0.089 [b]	498 [c]	Ref. (b)	130. [f]	2.52
GaP	150 [g]	0.79 [b]	0.14 [b]	582 [c]	Ref. (b)	80. [h]	3.59
AlP	450 [i]	0.63 [b]	0.20 [b]	719 [c]	Ref. (b)	50. [b]	2.53

a. J. I. Pankove, Optical Processes in Semiconductors (Dover Publications, New York, 1971), Appendix II.

b. P. Lawaetz, Phys. Rev. B4, 3460 (1971).

c. W. Richter, Springer Tracts in Modern Physics 78, Solid-State Physics, ed. by G. Hohler (Springer-Verlag, Berlin, 1976), p. 174.

d. S. Zwerdling, K. J. Button, B. Lax, and L. M. Roth, Phys. Rev. 118, 975 (1960).

e. M. Glicksman and K. Weiser, J. Phys. Chem. Solids 10, 337 (1959).

f. M. Cardona, K. L. Shaklee, and F. H. Pollack, Phys. Rev. 154, 696 (1967).

g. R. J. Cherry and J. W. Allen, J. Phys. Chem. Solids 23, 163 (1962).

h. P. J. Dean, G. Kaminsky, and R. B. Zettersirom, J. Appl. Phys. 38, 3551 (1967).

i. J. D. Wiley, Semiconductors and Semimetals, ed. by R. K. Willardson and A. C. Beer (Academic Press, New York, 1975), p. 141.

VI. RESULTS AND DISCUSSION FOR MATERIALS WITH SMALL SPIN-ORBIT SPLITTINGS

We numerically integrate the expressions for $\alpha_{h\to\ell}$, $\alpha_{h\to s}$, and $\alpha_{\ell\to s}$, and find that the intensity dependence of the absorption due to each direct transition can be fit to high accuracy by the functional form

$$\alpha_i(I) = \frac{\alpha_{oi}}{\sqrt{1 + I/(I_s)_i}} \quad , \tag{12}$$

where α_{oi} is the low-intensity absorption coefficient and $(I_s)_i$ is the saturation intensity of the i^{th} intervalence-band transition. Values of $(I_s)_{h\ell}$, $(I_s)_{hs}$, and $(I_s)_{\ell s}$ at λ=9.6 μm and T = 295 K are given in Table IV for the materials considered.

Most measurements of the saturable absorption in p-type semiconductors are interpreted in terms of an inhomogeneously broadened two-level model in which the reduction in the absorption coefficient is given by Eq. (1) of this chapter. The absorption coefficient from the sum of the three intervalence-band processes can be reasonably well approximated by Eq. (1) for intensities in the range in which most saturable absorption experiments have been performed ($I \lesssim 100$ MW/cm^2). For intensities low enough that the square roots in Eqs. (1) and (12) can be power series expanded, one has

$$\frac{1}{I_s} = \frac{1}{\alpha_o} \sum_j \frac{\alpha_{oj}}{(I_s)_j} \quad . \tag{13}$$

The values of α_{oj}/α_o for each of the three resonant transitions are listed in Table V. We have taken I_s to fit the result for the sum of the three processes for intensities up to 100 MW/cm^2. We find the saturation intensity to have a smooth behavior near room temperature and λ=9.6 μm (E_o = 129.8 meV). This allows one to describe the saturation near room temperature and near E_o by giving the values of I_s (at E_o = 129.8 meV and T = 295 K) and the slopes $\left.\frac{\partial I_s}{\partial E}\right|_{E_o}$ and $\left.\frac{\partial I_s}{\partial T}\right|_{T_o}$. The values of I_s, $\left.\frac{\partial I_s}{\partial E}\right|_{E_o}$, and $\left.\frac{\partial I_s}{\partial T}\right|_{T_o}$ are given in Table IV.

Values of the saturation intensities in the materials with small spin-orbit splittings are generally larger than the values in materials with larger spin-orbit splittings such as Ge and GaAs. This difference is primarily due to the relatively slow splitting between the valence bands with increasing $|k|$. As a result the resonant optical transitions occur at larger values of $|k|$. As discussed in Chapter 2, this leads to larger scattering rates for the states involved in the transitions and thus large values for the saturation intensity. The deformation potentials and the values of the optical matrix elements also play an important role in determining the value of the saturation intensity as previously discussed in this chapter.

TABLE IV. Parameters describing the saturation characteristics for heavy-hole to light-hole band transitions, heavy-hole to split-off band transitions, and light-hole to split-off band transitions for T_o=295K and E_o = 129.8 meV. Values of the saturation intensity are given due to the cumulative effect of all three direct intervalence band transitions. Also included are the first derivatives of the saturation intensity with respect to photon energy and temperature. All intensities are given in units of MW/cm^2.

Material	$(I_s)_{h\ell}$	$(I_s)_{hs}$	$(I_s)_{\ell s}$	I_s	$\left.\frac{\partial I_s}{\partial E}\right\|_{E_o}\left[\frac{MW}{cm^2}\frac{1}{meV}\right]$	$\left.\frac{\partial I_s}{\partial T}\right\|_{T_o}\left[\frac{MW}{cm^2}\frac{1}{^oK}\right]$
Si	301	127	161	175	3.3	1.7
InP [a]	745	---	97	159	8	1.0
GaP	1900	161	332	229	0.9	2.3
AlP	104	190	215	122	3.1	1.0

a) The h↔s transition in InP is not energetically allowed for this photon energy.

TABLE V. Values of $\frac{\alpha_{oj}}{\alpha_o}$ for transitions between the heavy- and light-hole bands, the heavy- and split-off bands, and the light- and split-off bands. All values are given for a photon energy of 129.8 meV (λ=9.6 μm) and room temperature conditions.

Material	$\frac{(\alpha_o)_{h\leftrightarrow\ell}}{\alpha_o}$	$\frac{(\alpha_o)_{h\leftrightarrow s}}{\alpha_o}$	$\frac{(\alpha_o)_{\ell\leftrightarrow s}}{\alpha_o}$
Si	0.37	0.39	0.24
InP [a]	0.39	----	0.61
GaP	0.14	0.58	0.28
AlP	0.71	0.19	0.10

a) The h↔s transition in InP is not energetically allowed for this photon energy.

VII. SUMMARY AND CONCLUSIONS

We have presented a theory describing the saturation of several p-type semiconductors with spin-orbit splittings large compared to the incident photon energy (such as Ge). The functional form of the decrease in the absorption coefficient with increasing intensity has been predicted, and values of the saturation intensity have been reported as a function of the photon energy and temperature of the material. We have analyzed the systematic dependence of the saturation intensity for the materials considered and found the large variation in values for I_s to be primarily due to the different deformation potential parameters and the different valence band structures. We predict the saturation intensity to be smaller for the materials with high hole mobility and large values of $(1/m_\ell^* - 1/m_h^*)$.

The theory was modified to also include p-type materials with small spin-orbit splittings (such as Si). The calculated values for these materials indicate that they are more difficult to saturate than several p-type semiconductors with large spin-orbit splittings. Thus, it seems likely that materials with large Δ will be more useful in the applications of saturable absorbers to CO_2 laser systems. In addition the residual (non-saturable) absorption is smaller for the materials with large Δ due to their smaller longitudinal optical phonon energy, which is desirable.

REFERENCES

1. A. J. Alcock and A. C. Walker, Appl. Phys. Lett. 25, 299 (1974).
2. D. J. Feldman and J. F. Figueira, Appl. Phys. Lett. 25, 301 (1974).
3. A. C. Walker and A. J. Alcock, Opt. Commun. 12, 430 (1974).
4. C. R. Phipps, Jr. and S. J. Thomas, Optics Lett. 1, 93 (1977).
5. R. L. Carlson, M. D. Montgomery, J. S. Ladish, and C. M. Lockhart, IEEE J. Quant. Electron. QE-13, 35D (1977).
6. F. Keilmann, IEEE J. Quant. Electron. QE-12, 592 (1976).
7. W. Kaiser, R. J. Collins, and H. Y. Fan, Phys. Rev. 91, 1380 (1953).
8. A. F. Gibson, C. A. Rosito, C. A. Raffo, and M. F. Kimmitt, Appl. Phys. Lett. 21, 356 (1972).
9. A. H. Kahn, Phys. Rev. 97, 1647 (1955).
10. R. Braunstein, J. Phys. Chem. Solids 8, 280 (1959).
11. W. M. Becker, A. K. Ramdas, and H. Y. Fan, J. Appl. Phys. 32, 2094 (1961).
12. R. Braunstein and E. O. Kane, J. Phys. Chem. Solids 23, 1423 (1962).
13. F. Matossi and F. Stern, Phys. Rev. 111, 472 (1958).
14. P. Lawaetz, Phys. Rev. B4, 3460 (1971).
15. J. D. Wiley, Solid State Commun. 8, 1865 (1970).
16. A. F. Gibson, C. A. Rosito, C. A. Raffo, and M. F. Kimmitt, Appl. Phys. Lett. 21, 356 (1972).
17. J. D. Wiley and M. DiDomenico, Jr., Phys. Rev. B2, 427 (1970).

18. D. M. Brown and R. Bray, Phys. Rev. 127, 1593 (1962).

19. E. M. Conwell, J. Phys. Chem. Solids 8, 236 (1959).

20. E. O. Kane, J. Phys. Chem. Solids 1, 82 (1956).

CHAPTER 4

I. INTRODUCTION

At room temperature, the absorption spectrum of p-Ge in the wavelength region of 2-25 μm is determined by direct intervalence-band transitions [1]. For light with a wavelength between 5 and 25 μm, the dominant transition occurs between the heavy- and light-hole bands, for wavelengths between 4 and 5 μm the dominant transition occurs between the light- and split-off hole bands; and for wavelengths between 2 and 4 μm the dominant transition occurs between the heavy- and split-off hole bands. For sufficiently high intensities, the heavy- to light-hole transitions have been shown to saturate due to a depletion of the population of holes in the resonant region of the heavy-hole band [2-5]. With a high-intensity pump laser saturating the heavy-to light-hole band transition, the transmission of a low intensity probe resonant between the heavy- and split-off hole bands is altered. If the wavelength of the pump laser is fixed and the wavelength of the probe is tuned, there is a spectral region for the probe in which the two optical transitions are coupled due to their sharing of common initial states in the heavy-hole band (Fig. 1). Those features have been experimentally observed in p-Ge by Keilmann and Kuhl [6]. Here, the rapid relaxation of the excited holes allows both a picosecond switching time and a broad usable bandwidth in the modulation of the probe transmission. In the experiment of Ref. (6), the wavelength of the pump laser was fixed at 9.6 μm and the probe was tuned in wavelength near 3 μm. In this chapter, we present a

Figure 1. Valence band structure of Ge for $\vec{k}$ in the [100] direction. The solid arrow shows the direct hole transitions between the heavy- and light-hole bands induced by light with a wavelength of 10 μm. The dotted arrow shows the direct hole transitions between the heavy- and split-off hole bands induced by light with a wavelength of 3 μm. For this spectral region of the pump and probe beams, the direct intervalence-band transitions are coupled due to a sharing of common initial hole states in the heavy-hole band.

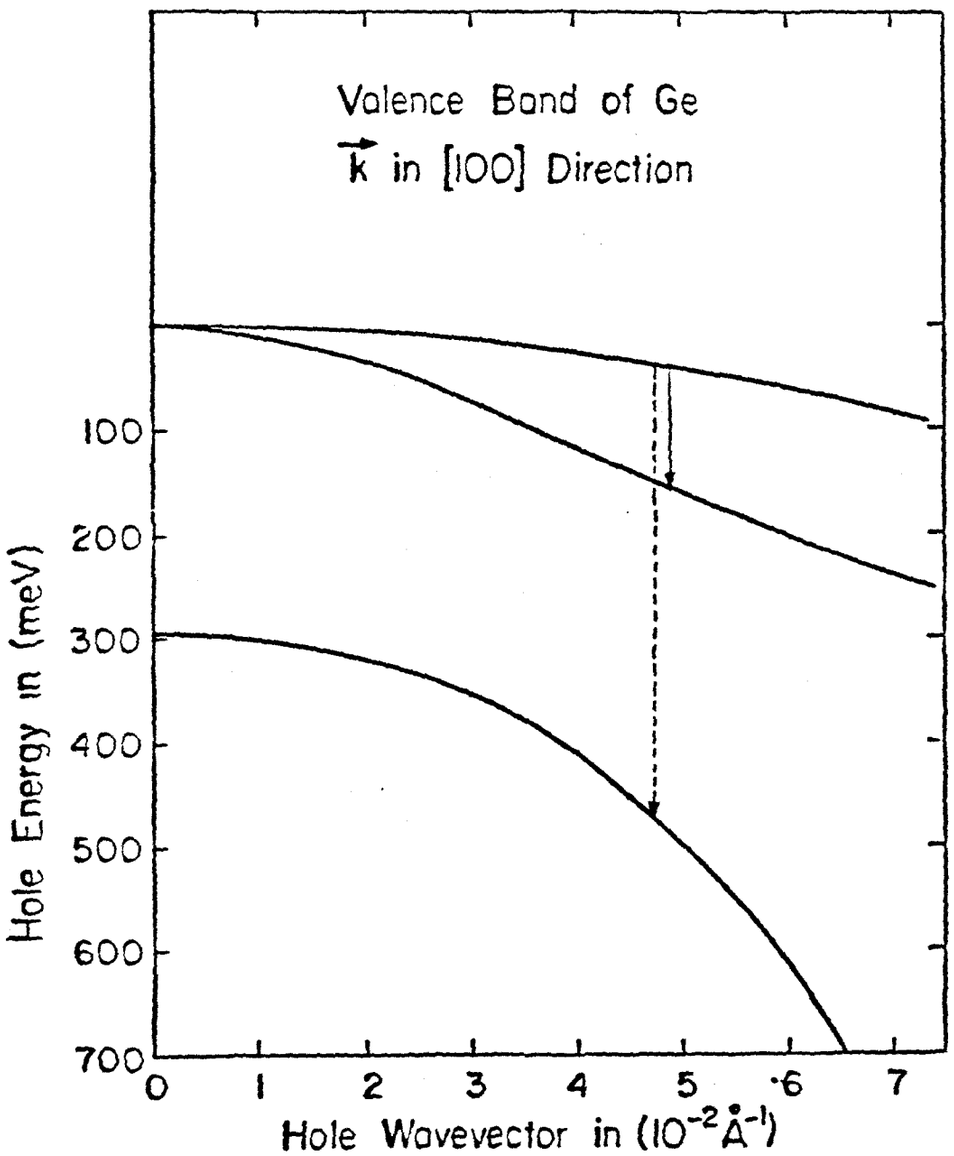
Valence Band of Ge
$\vec{k}$ in [100] Direction
Hole Energy in (meV)
100
200
300
400
500
600
700
0
1
2
3
4
5
6
7
Hole Wavevector in (10^{-2} Å^{-1})

theory describing the enhanced transmission of the 3 μm probe in the presence of the 10 μm pump in p-Ge.

II. THEORETICAL DESCRIPTION

We consider single quantum transitions between the heavy- and light-hole bands due to the pump laser and between the heavy- and split-off hole bands due to the probe. The absorption coefficient of the probe is given by

$$\alpha(I,\omega_2) = \frac{4\pi^2}{\sqrt{\epsilon}m^2\omega_2 c}\frac{N_h e^2}{3}\sum_{\underset{\sim}{k}}[f_h(\underset{\sim}{k})-f_s(\underset{\sim}{k})]|P_{hs}(\underset{\sim}{k})|^2$$

$$\frac{1/(\hbar\pi[T_2(\underset{\sim}{k})]_{hs})}{[\Omega_{hs}(\underset{\sim}{k})-\omega_2]^2+[1/T_2(\underset{\sim}{k})]^2_{hs}} \quad , \qquad (1)$$

where the subscripts h(s) designate the heavy- (split-off) hole band, N_h is the density of holes, I is the intensity of the pump, $\hbar\omega_2$ is the photon energy of the probe beam, ϵ is the dielectric constant, $f_i(\underset{\sim}{k})$ is the probability that a hole state with wavevector $\underset{\sim}{k}$ is occupied in band i, $\Omega_{hs}(k)$ is the angular frequency associated with the energy difference $[\epsilon_h(\underset{\sim}{k}) - \epsilon_s(\underset{\sim}{k})]$ where $\epsilon_i(\underset{\sim}{k})$ is the one-hole energy for a state with wavevector $\underset{\sim}{k}$ in band i, and $|P_{hs}(\underset{\sim}{k})|^2$ is the squared momentum matrix element between the Bloch states in the heavy- and split-off hole bands (summed over the two degenerate states in each band). Here,

$[T_2(\underset{\sim}{k})]_{hs}$ is defined by

$$\frac{2}{[T_2(\underset{\sim}{k})]_{hs}} = \sum_{c\underset{\sim}{k}'} [R_{h\underset{\sim}{k}\rightarrow c\underset{\sim}{k}'} + R_{s\underset{\sim}{k}\rightarrow c\underset{\sim}{k}'}] \quad , \tag{2}$$

where $R_{a\underset{\sim}{k}\rightarrow b\underset{\sim}{k}'}$ is the rate at which a hole in band a with wavevector $\underset{\sim}{k}$ is scattered into a state in band b with wavevector $\underset{\sim}{k}'$.

The dependence of the absorption coefficient on the intensity of the pump laser occurs through the distribution function in the heavy-hole band, $f_h(\underset{\sim}{k})$. We consider the case in which the probe is of sufficiently low intensity that it cannot saturate the transition [7]. Thus we take the distribution in the split-off hole band to be given by the equilibrium value. We calculate the distribution function for the heavy-hole band as a function of the intensity of the pump in the manner of Chapter 2.

The valence band structure of Ge has been calculated by several investigators to various degrees of accuracy [8-10]. The more exact of these calculations is given by Fawcett [8] where the interactions between the valence band and the two neighboring conduction bands are treated exactly rather than by perturbation methods. The result of the calculation indicates that for small k the heavy- and light-hole bands can be adequately described by a simpler calculation given by Kane [9], and that the split-off band is better approximated by a simpler calculation given by Dresselhaus, et al [10]. We calculate the dispersion curves for the heavy- and light-hole bands and the

momentum matrix elements following Kane [9]. The dispersion curve for the split-off band was taken to be

$$\varepsilon_s(k) = -\Delta - Ak^2 - Dk^4 \left[\sin^4\theta \cos^2\phi \sin^2\phi + \sin^2\theta \cos^2\theta\right] , \quad (3)$$

where Δ is the spin-orbit splitting (295 meV), A is a cyclotron resonance parameter, θ and ϕ are the polar and azimuthal angles (relative to a [100] axis), respectively, and D is determined by fitting to the results of Ref. (8) [11]. The angular dependence of the k^4 term in Eq. (3) is suggested by symmetry. The value of D used was 5×10^6 meV-$\text{A}^{\circ 4}$. For the small k region of interest, the fit of Eq. (3) to the results of Ref. (8) is very good. Of course, this result cannot be extended to large values of k. The cyclotron resonance parameters of Hensel and Suzuki [12] were used.

For room temperature conditions, the dominant scattering mechanism is phonon scattering for hole concentrations less than about $3\times10^{15}\text{cm}^{-3}$. For larger concentrations, one should also include the effect of hole-impurity and hole-hole scattering. Here we consider two cases; the low concentration case and the case of a hole concentration of $1.3\times10^{16}\text{cm}^{-3}$ (which corresponds to the experimental conditions in Ref. (6)). The hole-phonon, hole-impurity, and hole-hole scattering rates are treated as in Chapter 2.

III. RESULTS AND DISCUSSION

The calculated values for the absorption coefficient of the probe as a function of the photon energy of the probe are presented in Fig. (2) for a pump wavelength of 9.6 μm. All values of the absorption coefficient at a given photon energy are given relative to the small-signal absorption $\alpha_o(\omega_2)$ at that energy. To indicate the dependence of the absorption of the probe on the intensity of the pump, we plot $\alpha(I)/\alpha_o$ for I = 20,40,60, and 80 MW/cm^2. We note that the transmission of the probe is further enhanced as the pump intensity is increased due to the further depletion of the hole distribution in the resonant region of the heavy-hole band. We also note that for a given intensity and probe energy, values of α/α_o are larger for more heavily doped samples. This occurs because an increase in the hole concentration increases the hole-impurity and hole-hole scattering rates. Thus higher intensities are required to deplete the heavy-hole band population in the more heavily doped material.

The quantity that is presented by the authors of Ref. (6) is

$$\bar{\alpha}/\alpha_o \equiv \ell n\ T/\ell n\ T_o \quad , \tag{4}$$

where T is the transmission with the pump and T_o is the transmission without the pump. Because the intensities of the pump and probe beams change in space on a scale which is long compared with the wavelengths

Figure 2. Calculated spectral response for the absorption in p-Ge of a weak tunable probe in the presence of a saturating pump laser with a wavelength of 9.6 μm. Curves are shown for pump intensities of 20, 40, 60 and 80 MW/cm^2. The top figure illustrates the probe absorption for hole concentrations such that hole-hole and hole-impurity scattering can be neglected compared with hole-phonon scattering. The bottom figure illustrates the probe absorption for a hole concentration of $1.3 \times 10^{16} cm^{-3}$.

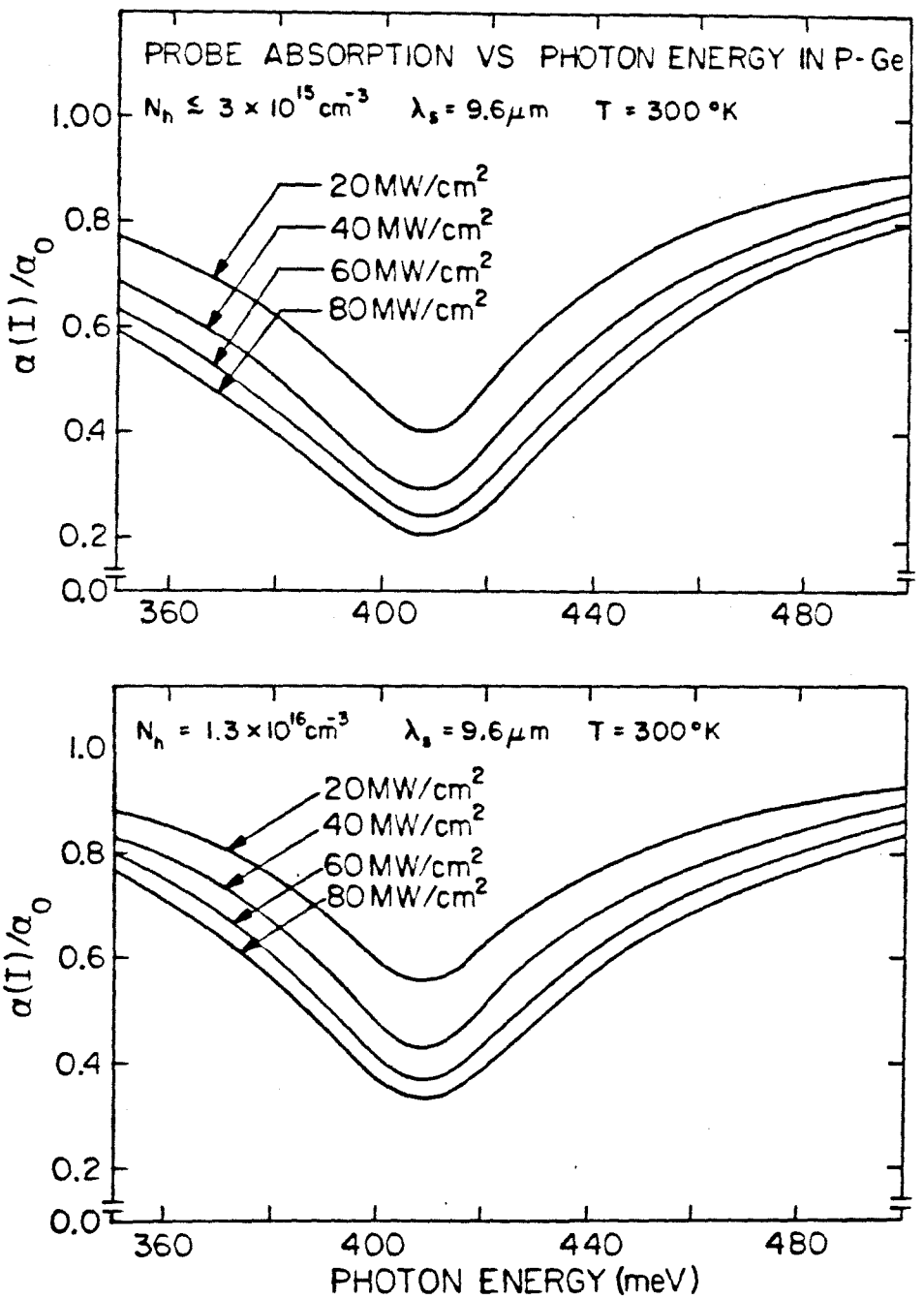
PROBE ABSORPTION VS PHOTON ENERGY IN P-Ge
$N_h \leq 3 \times 10^{15} cm^{-3}$ $\lambda_s = 9.6\mu m$ T = 300 °K
20 MW/cm²
40 MW/cm²
60 MW/cm²
80 MW/cm²
α(I)/α₀
1.00
0.8
0.6
0.4
0.2
0.0
360
400
440
480
$N_h = 1.3 \times 10^{16} cm^{-3}$ $\lambda_s = 9.6\mu m$ T = 300°K
20 MW/cm²
40 MW/cm²
60 MW/cm²
80 MW/cm²
α(I)/α₀
1.0
0.8
0.6
0.4
0.2
0.0
360
400
440
480
PHOTON ENERGY (meV)

of the beams and the carrier mean free paths, this ratio can be written as

$$\bar{\alpha}/\alpha_o = \frac{\ell n \left[\dfrac{\int I_{in}(\rho)\, e^{-\int_o^{\ell} \alpha(I(\rho,z))dz}\, d^2\rho}{\int I_{in}(\rho)\, d^2\rho} \right]}{(-\alpha_o \ell)} \quad . \tag{5}$$

Here z is the direction of propagation of the probe, ρ is the axial dimension of the probe, $I_{in}(\rho)$ is the incident intensity of the probe and ℓ is the sample length. The quantity which we calculate is $\alpha(I)$ (normalized to α_o which is separately calculated). If the experimental geometry was accurately known, it would be straightforward to perform the spatial integrals and make a direct comparison with the experiment but the experimental conditions were not accurately enough defined to make this practical. However, the calculated values of $\alpha(I)/\alpha_o$ account for the main qualitative features of the experimental results.

The experiments of Ref. (6) were done at room temperature with a pump laser at $\lambda = 9.6$ μm and a sample with $N_h = 1.3 \times 10^{16} cm^{-3}$. The intensity of the pump laser was estimated by the authors of Ref. (6) to vary between 80 MW/cm^2 and 7 MW/cm^2 as the beam passed through the absorbing sample. The pump was focused to a Gaussian spot size of

2w = 0.7 mm. The probe entered the sample from the opposite surface and was characterized by an elliptical cross section with 2w = 1.6 mm in the plane of incidence and 0.4 mm perpendicular to it. In addition the pump and probe beams were not colinear. Thus much of the probe was outside of the pumped region. Ideally one would like to have the spot size of the probe to be considerably less than the spot size of the pump. Under these experimental conditions, a dip in $\bar{\alpha}/\alpha_o$ was observed. The dip was centered at a probe energy of 417 meV, the minimum value of $\bar{\alpha}/\alpha_o$ was 0.82 and the FWHM of the dip was about 130 meV.

The calculated values of $\frac{\alpha(I)}{\alpha_o}$ predict the location of the saturation dip center to be at 410 meV, in close agreement with the experimental measurement of 417 meV. The location of the dip can be shifted to higher (lower) probe energies by adjusting the pump to higher (lower) photon energies. This allows a means to tune the maximum transmission of the probe by controlling the wavelength of the pump laser. It has been previously noted that the band structure results of Ref. (8) could account for the position of the dip [13].

Comparing the magnitude of the calculated dip in α/α_o with the experimental results, we see that the calculated values of the dip are larger than was measured. This is to be expected because, as we have previously noted, much of the probe passed through unpumped regions of the sample in the experiment.

The calculated value of the FWHM of the dip in α/α_o varies from about 70 to 110 meV for intensities in the 20-80 MW/cm^2 range. The

lineshape is non-Lorentzian (there is an inner dip in the curve) owing to the convolution of the Lorentzian lineshape of the probe with the hole distribution function in the heavy-hole band. The experimental results indicate a somewhat broader FWHM of about 130 meV. The experimental lineshape is approximately Lorentzian. Some of the discrepancy could be understood if the presence of the calculated inner dip was not experimentally observed owing to the broad frequency settings [14] of the probe used in measuring $\bar{\alpha}/\alpha_o$.

In Ref. (6), it was suggested that a homogeneous linewidth of about 80 meV for the heavy to split-off band transitions is required to account for the measured width of the dip in $\bar{\alpha}/\alpha_o$. This large width requires a hole lifetime in the split-off band of about 0.008 psec. We believe that this is an unphysically small value for the lifetime, and it is inconsistent by almost an order of magnitude with previous estimates [15]. (Theoretically, we find a value of about 0.06 psec.) In our calculations the width of the dip in α/α_o results primarily from band structure effects. Because of anisotropy in the band structure, the energy of the initial heavy-hole state resonant with the pump laser varies with the direction in $\underset{\sim}{k}$-space from about 20 to 60 meV. The energy of the initial heavy-hole state resonant with the probe laser also varies with direction in $\underset{\sim}{k}$-space. As a result, the value of the probe frequency for which the same heavy-hole states are resonant with both optical transitions will change with the particular direction in $\underset{\sim}{k}$-space. Thus anisotropy broadens the dip

in α/α_o compared with the result one would find in a spherical model for the band structure. In addition, the distribution of holes not directly depleted by the pump laser can be depleted by scattering into the depleted regions (Fig. 1 of Ch. 2). Also the curvature of the split-off hole band is greater than that of the heavy-hole band which further broadens the dip.

For semiconductors with the diamond or zincblende crystal structure, the valence band is similar to that of Ge and enhanced transmission of a probe by a saturating pump technique should be observable in these materials as well. As noted in Ref. (13), the location of the saturation dip can serve as a test of electronic band structure calculations. This method has been applied to testing the valence band structure calculations for Ge [13] and good agreement is noted. The results of the experiment are not surprising since the cyclotron resonance parameters are known to high accuracy for Ge. However, accurate cyclotron resonance parameters are not known for many of the III-V semiconductors, and the presence of laser-induced saturation dips should be measurable in many of these materials (as GaAs, AlSb, and InP). Such measurements provide useful information on the valence band structure for materials in which the cyclotron resonance parameters are not as well known as those for Ge.

IV. SUMMARY

We have presented a theory describing the enhanced transmission of a probe due to the presence of a saturating pump. Detailed calculations for p-Ge with a pump laser wavelength of 9.6 μm and probe energies between 350 and 500 meV have been shown. The results of the calculation are qualitatively consistent with existing experimental measurements; however, more experimental information is required for a detailed quantitative comparison.

REFERENCES

1. W. Kaiser, R. J. Collins, and H. Y. Fan, Phys. Rev. 91, 1342 (1953).
2. A. F. Gibson, C. A. Rosito, C. A. Raffo, and M. F. Kimmett, Appl. Phys. Lett, 21, 356 (1972).
3. C. R. Phipps, Jr. and S. J. Thomas, Opt. Lett. 1, 93 (1977).
4. R. L. Carlson, M. D. Montgomery, J. S. Ladish, and C. M. Lockhart, IEEE J. Quantum Electron. 13, 35D (1977).
5. F. Keilmann, IEEE J. Quantum Electron. 12, 592 (1976).
6. F. Keilmann and J. Kuhl, IEEE J. Quantum Electron. 14, 203 (1978).
7. For probe energies in the 360 to 480 meV range, we calculate a saturation intensity at room temperature which varies with photon energy between 35 and 55 MW/cm^2.
8. W. Fawcett, Proc. Phys. Soc. 85, 931 (1965).
9. E. O. Kane, J. Phys. Chem. Solids 1, 82 (1956).
10. G. Dresselhaus, A. F. Kip, and C. Kittel, Phys. Rev. 98, 368 (1955).
11. Using the theory in Ref. (10) to describe the split-off hole band yields Eq. (3) with D = 0.
12. J. C. Hensel and K. Suzuki, Phys. Rev, B9, 4219 (1974).
13. F. Keilmann, Solid State Commun, 25, 451 (1978).
14. The difference between photon energy settings of the probe is about 28 meV in the vicinity of the dip minimum.
15. J. B. Arthur, A. C. Baynham, W. Fawcett, and E. G. S. Paige, Phys. Rev. 152, 740 (1966).

CHAPTER 5

I. INTRODUCTION

Experimental attempts have been made to understand the response of the hole distribution to a high intensity pump laser of fixed wavelength by measuring the transmission of a weak tunable probe also resonant between the heavy- and light-hole bands [1-3]. Here the specific features of the absorption lineshape of the probe beam gives information on the distribution of hole states and fundamental relaxation constants. The absorption coefficient of the probe beam consists of two separate parts. One part is due to the decrease in the distribution of free-holes in the resonant region of the heavy-hole band induced by the saturating beam, and the second part results from the population difference's response to a forcing oscillation at the beat frequency Δ ($\Delta=\omega_+-\omega_-$) for a pump laser with frequency ω_+ and a probe laser with frequency ω_-. The first part can be accurately accounted for in the hole-burning model, while the contribution from the second part depends on the presence of pulsations of the difference in occupation probabilities for states in the resonant region of the heavy- and light-hole bands, which is not accounted for in the hole-burning model. The population pulsations act as a laser-induced grating which can scatter pump photons into the direction of the probe beam with the frequency of the probe, and vice versa. The contribution due to this Raman scattering can have a significant influence on the light transmission as measured along the probe direction. The two contributions to the probe absorption behave differently as the probe frequency ω_-

is detuned from the pump frequency ω_+. The hole-burning contribution has a linewidth as given by the homogeneous linewidth of the resonant transition, whereas the second part is more complex and depends on the dynamic model used to describe the pulsations of the population difference for the states in the resonant region. For cases in which the linewidths of each contribution are significantly different, one expects the existence of a double-dip saturation spectrum for the probe absorption coefficient as a function of the detuning Δ. In this chapter we present a calculation of the composite lineshape of a weak tunable probe beam in p-Ge in the presence of a high-intensity pump beam with a wavelength of 10.6 μm.

Theoretical discussions of the absorption of the probe have been presented for atomic systems with an inhomogeneous frequency distribution resulting from Doppler broadening [4-6]. Inhomogeneously broadened media which are not velocity-induced have also been considered [7-9]. Each of the calculations has analyzed the inadequacies of using only the hole-burning model to describe the probe absorption for several different experimental situations. In this chapter we present a calculation of the absorption lineshape of the probe beam in p-Ge by considering the initial- and final-hole states to form a continuum with the valence band structure determined by second-order degenerate $\underset{\sim}{k}\cdot\underset{\sim}{p}$ perturbation theory. A theoretical discussion of the probe absorption in p-Ge has also been presented; however, the treatment of the carrier relaxation is somewhat different from our calcu-

lational approach [10]. Our calculated results are in good agreement with the experimental measurements [3].

The chapter is organized in the following way: in Sec. II we present our theoretical approach, in Sec. III we give the results for p-Ge, and in Sec. V we summarize our conclusions.

II. THEORETICAL APPROACH

The absorption of light in the 10 μm region by p-type germanium is determined by direct intervalence-band transitions in which a free-hole in the heavy-hole band absorbs a photon and is excited to the light-hole band. For hole concentrations in the 10^{15}-10^{16} cm^{-3} range, the intervalence-band absorption is about two orders of magnitude greater than the other absorption mechanisms. We consider only the direct intervalence-band absorption process in the calculation.

We consider the case in which the medium is subjected to two electromagnetic waves (pump and probe laser beams) propagating along the z-axis and polarized along the same direction. We take the high-intensity pump beam to have a photon energy of $\hbar\omega_+$ and low-intensity probe beam to have a photon energy of $\hbar\omega_-$. The vector potential describing the waves is written as

$$\underset{\sim}{A}(z,t) = \tfrac{1}{2}(A_+ e^{i(\omega_+ t - k_+ z)} + A_- e^{i(\omega_- t - k_- z)})\,\underset{\sim}{\eta} + \text{c.c.}. \qquad (1)$$

We define k_- to be positive for the case of undirectional beams and negative for the case of opposing beams (as is the case in most pump-and-probe experiments).

Evaluating the matrix elements describing the effect of optical excitation (See Eqns. 6a and 6b of Chapter 2), we find that for the heavy- and light-hole bands the band index diagonal elements are determined by

$$\frac{d\sigma_{bb}(\underset{\sim}{k},t)}{dt} = \pm \left[\frac{ieA_+(\Sigma_{bc} \underset{\sim}{\eta}\cdot\underset{\sim}{P}_{bc}(\underset{\sim}{k}))}{2\hbar mc} \left(\sigma_{h\ell}(\underset{\sim}{k}) e^{i(\omega_+ t - k_+ z)} - \sigma_{\ell h}(\underset{\sim}{k})\, e^{-i(\omega_+ t - k_+ z)} \right) \right.$$

$$\left. + \frac{ieA_-(\Sigma_{bc} \underset{\sim}{\eta}\cdot\underset{\sim}{P}_{bc}(\underset{\sim}{k}))}{2\hbar mc} \left(\sigma_{h\ell}(\underset{\sim}{k})\, e^{i(\omega_- t - k_- z)} - \sigma_{\ell h}(\underset{\sim}{k})\, e^{-i(\omega_- t - k_- z)} \right) \right]$$

$$+ \sum_{ck'} R_{ck' \to bk}(\sigma_{cc}(\underset{\sim}{k}') - \sigma^e_{cc}(\underset{\sim}{k}')) - \sum_{ck'} R_{bk \to ck'}(\sigma_{bb}(\underset{\sim}{k}) - \sigma^e_{bb}(\underset{\sim}{k})) , \quad (2)$$

where the (-) sign is for the heavy-hole band and the (+) sign is for the light-hole band. The first terms on the right-hand side give the effect of optical excitation on $\sigma_{bb}(\underset{\sim}{k},t)$ and the remaining terms give the effect of the hole scattering. The off-diagonal elements are determined by (for frequencies near the resonant frequency)

$$\frac{d\sigma_{h\ell}(\underset{\sim}{k},t)}{dt} = \left[i\Omega(\underset{\sim}{k}) - \frac{1}{T_2(\underset{\sim}{k})} \right] \sigma_{h\ell}(\underset{\sim}{k})$$

$$- \left[\frac{ieA_+}{2\hbar mc} e^{-i(\omega_+ t - k_+ z)} + \frac{ieA_-}{2\hbar mc} e^{-i(\omega_- t - k_- z)} \right] (\sigma_{hh}(\underset{\sim}{k}) - \sigma_{\ell\ell}(\underset{\sim}{k})) . \quad (3)$$

Here, $\hbar\Omega(\underset{\sim}{k})$ is the angular frequency associated with the energy

difference $(\varepsilon_h(\underset{\sim}{k}) - \varepsilon_\ell(\underset{\sim}{k}))$ where $\varepsilon_i(\underset{\sim}{k})$ is the energy of the hole with wavevector $\underset{\sim}{k}$ in band i.

Since we are interested in the case for $(A_+ >> A_-)$, we write the one-hole density matrix as a perturbation expansion in the probe field magnitude:

$$\sigma(\underset{\sim}{k},t) = \sigma^{(0)}(\underset{\sim}{k},t) + \sigma^{(1)}(\underset{\sim}{k},t)\, A_- + \sigma^{(2)}(\underset{\sim}{k},t)\, A_-^2 + \ldots \qquad (4)$$

where $\sigma^{(0)}(\underset{\sim}{k},t)$ describes the one-hole density matrix subject to the high-intensity pump laser but with no probe laser, and $\sigma^{(1)}(\underset{\sim}{k},t)$ is the modification of $\sigma(\underset{\sim}{k},t)$ due to the presence of the probe beam (to first order in the probe field strength). The function $\sigma^{(0)}(\underset{\sim}{k},t)$ is used in Ch. 2 to compute the hole distribution function with no probe laser present. For small probe intensities, we consider $\sigma(\underset{\sim}{k},t)$ up to first-order in the field strength of the probe in our calculation of the probe absorption coefficient. For values of A_- such that $(A_+ \sim A_-)$ the calculational approach must be modified to include the higher terms in the perturbation.

We now expand $\sigma^{(i)}(k,t)$ for the heavy- and light-hole bands in a Fourier series of the form (for i = 0,1,2)

$$\sigma_{bb}^{(i)}(\underset{\sim}{k},t) = \sum_{mnp} \alpha_{bmnp}^{(i)}\, e^{i(mk_+ - nk_-)z}\, e^{ip\Delta t} \qquad (5a)$$

and

$$\sigma_{h\ell}^{(i)}(\underset{\sim}{k},t) = \sum_{mnp} \gamma_{mnp}^{(i)} e^{i(mk_+ - nk_-)z} e^{ip\Delta t} e^{-i(\omega_+ t - k_+ z)} . \qquad (5b)$$

In the band index diagonal matrix elements, we take into account the presence of a pulsation in the population of free holes in the resonant region due to a forcing oscillation at the beat frequency Δ ($\Delta=\omega_+-\omega_-$). This population pulsation is due to a nonlinear coupling of the free-hole distribution to the two laser beams with frequencies ω_+ and ω_-. The The simpler form for the time dependence of $\sigma_{h\ell}(\underset{\sim}{k},t)$ results from neglecting off-resonant components of the electromagnetic field which involve higher-order oscillations in the coupling of the two beams, such as the effect of second harmonic or frequency addition type oscillations. The spatial Fourier expansion is introduced to account for the spatial variation of the two fields with wavevectors k_+ and k_-.

The zeroth order solution to $\sigma(\underset{\sim}{k},t)$ (i.e., for $A_- = 0$) has previously been investigated in Chapter 2. For states in the resonant region, we calculated the hole distribution by considering only optical phonon scattering for states in the heavy-hole band and assuming that the rate at which free-holes are scattered into the states in the resonant region is given by the equilibrium value. In this approximation,

$$\sigma_{hh}^{(0)}(\underset{\sim}{k}) - \sigma_{\ell\ell}^{(0)}(\underset{\sim}{k}) = \frac{\sigma_{hh}^{e}(\underset{\sim}{k}) - \sigma_{\ell\ell}^{e}(\underset{\sim}{k})}{1 + \beta(\underset{\sim}{k})\,(T_h(\underset{\sim}{k}) + T_\ell(\underset{\sim}{k}))} , \qquad (6)$$

where all symbols have been previously defined by Eqs. (17c),(18a) and (18b) of Chapter 2.

The off-diagonal term is given by

$$\sigma^{(0)}_{h\ell}(\underset{\sim}{k},t) = \gamma^{(0)}_{000}(\underset{\sim}{k},t)\, e^{-i(\omega_+ t - k_+ z)} \quad , \tag{7}$$

where

$$\gamma^{(0)}_{000}(\underset{\sim}{k},t) = \frac{-ieA_+}{2\hbar mc}\left(\sum_{bc} \underset{\sim}{\eta}\cdot\underset{\sim}{P}_{bc}(\underset{\sim}{k})\right)\left(\sigma^{e}_{hh}(\underset{\sim}{k}) - \sigma^{e}_{\ell\ell}(\underset{\sim}{k})\right)\frac{[1/T_2(\underset{\sim}{k}) - i(\Omega(\underset{\sim}{k})-\omega_+)]}{[\Omega(\underset{\sim}{k})-\omega]^2 + 1/(T_2(\underset{\sim}{k}))^2[1+I/\ell(\underset{\sim}{k})]}, \tag{8}$$

and $\ell(\underset{\sim}{k})$ is defined by Eq. (35) of Chapter 2 [11].

Here, $\sigma^{e}_{hh}(\underset{\sim}{k})$ [$\sigma^{e}_{\ell\ell}(\underset{\sim}{k})$] is defined to be the one-hole density matrix in thermal equilibrium. The imaginary part of $\gamma^{(0)}_{000}(\underset{\sim}{k},t)$ can be related to the absorption coefficient of the pump by performing the integration over all $\underset{\sim}{k}$-space.

We now examine the solution of $\sigma(\underset{\sim}{k},t)$ to first-order in the probe field strength. Using the calculated values of $\sigma^{(0)}(\underset{\sim}{k},t)$ above, we can use Eqs. (2), (3) and (5) to write expressions for $\sigma^{(1)}(\underset{\sim}{k},t)$, which can be related to the probe absorption coefficient (details in Appendix A).

The term proportional to $\mathrm{Re}(\Xi(\underset{\sim}{k}))$ in Eq. (A7) describes the effect of the non-linear coupling of the pump and probe beams. This contribution results from the response of the free-holes to the component in the hole distribution which oscillates at the beat frequency Δ. This modulation of the hole distribution leads a small amplitude modulation of the strong

pump field and to the appearance of an additional signal at the frequency of the probe field, and consequently to the additional term in the probe absorption coefficient. For the beat frequency much less than $1/T_h(\underset{\sim}{k})$ and $1/T_\ell(\underset{\sim}{k})$, the contribution due to the coupling of the pump and probe is approximately equal to the contribution predicted from the hole-burning model. As the beat frequency Δ is increased by detuning so that Δ is comparable with the scattering rates for holes in the resonant region of the heavy- and light-hole bands, the contribution from this additional signal is decreased. And for Δ much greater than the scattering rates for the initial and final hole states, the hole distribution cannot follow the variation in the forcing frequency Δ and the additional contribution to the absorption coefficient becomes vanishingly small.

The other term in the absorption coefficient of the probe is due to the modification of the free-hole distribution in the presence of the high-intensity pump beam. The absorption coefficient of the probe would be determined entirely from this term if one neglects the coupling of the two electromagnetic fields. Here, the intensity dependence is completely contained in the distribution functions $f_h^o(\underset{\sim}{k})$ and $f_\ell^o(\underset{\sim}{k})$. This contribution is analogous to the hole-burning response of a Doppler broadened gaseous medium by a saturating beam.

We now examine the difference in the one-hole occupation probabilities $(f_h(\underset{\sim}{k}) - f_\ell(\underset{\sim}{k}))$ for states in the resonant region for the pump and probe

optical transitions. In the absence of the probe wave, the population difference is given by $(f_h^o(\underset{\sim}{k}) - f_\ell^o(\underset{\sim}{k}))$. The distribution functions $f_h^o(\underset{\sim}{k})$ and $f_\ell^o(\underset{\sim}{k})$ are calculated in the manner of Chapter 2. The difference in the one-hole occupation probabilities is modified when the probe field is taken into account. To lowest order in the probe field,

$$\sigma_{hh}(\underset{\sim}{k}) - \sigma_{\ell\ell}(\underset{\sim}{k}) = (\alpha^{(0)}_{h000}(\underset{\sim}{k}) - \alpha^{(0)}_{\ell 000}(\underset{\sim}{k}) + A_-[(\alpha^{(1)}_{h11-1}(\underset{\sim}{k}) - \alpha^{(1)}_{\ell 11-1}(\underset{\sim}{k})) \times e^{[-i(k_+ - k_-)z - \Delta t]} + c.c.\ ] \quad , \tag{9}$$

which yields a term in $(f_h(\underset{\sim}{k}) - f_\ell(\underset{\sim}{k}))$ which oscillates at the beat frequency. The spatial dependence of the second term is such that for fixed time, there exists a periodic variation in the one-hole occupation probabilities. Using Eqs. (2), (3) and (5), we solve for $(\alpha^{(1)}_{h11-1}(\underset{\sim}{k}) - \alpha^{(1)}_{\ell 11-1}(\underset{\sim}{k}))$ to determine the beat frequency oscillation of the population difference as a function of the frequencies of the pump and probe and the intensity of the pump.

There exists a d.c. component in $(\sigma_{hh}(\underset{\sim}{k}) - \sigma_{\ell\ell}(\underset{\sim}{k}))$ which is second-order in the probe field. The second-order d.c. component is given by the following system of equations:

$$[1/T_h(\underset{\sim}{k})]\alpha^{(2)}_{h000}(\underset{\sim}{k}) + \frac{ieA_+}{2mc\hbar}(\Sigma_{bc}\, \underset{\sim}{\eta}\cdot\underset{\sim}{P}_{bc})(\gamma^{(2)}_{000}(\underset{\sim}{k}) - \gamma^{(2)*}_{000}(\underset{\sim}{k})) = \frac{-ie}{2mc\hbar}(\Sigma_{bc}\, \underset{\sim}{\eta}\cdot\underset{\sim}{P}_{bc})(\gamma^{(1)}_{-1-11}(\underset{\sim}{k}) - \gamma^{(1)*}_{-1-11}(\underset{\sim}{k})) \quad , \tag{10a}$$

$$[1/T_\ell\ (\underset{\sim}{k})]\alpha^{(2)}_{\ell 000}(\underset{\sim}{k}) - \frac{ieA_+}{2mc\hbar}\ (\Sigma_{bc}\ \underset{\sim}{\eta}\cdot\underset{\sim}{P}_{bc})(\gamma^{(2)}_{000}(\underset{\sim}{k})-\gamma^{(2)*}_{000}(\underset{\sim}{k}))$$

$$= \frac{ie}{2mc\hbar}\ (\Sigma_{bc}\ \underset{\sim}{\eta}\cdot\underset{\sim}{P}_{bc})(\gamma^{(1)}_{-1-11}(\underset{\sim}{k})-\gamma^{(1)*}_{-1-11}(\underset{\sim}{k})) \quad , \tag{10b}$$

and

$$[1/T_2(\underset{\sim}{k})+i(\Omega-\omega_+)]\ \gamma^{(2)}_{000}(\underset{\sim}{k}) + \frac{ieA_+}{2mc\hbar}\ (\Sigma_{bc}\ \underset{\sim}{\eta}\cdot\underset{\sim}{P}_{bc})(\alpha^{(2)}_{h000}(\underset{\sim}{k})-\alpha^{(2)}_{\ell 000}(\underset{\sim}{k}))$$

$$= \frac{-ie}{2mc\hbar}(\Sigma_{bc}\ \underset{\sim}{\eta}\cdot\underset{\sim}{P}_{bc})(\alpha^{(1)}_{h11-1}(\underset{\sim}{k})-\alpha^{(1)}_{\ell 11-1}(\underset{\sim}{k})) \quad . \tag{10c}$$

The d.c. population difference (for $\Delta\neq 0$) correct to second-order in the field strength of the probe is given by

$$(\sigma_{hh}(\underset{\sim}{k}) - \sigma_{\ell\ell}(\underset{\sim}{k}))_{d.c.} = (\alpha^{(0)}_{h000}(\underset{\sim}{k})-\alpha^{(0)}_{\ell 000}(\underset{\sim}{k})+A_-^2(\alpha^{(2)}_{h000}(\underset{\sim}{k})-\alpha^{(2)}_{\ell 000}(\underset{\sim}{k})), \tag{11}$$

where

$$(\alpha^{(2)}_{h000}-\alpha^{(2)}_{\ell 000}) = \frac{-ieA_+}{2mc\hbar}(\Sigma_{bc}\ \underset{\sim}{\eta}\cdot\underset{\sim}{P}_{bc})(T_h+T_\ell)(\gamma^{(2)}_{000}-\gamma^{(2)*}_{000})$$

$$\frac{-ie}{2mc\hbar}(\Sigma_{bc}\ \underset{\sim}{\eta}\cdot\underset{\sim}{P}_{bc})(T_h+T_\ell)(\gamma^{(1)}_{-1-11}-\gamma^{(1)*}_{-1-11}) \quad . \tag{12}$$

This term represents the effect of the probe field on the optical transition rate between states in the heavy- and light-hole bands. We find that the change in the absorption of the probe due to the nonlinear coupling of the two beams can be explained by accounting for

$(\alpha^{(2)}_{h000}(\underset{\sim}{k}) - \alpha^{(2)}_{\ell 000}(\underset{\sim}{k}))$, which produces a small change in the rate of energy absorption of the pump.

We proceed to calculate the absorption coefficient of the probe and to analyze the quantities which describe the nonlinear coupling of the pump and probe beams.

III. RESULTS AND DISCUSSION OF THE CALCULATION

We calculate the lineshape for the absorption coefficient of the probe beam in the presence of a high-intensity pump laser by numerically integrating Eq. (A7). We consider the case in which the pump laser is at a fixed wavelength and the probe can be tuned in wavelength in the vicinity of the resonant region of the pump. The probe absorption coefficient is calculated for a pump laser at 10.6 μm ($\hbar\omega$ = 117 meV), since experimental information exists for this case; however, the theory presented can be applied for other pump and probe wavelengths. Using Eq. (A7) we calculate $\alpha(I)/\alpha_o$ versus the photon energy of the probe. All values of the absorption coefficient at a given probe energy are given relative to the small-signal absorption coefficient α_o at that energy. The calculation was performed for room temperature conditions. To indicate the dependence of the absorption coefficient of the probe on the intensity of the pump, values of $\alpha(I)/\alpha_o$ are calculated for several pump intensities. We find that the absorption coefficient of the probe is further decreased as the pump intensity is

increased. This is due to further depletion of the pertinent states in the resonant region of the heavy-hole band.

The experiments of Ref. (3) were done at room temperature with a high-intensity laser at λ = 10.6 μm and a sample with $N_h = 7.1 \times 10^{15} cm^{-3}$. The polarization directions were parallel for the pump and probe waves. The saturator and probe were in approximately opposite directions, with the saturator being 16^o out of the probe's plane of incidence. The intensity of the saturating beam was estimated by the author to be 11 and 95 MW/cm^2 at its center just inside the sample. However, there is a note added in proof where the authors have questioned the calibration of their detectors in measuring the beam intensities. Since the intensity of the pump is not known in the measurements, we choose to test our calculated results with these measurements by fitting the pump intensity so that the magnitude of the absorption reduction at $\Delta = 0$ be the same as the measured magnitude of the absorption dip. This requires that the pump intensity be considerably less than the intensity approximated in Ref. (3); however, these lower intensities are more consistent with other measurements of the saturation characteristics of p-type germanium [12-14]. Without accurate knowledge of the experimental beams, a detailed comparison of the dip magnitude is not possible. The experimental results of Ref. (3) are also shown in Fig. (1), together with the calculated values of $\alpha(I)/\alpha_o$ for pump intensities of 0.48 and 2.0 MW/cm^2. We find good agreement with the measured results.

Figure 1. Probe absorption versus photon energy of the probe in p-Ge for a pump laser at 10.6 μm (117 meV) and room temperature conditions. The top line shows the calculated values of $\alpha(I)$ $\alpha(I)/\alpha_o$ for a pump intensity of 0.48 MW/cm^2 and the bottom line shows the calculated values for a pump intensity of 2.0 MW/cm^2. The experimental data were taken from Ref. (3).

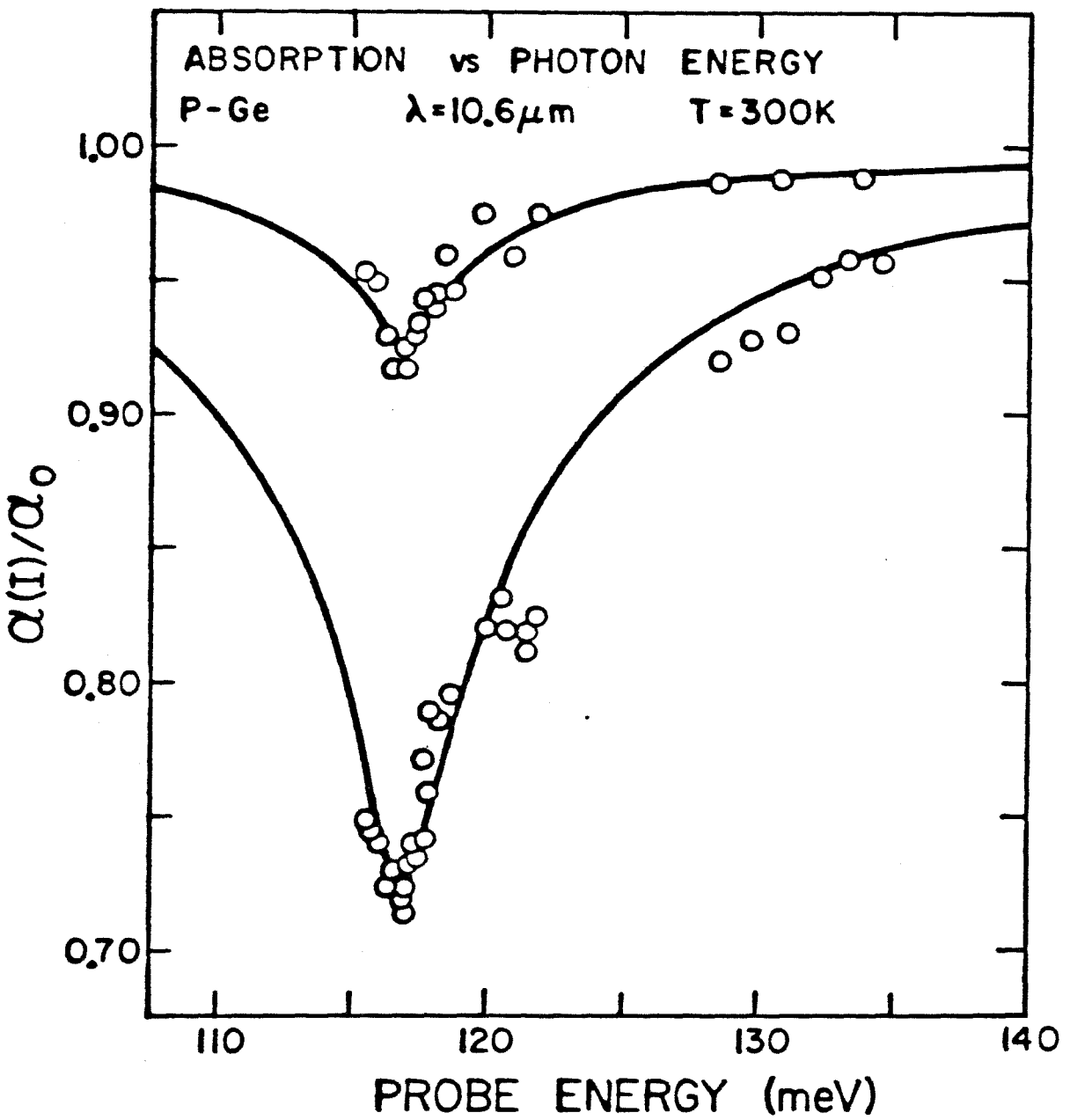
ABSORPTION vs PHOTON ENERGY
P-Ge λ=10.6μm T=300K
1.00
0.90
0.80
0.70
α(I)/α₀
110
120
130
140
PROBE ENERGY (meV)

The absorption lineshape of the probe in non-Lorentzian owing to the effect of the two separate contributions to $\alpha(I)$. The hole-burning contribution accounts for most of the broadness in $\alpha(I)/\alpha_o$ where the width is determined by the homogeneous linewidth of the transition. The shape of $\alpha(I)/\alpha_o$ from this term results from convoluting the Lorentzian lineshape of the probe with the hole distribution in the heavy- and light-hole bands as modified by the high-intensity pump. The other contribution is due to the nonlinear coupling of the pump and probe fields as previously discussed. Due to the coupling of the two electromagnetic fields, there exists a temporal and spatial modulation in the distribution of hole states in the resonant region. This Raman type modulator oscillates at the beat frequency of the two waves with a spatial variation determined by $(k_+-k_-)z$. This modulator can scatter light from the pump beam into the direction of the probe beam with the frequency of the probe photons, and vice versa. These population pulsations are treated in a microscopic picture; however, one can get an understanding of the coupling of the beams by considering the scattering to be due to a diffraction grating formed from a periodic variation in the index of refraction. The intensity resulting from the two fields at ω_+ and ω_- is given by

$$I = I_+ + I_- + 2\sqrt{I_+ I_-}\cos(\Delta t-(k_+-k_-)z+(\phi_+-\phi_-)) \qquad (13)$$

where I_+ (I_-) is the pump (probe) intensity, and ϕ_+ (ϕ_-) is the phase associated with the pump (probe) field. That is, there exists a term

in the total intensity due to the interference of the two waves which oscillates at the beat frequency and has a spatial variation given by $(k_+ - k_-)z$. And since the index of refraction is a function of intensity from nonlinear effects [15-16], we see that the index of refraction can be modulated with the same spatial and temporal dependence provided the medium can respond to the forcing oscillation at the beat frequency Δ. Otherwise, an averaged intensity is seen and the modulation of the index of refraction is averaged out. For Δ comparable to $1/T_h$ $1/T_\ell$, there exists a periodic variation in the index of refraction which can transfer some of the saturating wave into the probe or vice versa. For beat frequencies small compared to the reciprocal lifetimes of the initial and final hole states, energy is transferred from the pump to the probe and the absorption coefficient of the probe is reduced. And as Δ is increased so that it is much greater than $1/T_h$ and $1/T_\ell$, there is a small energy transfer from the probe to the pump so that there is a small increase in the probe absorption coefficient at these wavelengths.

The correction to the hole-burning model is contained in the factor $[1 - I_+/\ell(\underset{\sim}{k})\ \mathrm{Re}(\Xi(\underset{\sim}{k}))]$ in Eq. (A7). In Fig. (2) we show the results for this factor versus the energy separation between the heavy- and light-hole bands for $\underset{\sim}{k}$ in the [111] and [100] directions and Δ=0. The calculated values are for intensities of 0.48 and 2.0 MW/cm^2. The dependence of $\mathrm{Re}(\Xi(\underset{\sim}{k}))/\ell(\underset{\sim}{k})$ in Fig. (2) is contained in the $\underset{\sim}{k}$-dependence of the one-hole energies, momentum matrix elements and hole scat-

Figure 2. Variation of the factor $(1-I_+/\ell(\underset{\sim}{k})\ \mathrm{Re}\Xi)$ in $\underset{\sim}{k}$-space for $\underset{\sim}{k}$ in the [111] and [100] directions and the pump and probe beams fixed at 10.6 μm. The values of the factor are shown as a function of the energy separation $\hbar\Omega(\underset{\sim}{k})$ for states in the heavy- and light-hole bands. The dashed (solid) curve shows the calculated values for a pump intensity of 0.48 MW/cm^2 (2.0 MW/cm^2).

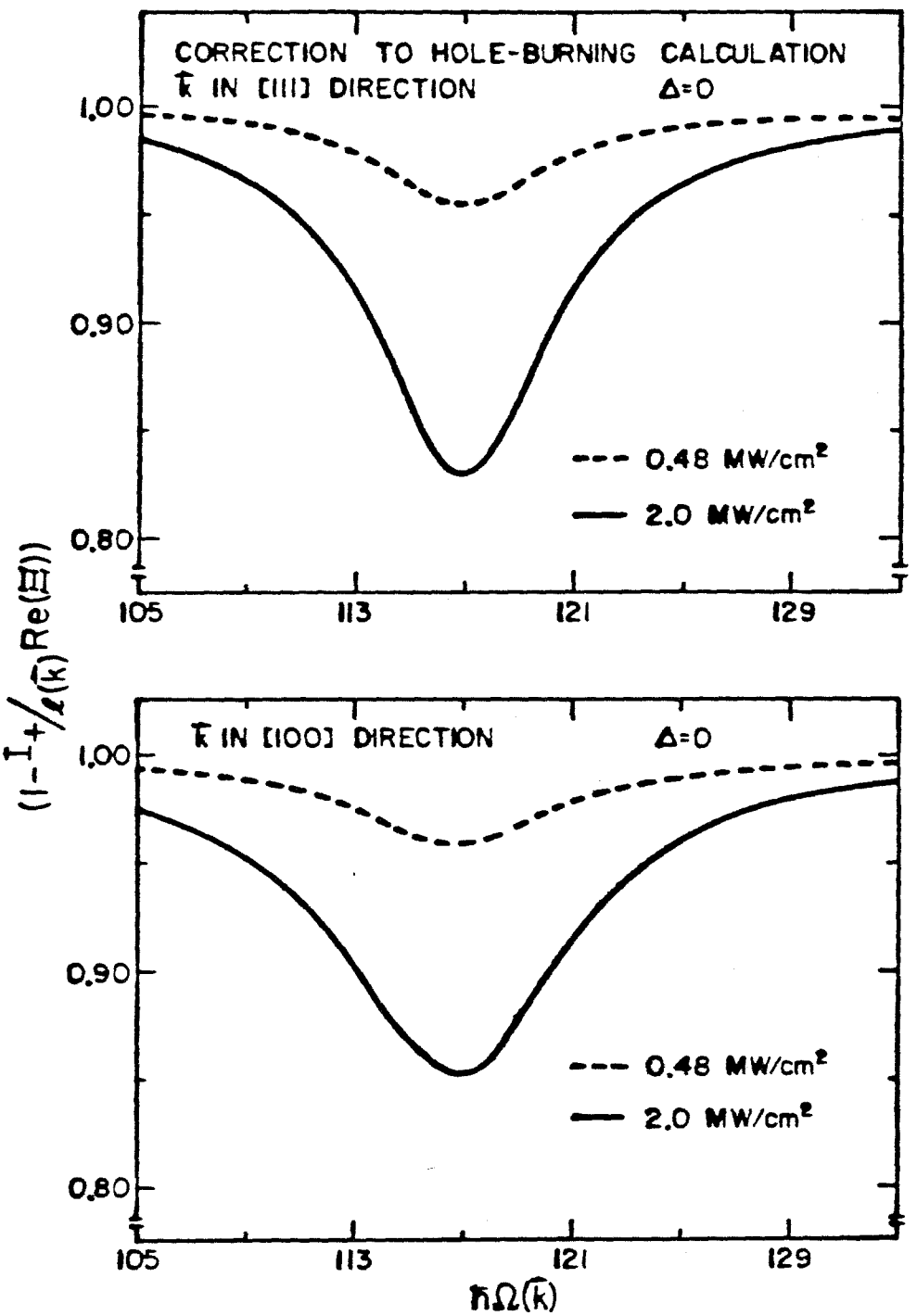
CORRECTION TO HOLE-BURNING CALCULATION
k̄ IN [111] DIRECTION
Δ=0
1.00
0.90
0.80
0.48 MW/cm²
2.0 MW/cm²
105
113
121
129
k̄ IN [100] DIRECTION
Δ=0
1.00
0.90
0.80
0.48 MW/cm²
2.0 MW/cm²
105
113
121
129
$(1-I_+/\mathcal{I}(\bar{k})\,\mathrm{Re}(\Xi))$
$\hbar\Omega(\bar{k})$

Figure 3. Variation of the factor $(1 - I_+/\ell(\underset{\sim}{k})\ \mathrm{Re}\Xi)$ vs $\hbar\Omega(\underset{\sim}{k})$ for $\underset{\sim}{k}$ in the [111] direction and a pump laser at 10.6 μm. The top figure is for $\Delta = -4.56\times10^{12}\mathrm{cm}^{-1}$ ($\hbar\omega_- = 120$ meV) and the bottom figure is for $\Delta = -9.11\times10^{12}\mathrm{sec}^{-1}$ ($\hbar\omega_- = 123$ meV). The dashed (solid) curve in each figure is for a pump intensity of 0.48 (2.0) $\mathrm{MW/cm}^2$. The calculated values are for T=300K.

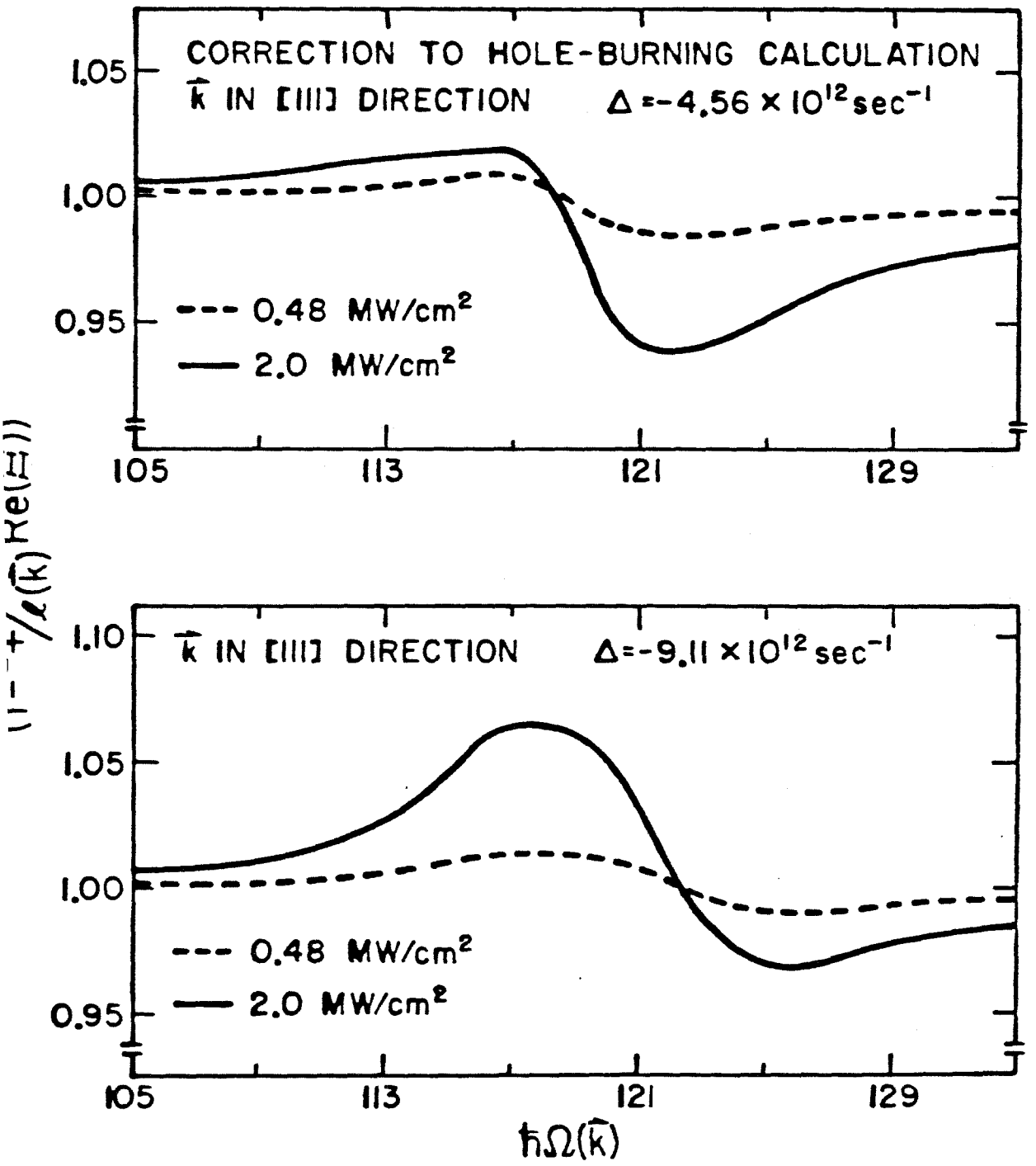
CORRECTION TO HOLE-BURNING CALCULATION
$\vec{k}$ IN [111] DIRECTION $\Delta = -4.56 \times 10^{12}\,sec^{-1}$
0.48 MW/cm²
2.0 MW/cm²
1.05
1.00
0.95
105
113
121
129
$\vec{k}$ IN [111] DIRECTION $\Delta = -9.11 \times 10^{12}\,sec^{-1}$
0.48 MW/cm²
2.0 MW/cm²
1.10
1.05
1.00
0.95
105
113
121
129
$\hbar\Omega(\vec{k})$
$(1 - \epsilon^{-1}/\epsilon(\vec{k}))\,Re(\Pi)$

tering rates. We immediately note that the term describing the coupling of the pump and probe beams in $\alpha(I)/\alpha_o$ depends on the particular direction in $\underset{\sim}{k}$-space due to the presence of anisotropy in the valence band.

In Fig. (3) we show the results for $[1 - I_+/\ell(\underset{\sim}{k})\ \mathrm{Re}(\Xi(\underset{\sim}{k}))]$ versus the detuning Δ for $\underset{\sim}{k}$ in the [111] direction. The top figure is for $\Delta = 4.56\times10^{12}\mathrm{sec}^{-1}$ which corresponds to $\hbar\omega_- = 120$ meV and the bottom figure is for $\Delta = -9.11\times10^{12}\mathrm{sec}^{-1}$ which corresponds to $\hbar\omega_- = 123$ meV. Using Figs. (2) and (3), we see that for small detuning ($\Delta << 1/T_2$), the factor is less than unity for all values of $\hbar\Omega(\underset{\sim}{k})$, and the probe absorption is reduced as compared to the hole-burning results. As the detuning is increased, the factor $[1 - I_+/\ell(\underset{\sim}{k})\ \mathrm{Re}\ \Xi]$ also increases and exceeds unity for some values of $\hbar\Omega(\underset{\sim}{k})$ as shown in Fig. (3). For example, from the bottom figure of Fig. (3) we see that for states with $\hbar\Omega(\underset{\sim}{k})$ less than about $\hbar\omega_-$, the probe absorption is increased as compared to the hole-burning calculation, and for $\hbar\Omega(\underset{\sim}{k})$ greater than about $\hbar\omega_-$, the probe absorption is decreased as compared to the hole-burning calculation.

The component in the difference of the one-hole occupation probabilities for states in the heavy- and light-hole bands which oscillates at the beat frequency is described by the coefficients $A_-(\alpha^{(1)}_{hl1-1}(\underset{\sim}{k}) - \alpha^{(1)}_{\ell l1-1}(\underset{\sim}{k}))$. Using Eqs. (7),(8) and (10), we numerically calculate $A_-(\alpha^{(1)}_{hl1-1} - \alpha^{(1)}_{\ell l1-1})$ as a function of the detuning. Room temperature

values of the real part of $\left[\frac{A_-(\alpha^{(1)}_{h11-1}-\alpha^{(1)}_{\ell11-1})}{\alpha^{(0)}_{h000}-\alpha^{(0)}_{\ell000}}\times\sqrt{I_+/I_-}\right]$

are shown in Fig. (4) for a high-intensity laser with $\lambda = 10.6$ μm. The values are shown for pump intensities of $I = 0.48$ and 2.0 MW/cm^2 and beat frequencies of zero and -4.56×10^{12} sec^{-1} ($\hbar\omega_- = 120$ meV). We note that the magnitude of the pulsation increases with increasing intensity. In addition, we see that the magnitude of the pulsation is a maximum for zero beat frequency and decreases as the pump and probe are detuned. For zero beat frequency, values of the real part of $(\alpha^{(1)}_{h11-1} - \alpha^{(1)}_{\ell11-1})$ are peaked at $\hbar\Omega(\underset{\sim}{k}) = 117$ meV and have a Lorentzian shape for states with $\hbar\Omega(k)$ in the resonant region. As the pump and probe are detuned, the structure of $\mathrm{Re}(\alpha^{(1)}_{h11-1} - \alpha^{(1)}_{\ell11-1})$ vs $\hbar\Omega(\underset{\sim}{k})$ becomes more complicated as shown in the bottom figure of Fig. (4) with two peaks located at approximately $\hbar\Omega(\underset{\sim}{k}) = \hbar\omega_+$ and $\hbar\Omega(\underset{\sim}{k}) = \hbar\omega_-$.

We have so far considered the effect of the high-intensity pump laser on the absorption coefficient of the probe. In addition, there exists a d.c. component in $(f_h(\underset{\sim}{k}) - f_\ell(\underset{\sim}{k}))$ which is second-order in the field amplitude of the probe laser as shown in Eqs. (11) and (12). The first term on the right-hand side of Eq. (11) gives the effect of the probe field on the absorption coefficient of the pump laser. It is smaller than the zeroth order term by approximately I_-/I_+. For ($I_- \ll I_+$) the term has a negligible effect on the measured absorption coefficient of the pump; however, the term does account for a small change

Figure 4. Room temperature values of $\mathrm{Re}\left[\frac{-A_-(\alpha_{h11-1}-\alpha^{(1)}_{\ell 11-1})}{\alpha^{(0)}_{h000}-\alpha^{(0)}_{\ell 000}}\times\sqrt{I_+/I_-}\right]$ versus $\hbar\Omega(\underset{\sim}{k})$ for $\underset{\sim}{k}$ in the [111] direction and a pump laser at 10.6 μm. The top figure shows the factor for $\Delta = 0$ and the bottom figure for $\Delta = -4.56\times10^{12}\,\mathrm{sec}^{-1}$. The dashed (solid) curve in each figure is for a pump intensity of 0.48 (2.0) $\mathrm{MW/cm}^2$.

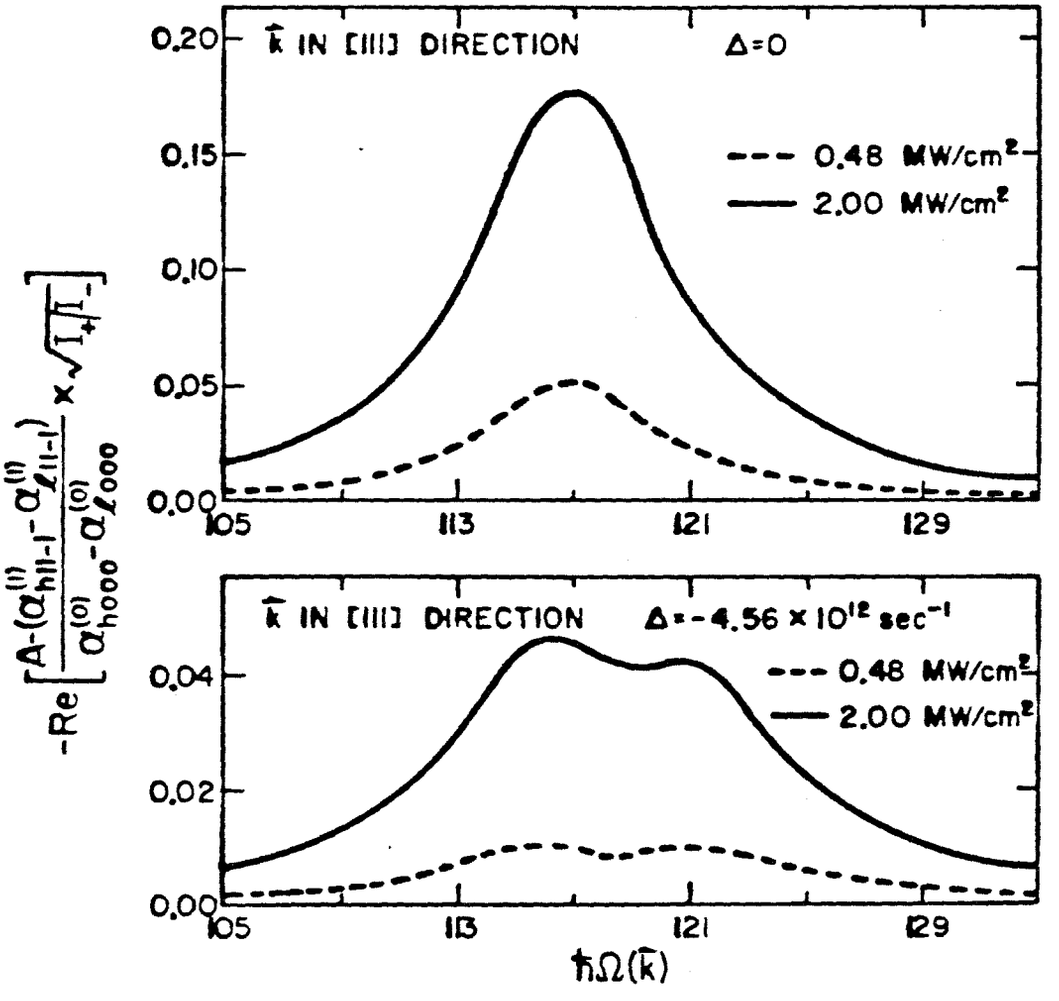
$\hat{k}$ IN [111] DIRECTION
Δ=0
0.48 MW/cm²
2.00 MW/cm²
0.20
0.15
0.10
0.05
0.00
105
113
121
129
$\hat{k}$ IN [111] DIRECTION
Δ=-4.56 × 10¹² sec⁻¹
0.48 MW/cm²
2.00 MW/cm²
0.04
0.02
0.00
105
113
121
129
ħΩ(k̄)
$-Re\left[\frac{A-(\alpha^{(1)}_{hll-l}-\alpha^{(1)}_{ll-l})}{\alpha^{(0)}_{hooo}-\alpha^{(0)}_{looo}}\times\sqrt{I_4 I_-}\right]$

in the energy absorbed by the medium from the pump field. The second term on the right-hand side of Eq. (11) is proportional to the energy absorbed by the probe beam. Eq. (11) is an energy balance equation which states that an increase in the transmission of the probe beam occurs at the expense of the pump beam or vice versa.

IV. SUMMARY AND CONCLUSIONS

We have presented a theory describing the absorption lineshape of a low-intensity probe laser which is tuned in the vicinity of a high-intensity pump laser at a fixed frequency. Values of the probe absorption coefficient are calculated at room temperature for a pump laser with a wavelength of 10.6 μm. We find that the absorption coefficient of the probe is modified by the high intensity pump which saturates the resonant transitions. The absorption coefficient of the probe has two separate contributions: one being due to the depletion of free holes in the resonant region of the heavy-hole band and the other being due to a non-linear coupling of the pump and probe beams which allows an energy transfer of photons in the pump beam to the probe beam and vice versa. The composite lineshape of the probe absorption coefficient due to these contributions is non-Lorentzian. The calculated results are compared with the experimental measurements and good agreement is found. The theory presented can be applied to other wavelengths of the pump and probe (for wavelengths in the 8-25 μm region) and to other p-type semiconductors with a valence band structure similar to that of Ge.

APPENDIX A: EQUATION FOR PROBE ABSORPTION COEFFICIENT

The current density owing to the intervalence-band transitions induced by the probe is given by (where $\underset{\sim}{J} = \sum_{\underset{\sim}{k}} \underset{\sim}{J}(\underset{\sim}{k})$)

$$\underset{\sim}{J}_{-}(\underset{\sim}{k}) = \frac{N_h e}{m} \mathrm{Tr}(\sigma(\underset{\sim}{k},t)\, \underset{\sim}{P}_{h\ell}(\underset{\sim}{k}))$$

$$= \frac{N_h e}{m} e^{-i(\omega_- t - k_- z)}\, \underset{\sim}{P}_{h\ell}(\underset{\sim}{k})\, [A_-\, \gamma^{(1)}_{-1-1\ 1}(\underset{\sim}{k})] + \mathrm{cc.} \qquad \text{(A1)}$$

The power gained by the probe from states with wavevector $\underset{\sim}{k}$ is given by the time average

$$\frac{1}{\omega_- c} \langle A_- \underset{\sim}{\eta}\cdot \frac{d\underset{\sim}{J}_-}{dt}(\underset{\sim}{k})\rangle = \frac{N_h e}{m\omega_-} \frac{8\pi}{\sqrt{\varepsilon}\ \omega_-^2} I_-\ \mathrm{Im}(\gamma^{(1)}_{-1-1\ 1}(\underset{\sim}{k})) \quad , \qquad \text{(A2)}$$

where I_- is the intensity of the probe beam. Using the Fourier expansions, we find $\gamma^{(1)}_{-1-1\ 1}(\underset{\sim}{k})$ to be determined by the following set of algebraic equations which are first-order in the probe field strength.

$$[1/T_h\ (\underset{\sim}{k}) - i\Delta]\ \alpha^{(1)}_{h11-1}(\underset{\sim}{k}) + \frac{ie}{2mc\hbar} A_+ (\sum_{bc} \underset{\sim}{\eta}\cdot\underset{\sim}{P}_{bc})(\gamma^{(1)}_{11-1}(\underset{\sim}{k}) - \gamma^{(1)*}_{-1-11}(\underset{\sim}{k})) = \frac{-ie}{2mc\hbar}\gamma^{(0)}_{000}(\underset{\sim}{k}) \qquad \text{(A3)}$$

$$[1/T_\ell\ (\underset{\sim}{k}) - i\Delta]\ \alpha^{(1)}_{\ell 11-1}(\underset{\sim}{k}) - \frac{ie}{2mc\hbar} A_+ (\sum_{bc} \underset{\sim}{\eta}\cdot\underset{\sim}{P}_{bc})(\gamma^{(1)}_{11-1}(\underset{\sim}{k}) - \gamma^{(1)*}_{-1-1\ 1}(\underset{\sim}{k})) = \frac{ie}{2mc\hbar}\gamma^{(0)}_{000}(\underset{\sim}{k}) \qquad \text{(A4)}$$

$$[\,1/T_2(\underset{\sim}{k})+i(\Omega-\omega_+-\Delta)\,]\gamma^{(1)}_{11-1}(\underset{\sim}{k})+\frac{ie}{2mch}A_+(\alpha^{(1)}_{h11-1}(\underset{\sim}{k})-\alpha^{(1)}_{\ell\ 11-1}(\underset{\sim}{k}))=0 \qquad (A5)$$

$$[1/T_2(\underset{\sim}{k})+i(\Omega-\omega_+-\Delta)]\,\gamma^{(1)}_{-1-1\ 1}(\underset{\sim}{k})+\frac{ie}{2mch}A_+(\alpha^{(1)*}_{h11-1}(\underset{\sim}{k})-\alpha^{(1)*}_{11-1}(\underset{\sim}{k}))$$

$$=\frac{-ie}{2mch}(\alpha^{(0)}_{h000}(\underset{\sim}{k})-\alpha^{(0)}_{\ell000}(\underset{\sim}{k}))\ . \qquad (A6)$$

Using Eqs.(A3-A6), we solve for $\mathrm{Im}(\gamma^{(1)}_{-1-1\ 1}(\underset{\sim}{k}))$ in terms of the zero-order expansion. We find that the absorption coefficient of the probe in the presence of the pump laser is given by (after performing the integration over all $\underset{\sim}{k}$-space)

$$\alpha_-(I_+)=\frac{2\pi^2 N_h e^2}{\sqrt{\varepsilon}m^2\omega_- c}\sum_{\underset{\sim}{k}}(f^o_h(\underset{\sim}{k})-f^o_\ell(\underset{\sim}{k}))\ \frac{\frac{1}{\hbar}\frac{1}{\pi T_2(\underset{\sim}{k})}}{(\Omega(\underset{\sim}{k})-\omega_-)^2+(\frac{1}{T_2}(\underset{\sim}{k}))^2}(\sum_{bc}|\underset{\sim}{\eta}\cdot\underset{\sim}{P}_{bc}|^2)$$

$$\times\,[1-\frac{I_+}{\ell(\underset{\sim}{k})}\,\mathrm{Re}(\Xi(\underset{\sim}{k}))]\quad , \qquad (A7)$$

where I_+ is the light intensity of the pump laser. Here, $f^o_h(\underset{\sim}{k})$ and $f^o_\ell(\underset{\sim}{k})$ are the one-hole distribution functions in the heavy- and light-hole bands in the presence of the high-intensity pump laser. In addition, we have defined the auxiliary functions

$$\ell(k)=\frac{\hbar^2 c\sqrt{\varepsilon}\ m^2\omega_+^2}{(T_h\ (\underset{\sim}{k})+T_\ell\ (\underset{\sim}{k}))\ T_2(\underset{\sim}{k})\ 2\pi e^2\sum_{bc}|\underset{\sim}{\eta}\cdot\underset{\sim}{P}_{bc}|^2}\ , \qquad (A8)$$

and

$$\mathrm{Re}(\Xi(\underset{\sim}{k})) = \frac{A(B+C) + E(D+F)}{(B+C)^2 + (D+F)^2} \quad , \tag{A9}$$

where we have defined

$$A(\underset{\sim}{k}) = \frac{1 + (\Omega-\omega_+ +\Delta)(\Omega-\omega_+)(T_2(\underset{\sim}{k}))^2}{1 + (\Omega-\omega_+)^2(T_2(\underset{\sim}{k}))^2} + \frac{1 - (\Omega-\omega_+ +\Delta)^2(T_2(\underset{\sim}{k}))^2}{1 + (\Omega-\omega_+ +\Delta)^2(T_2(\underset{\sim}{k}))^2} \quad , \tag{A10}$$

$$B(\underset{\sim}{k}) = \frac{2(T_h + T_\ell)^2}{[(T_h)^{-1} + (T_\ell)^{-1}]^2 + 4\Delta^2}\left[\frac{1}{T_h T_\ell}\left(\frac{1}{T_h T_\ell} + \Delta^2\right)\right] \quad , \tag{A11}$$

$$C(\underset{\sim}{k}) = 2\left[\frac{1 + (\Omega-\omega_+ -\Delta)(\Omega-\omega_+ +\Delta)(T_2)^2 + 2\Delta^2(T_2)^2}{[1+(\Omega-\omega_+ -\Delta)(\Omega-\omega_+ +\Delta)(T_2)^2]^2 + 4\Delta^2(T_2)^2}\right]\frac{I_+}{\ell(\underset{\sim}{k})} \quad , \tag{A12}$$

$$D(\underset{\sim}{k}) = \frac{2\Delta T_2\,[-1 + (\Omega-\omega_+ -\Delta)(\Omega-\omega_+ +\Delta)(T_2)^2]}{[1 + (\Omega-\omega_+ -\Delta)(\Omega-\omega_+ +\Delta)(T_2)^2]^2 + [2\Delta T_2]^2}\;\frac{I_+}{\ell(\underset{\sim}{k})} \quad , \tag{A13}$$

$$E(\underset{\sim}{k}) = \frac{-\Delta T_2}{1+(\Omega-\omega_+)^2(T_2)^2} - \frac{2(\Omega-\omega_+ +\Delta)\,T_2}{1+(\Omega-\omega_+ +\Delta)^2(T_2)^2} \quad , \tag{A14}$$

and

$$F(\underset{\sim}{k}) = \frac{2\Delta(T_h + T_\ell)}{(1/T_h + 1/T_\ell)^2 + (2\Delta)^2}\left[(1/T_h + 1/T_\ell)^2 + 2\left(\Delta^2 - \frac{1}{T_h T_\ell}\right)\right] . \tag{A15}$$

Here we have continued with the notation in which a subscript (+) refers to the pump laser and a (-) refers to the probe laser.

REFERENCES

1. F. Keilmann, IEEE J. Quantum Electron. 12, 592 (1976).
2. P. J. Bishop, A. F. Gibson, and M. F. Kimmitt, J. Phys. D9, L101 (1976).
3. F. Keilmann, Appl. Phys. 14, 29 (1977).
4. E. V. Baklanov and V. P. Chebotaev, Zh. Eksp. Teor. Fiz. 61, 922 (1971) [Sov. Phys. JETP 34, 490 (1972)].
5. E. V. Baklanov and V. P. Chevotaev, Zh. Eksp. Teor. Fiz. 60, 552 (1971) [Sov. Phys. JETP 33, 300 (1971)].
6. S. Haroche and F. Hartmann, Phys. Rev. A6, 1280 (1972).
7. M. Sargent III, Appl. Phys. 9, 127 (1976).
8. M. Sargent III, P. E. Toschek, and H. G. Danielmeyer, Appl. Phys. 11, 55 (1976).
9. M. Sargent III, P. E. Toschek, Appl. Phys. 11, 107 (1976).
10. M. Sargent III, Opt. Commun. 20, 298 (1977).
11. In the momentum matrix elements of Eq. (8), we perform the sum on bands for b in the heavy-hole band, and c in the light-hole band. For the remainder of this paper, we omit the "in h" in the sum over b and the "in ℓ" in the sum over c.
12. A. F. Gibson, C. A. Rosito, C. A. Raffo, and M. F. Kimmitt, Appl. Phys. Lett. 21, 356 (1972).
13. C. R. Phipps, Jr. and S. J. Thomas, Opt. Lett. 1, 93 (1977).
14. R. L. Carlson, M. D. Montgomery, J. S. Ladish, and C. M. Lockhart, IEEE J. Quantum Electron. 13, 35D (1977).

15. J. Wynne, Phys. Rev. 178, 1295 (1969).

16. C. Phipps, Jr., D. Watkins, and S. Thomas, Proc. on the International Conf. on Lasers '79 (STS Press, Alexandria, Va., 1980), paper Q. 5.

CHAPTER 6

I. INTRODUCTION

The absorption of light in the 10 μm region by p-type germanium is determined by direct intervalence-band transitions in which a free hole in the heavy-hole band absorbs a photon and is excited to the light-hole band [1]. Since the absorption of light modifies the distribution of free holes, one expects a change in the sample conductivity upon illumination. Because the density of states in the heavy-hole band is much greater than that in the light-hole band, the photo-excited holes primarily scatter into high energy states in the heavy-hole band. Thus the dominant change in the distribution function is an increase in the average energy of occupied states in this band. For temperatures and doping levels for which phonon scattering dominates the momentum relaxation, the conductivity decreases upon illumination because the rate of phonon scattering increases with increasing hole energy. For lower temperatures or higher doping levels where ionized impurity scattering dominates the momentum relaxation, the conductivity increases with illumination because ionized impurity scattering decreases with increasing hole energy. These photoconductive effects have been observed experimentally [2-7] and have been shown to influence the performance of p-Ge photon drag detectors [8-10]. In this chapter we present a calculation of the photoconductive response of p-Ge upon illumination by 10.6 μm light as a function of doping level, temperature and intensity.

Previous calculations of this photoconductive response have been based on idealized models in which the Ge valence bands have been replaced by a set of discrete energy levels, each characterized by an effective mobility [6,7]. In addition, the effects of saturation of the intervalence-band transitions were not included, so that the results could only be applied for low intensities. Here we describe the Ge valence band using degenerate $\underset{\sim}{k}\cdot\underset{\sim}{p}$ perturbation theory. We calculate the hole distribution as a function of the laser intensity in both the linear and nonlinear regimes. Using the calculated hole distribution, we determine the photoconductive response. We find reasonable agreement with experimental results. There are no adjustable parameters in the theory.

The paper is organized in the following way: in Sec. II we present our theoretical approach, in Sec. III we give our results for the change in the conductivity, and in Sec. IV we summarize our conclusions.

II. THEORETICAL CALCULATION

The valence bands of Ge consist of three two-fold degenerate bands: the heavy-hole, the light-hole, and the split-off hole bands. In thermal equilibrium the occupied hole states are in the heavy- and light-hole bands only. We consider the intervalence-band photoconductivity of p-Ge when the sample is pumped by a CO_2 laser. Since the laser does not couple free-holes to states in the split-off

hole band, only the heavy- and light-hole bands need to be considered. The d.c. current density owing to free-holes is given by

$$\underset{\sim}{J} = \left(\frac{1}{2\pi}\right)^3 N_h\, e \sum_b \int f_b(\underset{\sim}{k})\, \underset{\sim}{v}_{bk}\, d^3k \quad , \tag{1}$$

where N_h is the density of holes, b labels the band index, $\underset{\sim}{k}$ is the wavevector, $f_b(\underset{\sim}{k})$ is the one-hole distribution function and $\underset{\sim}{v}_{bk}$ is the group velocity of the carrier with wavevector $\underset{\sim}{k}$ in band b.

In order to calculate the current density and thus determine the conductivity, it is necessary to find the distribution function in the presence of the exciting laser and a small applied d.c. electric field. The distribution functions in the heavy- and light-hole bands are determined by solving the following equations [11] (see Eqs. 17a and 17b of Chapter 2).

$$\beta(\underset{\sim}{k})(f_h(\underset{\sim}{k})-f_\ell(\underset{\sim}{k})) + \frac{e}{\hbar}\underset{\sim}{E}\cdot\nabla_{\underset{\sim}{k}} f_h(\underset{\sim}{k}) = -\sum_{\underset{\sim}{ck'}} [R_{\underset{\sim}{hk}\to\underset{\sim}{ck'}} f_h(\underset{\sim}{k}) - R_{\underset{\sim}{ck'}\to\underset{\sim}{hk}} f_c(\underset{\sim}{k'})] \quad , \tag{2a}$$

and

$$\beta(\underset{\sim}{k})(f_h(\underset{\sim}{k}) - f_\ell(\underset{\sim}{k})) - \frac{e}{\hbar}\underset{\sim}{E}\cdot\nabla_{\underset{\sim}{k}} f_\ell(\underset{\sim}{k}) = \sum_{\underset{\sim}{ck'}} [R_{\underset{\sim}{\ell k}\to\underset{\sim}{ck'}} f_\ell(\underset{\sim}{k}) - R_{\underset{\sim}{ck'}\to\underset{\sim}{\ell k}} f_c(\underset{\sim}{k'})] \quad , \tag{2b}$$

where $\beta(\underset{\sim}{k})$ is given by Eq. (17c) of Chapter 2. The term proportional to β in Eqs. (2a) and (2b) describes the change in the distribution due

to optical excitation, the term proportional to E describes the acceleration of the holes by the electric field and the terms proportional to R describe the scattering of the holes. The one-hole energies and momentum matrix elements are determined by degenerate $\underset{\sim}{k}\cdot\underset{\sim}{p}$ perturbation theory [12]. The cyclotron resonance parameters of Ref. (13) are used in the calculation. The hole scattering rates are treated in the manner of Chapter 2.

In small d.c. electric fields, the distribution of carriers can be described by the sum of a small drift term and the distribution function without an electric field. Thus in small electric fields, we write

$$f_b(\underset{\sim}{k}) = f_b^o(\underset{\sim}{k}) + g_b(\underset{\sim}{k}) \quad , \tag{3}$$

where $f_b^o(\underset{\sim}{k})$ is the distribution function subject to the high-intensity laser but with no external electric field, and $g_b(\underset{\sim}{k})$ is the modification of $f_b(\underset{\sim}{k})$ due to the presence of the electric field. Here, it is assumed that $g_b(\underset{\sim}{k}) << f_b^o(\underset{\sim}{k})$. The function $f_b^o(\underset{\sim}{k})$ is computed as in Chapter 2. Using Eq. (3), we write Eqs. (2) to first order in the electric field

$$\beta(\underset{\sim}{k})(g_h(\underset{\sim}{k})-g_\ell(\underset{\sim}{k})) + \frac{e}{\hbar}\underset{\sim}{E}\cdot\nabla_{\underset{\sim}{k}} f_h^o(\underset{\sim}{k}) = -\sum_{c\underset{\sim}{k}'}[R_{h\underset{\sim}{k}\rightarrow c\underset{\sim}{k}'}g_h(\underset{\sim}{k})-R_{c\underset{\sim}{k}'\rightarrow h\underset{\sim}{k}}g_c(\underset{\sim}{k}')] \quad , \tag{4a}$$

and

$$\beta(\underset{\sim}{k})(g_h(\underset{\sim}{k})-g_\ell(\underset{\sim}{k})) - \frac{e}{\hbar}\,\underset{\sim}{E}\cdot\nabla_{\underset{\sim}{k}} f^o_\ell(\underset{\sim}{k}) = \sum_{c\underset{\sim}{k}'} [R_{\ell\underset{\sim}{k}\to c\underset{\sim}{k}'}\, g_\ell(\underset{\sim}{k}) - R_{c\underset{\sim}{k}'\to\ell\underset{\sim}{k}}\, g_c(\underset{\sim}{k}')] \,. \tag{4b}$$

We assume that a relaxation time approximation can be made for the low d.c. field; that is, the rate of change of $g_h(\underset{\sim}{k})$ due to collisions can be approximated by

$$\sum_{c\underset{\sim}{k}'} [R_{h\underset{\sim}{k}\to c\underset{\sim}{k}'}\, g_h(\underset{\sim}{k}) - R_{c\underset{\sim}{k}'\to h\underset{\sim}{k}}\, g_c(\underset{\sim}{k}')] = \frac{g_h(\underset{\sim}{k})}{\tau_h(\underset{\sim}{k})} \,, \tag{5}$$

and a similar expression for the effect of collisions on $g_\ell(\underset{\sim}{k})$. Here, $\tau_h(\underset{\sim}{k})$ $[\tau_\ell(\underset{\sim}{k})]$ is the momentum relaxation time due to scattering of holes with wavevector $\underset{\sim}{k}$ in the heavy- [light-] hole band by phonons and ionized impurities [14].

Using Eqs. (4) and the relaxation time approximation, we write expressions for $g_b(\underset{\sim}{k})$ in terms of the functions $f^o_b(\underset{\sim}{k})$. Taking the d.c. electric field to be in the z-direction, we have

$$g_h(\underset{\sim}{k}) = \frac{-e}{\hbar}\,\tau_h|E|\,\frac{\partial f^o_h}{\partial k_z}\left[\frac{1+\beta\tau_\ell\left(\dfrac{\partial f^o_\ell/\partial k_z}{\partial f^o_h/\partial k_z}+1\right)}{1+\beta(\tau_h+\tau_\ell)}\right] \,, \tag{6a}$$

and

$$g_\ell(\underset{\sim}{k}) = \frac{-e}{\hbar}\tau_\ell|E|\frac{\partial f_\ell^o}{\partial k_z}\left[\frac{1+\beta\tau_h\left(\frac{\partial f_h^o/\partial k_z}{\partial f_\ell^o/\partial k_z}+1\right)}{1+\beta(\tau_h+\tau_\ell)}\right] \quad . \tag{6b}$$

Since $\underset{\sim}{v}_b(\underset{\sim}{k}) = -\underset{\sim}{v}_b(-\underset{\sim}{k})$ and $f_b^o(\underset{\sim}{k}) = f_b^o(-\underset{\sim}{k})$, we can write

$$J_z = 2\left(\frac{1}{2\pi}\right)^3 e N_h \sum_b \int g_b(\underset{\sim}{k})\, v_{bz}(\underset{\sim}{k})\, d^3k \quad . \tag{7}$$

Integrating Eq. (7) by parts the conductivity is given by

$$\sigma = 2\left(\frac{1}{2\pi}\right)^3 \frac{e^2}{\hbar} N_h \int d^3k\, f_h^o(\underset{\sim}{k}) \frac{\partial}{\partial k_z}\left[\tau_h\, v_{hz}\left(\frac{1+\beta\tau_\ell\left(\frac{\partial f_\ell^o/\partial k_z}{\partial f_h^o/\partial k_z}+1\right)}{1+\beta(\tau_h+\tau_\ell)}\right)\right]$$
$$+ 2\left(\frac{1}{2\pi}\right)^3 \frac{e^2}{\hbar} N_h \int d^3k\, f_\ell^o(\underset{\sim}{k}) \frac{\partial}{\partial k_z}\left[\tau_\ell\, v_{\ell z}\left(\frac{1+\beta\tau_h\left(\frac{\partial f_h^o/\partial k_z}{\partial f_\ell^o/\partial k_z}+1\right)}{1+\beta(\tau_h+\tau_\ell)}\right)\right] . \tag{8}$$

The factor

$$Z_h = \frac{1+\beta\tau_\ell\left(\frac{\partial f_\ell^o/\partial k_z}{\partial f_h^o/\partial k_z}+1\right)}{1+\beta(\tau_h+\tau_\ell)} \tag{9}$$

appearing in the heavy-hole band contribution to the conductivity and the analogous factor Z_ℓ present some numerical difficulties owing to the peaked nature of the terms involved. This factor differs significantly from unity only if $\beta\tau_h \gtrsim 1$ [15]. We note that β is sharply peaked in the resonant region of the optical transition and negligibly small outside of this region. Thus we need only evaluate $\partial f^o/\partial k_z$ in the vicinity of the resonant region. At low light intensities where saturation of the optical transitions does not occur ($I \leq 1$ MW/cm^2), $\beta\tau_h$ is small compared to unity even in the resonant region, and Z_h is essentially one. At high intensities where saturation does occur, Z_h differs from unity in the resonant region. However, for the range of intensities considered in this paper ($I \leq 10$ MW/cm^2), this difference still does not make a large contribution to the integral in Eq. (8) because of limited range over which it occurs.

To estimate the value of Z_h, we only need to know the distribution function in the resonant region. We have found in Chapter 2 that these functions can be reasonably approximated by a simple analytical form for states in the resonant region,

$$f_h^o(\underset{\sim}{k}) \simeq f_h^e(\underset{\sim}{k}) - \frac{\beta(\underset{\sim}{k})\, T_h^{op}(f_h^e(\underset{\sim}{k}) - f_\ell^e(\underset{\sim}{k}))}{1 + \beta(\underset{\sim}{k})\,(T_h^{op} + T_\ell)} \quad , \tag{10a}$$

and

$$f_\ell^o(\underset{\sim}{k}) \simeq f_\ell^e(\underset{\sim}{k}) + \frac{\beta(\underset{\sim}{k})\, T_\ell(\underset{\sim}{k})\,(f_h^e(\underset{\sim}{k}) - f_\ell^e(\underset{\sim}{k}))}{1 + \beta(\underset{\sim}{k})\,(T_h^{op} + T_\ell)} \quad . \tag{10b}$$

where $f^e(\underset{\sim}{k})$ is the equilibrium distribution,

$$\frac{1}{T_\ell(\underset{\sim}{k})} = \sum_{b\underset{\sim}{k}'} R_{\ell\underset{\sim}{k}\to b\underset{\sim}{k}'} \quad , \tag{11}$$

and T_h^{op} is defined for the heavy-hole band analogous to Eq. (11) except that only optical phonon scattering is included.

In the resonant region, the distribution functions in Eqs. (10a) and (10b) have a peaked structure owing to the Lorentzian factor contained in β. Taking the other factors in Eqs. (10) to be slowly varying in the resonant region, we approximate

$$\frac{\partial f^o}{\partial k_z} \simeq \frac{\partial f^o}{\partial \beta}\frac{\partial \beta}{\partial k_z} \quad . \tag{12}$$

With this approximation we

$$\frac{\partial f_\ell^o}{\partial k_z} \Big/ \frac{\partial f_h^o}{\partial k_z} \simeq T_\ell \Big/ T_h^{op} \quad , \tag{13}$$

and thus a simple analytical expression for Z_h. To calculate the conductivity we must also evaluate the derivative of Z_h with respect to k_z. In evaluating this derivative, we take the factors other than β to be slowly varying in the resonant region and take the change in β to occur primarily through the Lorentzian factor which depends on $\Omega(\underset{\sim}{k})$; that is, we approximate

$$\frac{\partial Z_h}{\partial k_z} \simeq \frac{\partial Z_h}{\partial \beta} \frac{\partial \beta}{\partial \Omega} \frac{d\Omega}{dk_z} \quad . \tag{14}$$

With this approximation, we have

$$\frac{\partial Z_h}{\partial k_z} = \left[\tau_h + \tau_\ell \left(\frac{T_\ell}{T_h^{op}} \right) \right] \frac{d\Omega}{dk_z} \frac{2\beta}{(1+\beta(\tau_h+\tau_\ell))^2} \frac{(\Omega-\omega)}{(\Omega-\omega)^2 + (1/T_2)^2} \quad . \tag{15}$$

We treat the factor Z_ℓ which appears in the light-hole contribution to the conductivity in a similar way. We note that the expression in Eq. (15) is vanishingly small outside of the resonant region and changes sign as $\Omega(\underset{\sim}{k})$ crosses ω. As a result this term tends to cancel in the $\underset{\sim}{k}$-space integration. The inclusion of the terms containing $\partial Z_h/\partial k_z$ and $\partial Z_\ell/\partial k_z$ makes a contribution of less than 20% to the calculation of the photoinduced change in the conductivity at the highest intensities we consider.

III. RESULTS OF $\Delta\sigma(I)$

We compute the conductivity due to free holes by numerically integrating Eq. (8). For very lightly doped (near intrinsic) samples, we also include a term due to free electrons. We assume that the electron contribution is not much modified by illumination because the absorption cross section for electrons is nearly two orders of magnitude smaller than that for holes [16].

In Fig. (1) we show the calculated results for $(-\Delta\sigma/\sigma I)$ vs N_h in the low intensity regime where $\Delta\sigma$ is proportional to I. The calculation was done for room temperature Ge illuminated by λ = 10.6 μm light. The conductivity has decreased upon illumination. The primary effect of illumination on the hole distribution is to increase the population of high energy holes in the heavy-hole band. At room temperature and for the doping levels considered here, hole-phonon scattering limits the conductivity. Since hole-phonon scattering rates increase with increasing hole energy, the conductivity decreases with illumination. For hole densities between about 10^{14} - $4x10^{15}cm^{-3}$, $(-\Delta\sigma/\sigma I)$ is essentially independent of N_h. In this region hole-impurity scattering makes a negligible contribution to the scattering rates. For hole densities greater than about $4x10^{15}cm^{-3}$, $(-\Delta\sigma/\sigma I)$ decreases with increasing N_h. In this regime, hole-impurity scattering begins to play a role in limiting the mobility. Hole-impurity scattering rates decrease with increasing hole energy. As a result the fractional increase in the total scattering rate (hole-phonon plus hole-impurity) does not increase as much with increasing hole energy in the more heavily doped samples. In addition, the hole distribution is not as strongly modified by illumination of a given intensity in the more heavily doped samples due to the increase in hole-ionized impurity and hole-hole scattering which tends to maintain the equilibrium distribution. For hole densities less than

Figure 1. Values of $(\frac{\Delta\sigma}{\sigma I})$ vs the hole concentration in p-Ge for CO_2 laser excitation at 10.6 μm, room temperature and low light intensities. The calculated values of $(\frac{\Delta\sigma}{\sigma I})$ are shown by the solid curve. The experimental data are taken from: x Ref. (4), Δ Ref. (5), ■ Ref. (6), ● Ref. (7), and O Ref. (9). Error bars are reported only in Refs. (5) and (7).

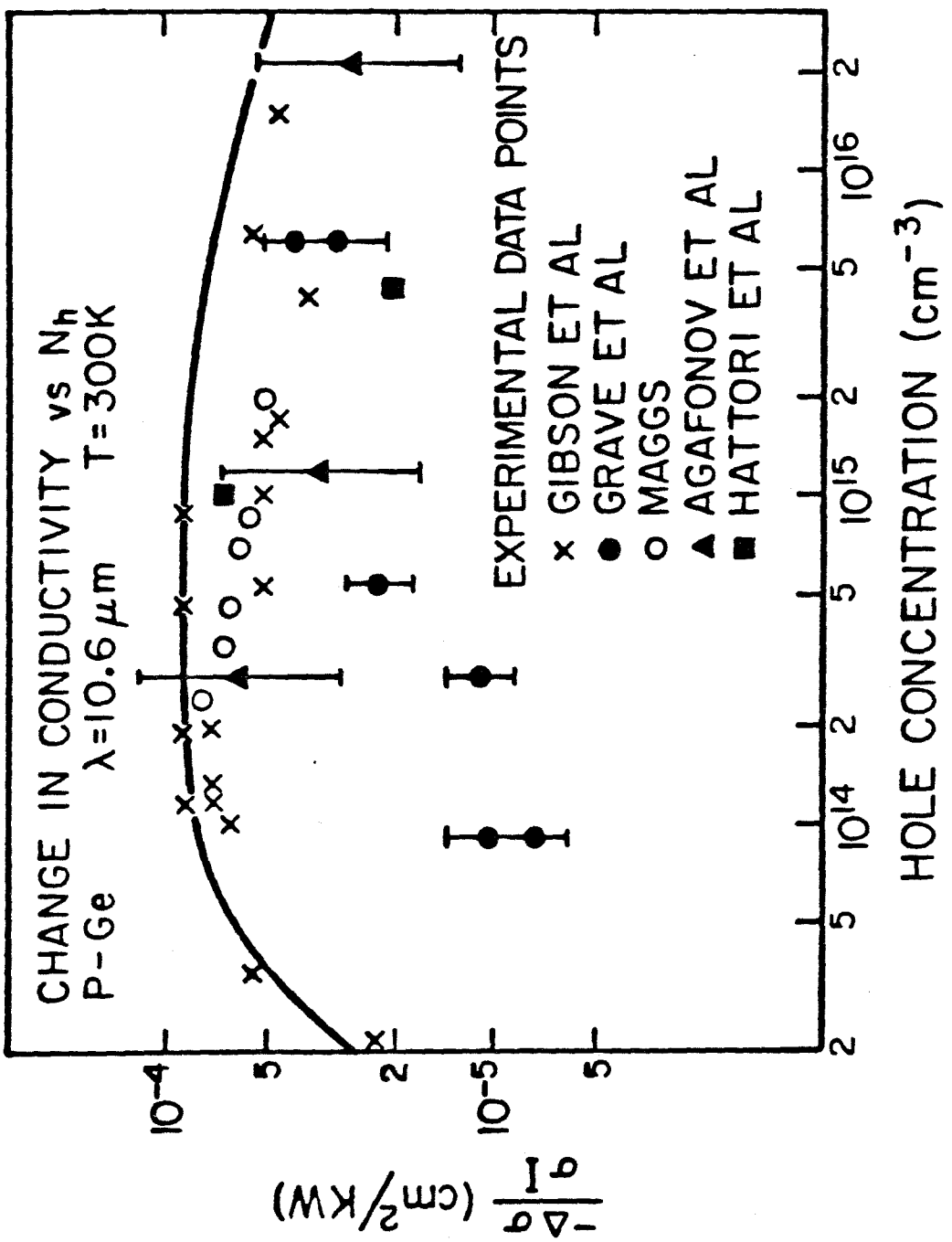
CHANGE IN CONDUCTIVITY vs N_h
P-Ge λ=10.6 μm T=300K
EXPERIMENTAL DATA POINTS
x GIBSON ET AL
● GRAVE ET AL
o MAGGS
▲ AGAFONOV ET AL
■ HATTORI ET AL
$\frac{-\Delta\rho}{\rho I}$ (cm²/KW)
HOLE CONCENTRATION (cm⁻³)
10⁻⁴
10⁻⁵
5
2
10¹⁴
10¹⁵
10¹⁶

about $10^{14}cm^{-3}$, $(-\Delta\sigma/\sigma I)$ decreases with decreasing hole density. This decrease is due to the increased contribution to the conductivity of free electrons whose distribution is not strongly modified by illumination. (In Ge at 300K, the intrinsic density is about $2x10^{13}cm^{-3}$).

Also shown in Fig. (1) are the available experimental results. There is considerable variation in the results reported by the various authors. Our calculated values are in fairly good agreement with the data of Gibson et al [4] and those of Maggs [9].

In Fig. (2), we present our results for the temperature dependence of $(\Delta\sigma/\sigma I)$ for a hole concentration of $2x10^{16}cm^{-3}$. We choose this value for the hole density since experimental measurements exist and the change in the conductivity was observed to change sign over the temperature range that was reported [5]. We note that the change in the conductivity is negative for temperatures greater than about 100K and becomes positive for lower temperatures. In the higher temperature regime, hole-phonon scattering plays a greater role in determining the momentum relaxation than hole-impurity scattering and thus the conductivity decreases upon illumination. In the lower temperature regime hole-ionized impurity scattering dominates the momentum relaxation and the conductivity increases upon illumination. The temperature at which $\Delta\sigma$ changes sign depends on the doping level. At lower doping levels, the sign change in $\Delta\sigma$ occurs at lower temperatures. This effect has been observed experimentally [5]. In addition, we note that the magnitude of $|\Delta\sigma/\sigma I|$ decreases as the temperature

Figure 2. Calculated values of the normalized change in the conductivity of p-Ge vs temperature for light at 10.6 μm, a hole concentration of 2.0×10^{16} cm^{-3} and low intensity excitation. The experimental data are taken from: ▲ Ref. (5) and ● Ref. (3). Error bars are only reported in Ref. (5).

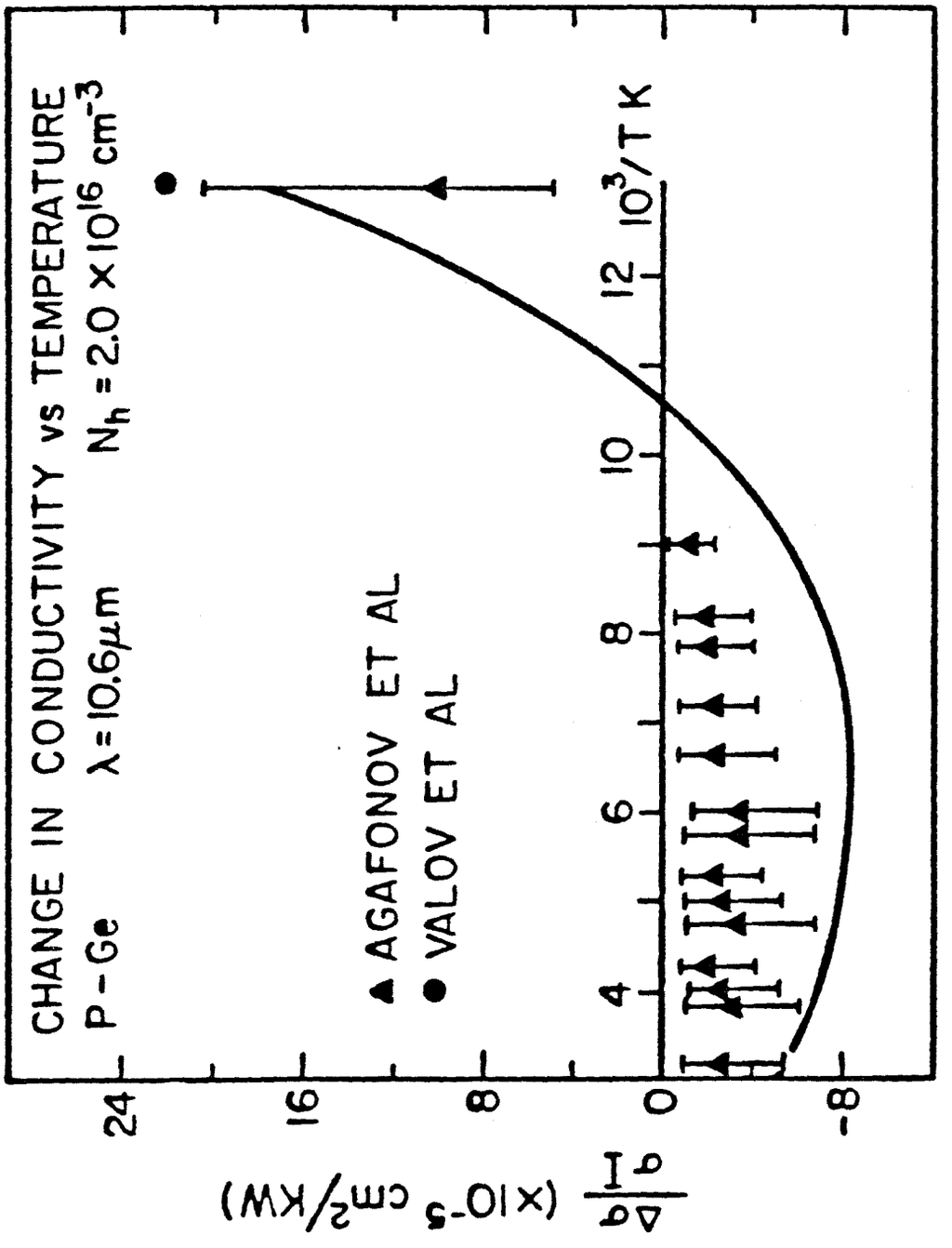
CHANGE IN CONDUCTIVITY vs TEMPERATURE
P-Ge λ=10.6μm $N_h = 2.0 \times 10^{16}$ cm^{-3}
▲ AGAFONOV ET AL
● VALOV ET AL
$\frac{\Delta}{q}\frac{q}{I}$ (x10^{-5} cm^2/KW)
24
16
8
0
-8
4
6
8
10
12
10^3/T K

increases from about 150K. This decrease is due to a decrease in the rate of phonon scattering at the lower temperatures. As a result of the decreased scattering rate, the hole distribution is more strongly modified by a given light intensity at the lower temperatures. The experimental results of Refs. (3) and (5) are included in Fig. (2). The data show the same qualitative features as the calculated results. The calculation gives somewhat larger values for $|\Delta\sigma/\sigma I|$ than were observed in Ref. (5). From Fig. (1), we note that the room temperature results reported in Ref. (5) are systematically smaller than those of Refs. (4) and (9).

Because of interest in the performance of photon-drag detectors at high laser intensities [8-10], we also examine the photoconductive response of p-Ge at intensities for which saturation effects are important. In Fig. (3), we present the results of our calculation of $(-\Delta\sigma/\sigma I)$ as a function of N_h for different light intensities. The curve for 0.05 MW/cm^2 is in the linear regime. At the higher intensities, $(-\Delta\sigma/\sigma)$ increases with increasing intensity at a rate which is slower than linear. The nonlinear behavior is due to saturation of the intervalence-band transitions. The shape of the curves at any given intensity are similar. We are not aware of any direct measurements of $(\Delta\sigma/\sigma I)$ at these high intensities; however, both saturable absorption[17,18] and non-linear photon-drag voltages [9,10] have been seen experimentally. It is possible that this saturation effect could account for some of the variation in the experimental results shown in Fig. (1).

Figure 3. Values of $(-\frac{\Delta\sigma}{\sigma I})$ vs the hole concentration in p-Ge for λ = 10.6 μm and T = 300 K. The solid curves are our calculated values for intensities of 0.05 (linear regime), 1, 5, and 10 MW/cm^2.

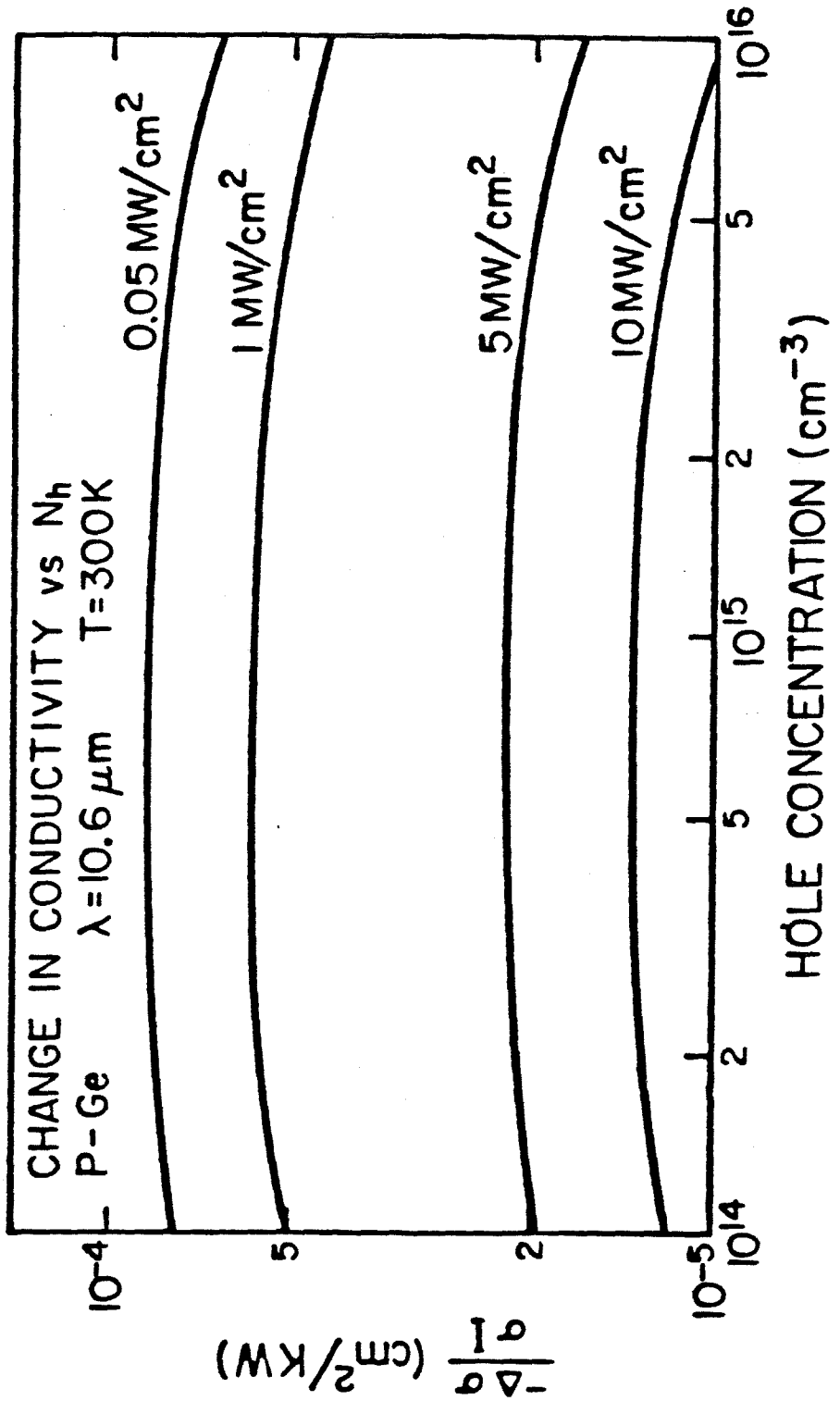
CHANGE IN CONDUCTIVITY vs N_h
P-Ge λ=10.6 μm T=300K
0.05 MW/cm²
1 MW/cm²
5 MW/cm²
10 MW/cm²
10^{-4}
5
2
10^{-5}
10^{14}
2
5
10^{15}
2
5
10^{16}
HOLE CONCENTRATION (cm^{-3})
$\frac{-\Delta\rho}{\rho I}$ (cm^2/KW)

IV. SUMMARY AND CONCLUSIONS

We have presented a theory of the photoconductive response of p-Ge for light with a wavelength of 10.6 μm. Values of $(\Delta\sigma/\sigma I)$ are calculated as a function of doping level in the low intensity regime at room temperature. We have also reported the temperature dependence of $(\Delta\sigma/\sigma I)$ at a fixed hole concentration in the low intensity regime. The effect of saturation at high light intensities was investigated. The theory presented can be applied to other p-type semiconductors with a valence band structure similar to that of Ge.

REFERENCES

1. W. Kaiser, R. J. Collins, and H. Y. Fan, Phys. Rev. 91, 1342 (1953).
2. A. M. Danishevskii, A. A. Kastal'skii, B. S. Ryvkin, S. M. Ryvkin, and I. D. Yaroshetskii, JETP Lett. 10, 302 (1969).
3. P. M. Valov, I. D. Yaroshetskii, and I. N. Yassievich, JETP Lett. 20, 204 (1974).
4. A. F. Gibson and P. N. D. Maggs, J. Phys. D: Appl. Phys. 7, 292 (1974).
5. V. G. Agafonov, P. M. Valov, B. S. Ryvkin, and I. D. Yarosketskii, Sov. Phys. Semicond. 9, 571 (1975).
6. H. Hattori, O. Fujitani, and M. Umeno, J. Phys. Soc. Japan 36, 485 (1974).
7. T. Grave and F. Keilmann, Z. Physik B32, 347 (1979).
8. A. F. Gibson, M. F. Kimmitt, P. N. D. Maggs, and B. Norris, J. Appl. Phys. 46, 1413 (1975).
9. P. J. Bishop, A. F. Gibson, and M. F. Kimmitt, IEEE J. of Quantum Electron. QE-9, 1007 (1973). Values of $\frac{\Delta\sigma}{\sigma I}$ quoted in this paper were measured by P. Maggs.
10. T. Kamibayashi, S. Yonemochi, and T. Miyakawa, Appl. Phys. Lett. 22, 119 (1973).
11. We have assumed that there exists no impact ionization processes in which a hole is sufficiently energetic ($\geq$ the band gap) to relax by an electron-hole pair production. This energy relaxation mechanism may be important at very high intensities; however, the

experiments of Ref. (17) indicate that this process is negligible over the range of intensities presented in this paper.

12. E. O. Kane, J. Phys. Chem. Solids 1, 82 (1956).

13. J. C. Hensel and K. Suzuki, Phys. Rev. B9, 4219 (1974).

14. Hole-hole scattering is included in the calculation of the distribution f^o, but it is not included in the momentum relaxation rates. For hole-hole scattering, the total momentum is not changed; thus, it has little influence on the mobility.

15. For p-Ge and hole states in the resonant region, τ_h is much greater than τ_ℓ.

16. P. J. Bishop and A. F. Gibson, Appl. Optics 12, 2549 (1973).

17. C. R. Phipps, Jr., and S. J. Thomas, Opt. Lett. 1, 93 (1977).

18. A. F. Gibson, C. A. Rosito, C. A. Raffo, and M. F. Kimmitt, Appl. Phys. Lett. 21, 356 (1972).